Energy Research and Development Division
FINAL PROJECT REPORT

CLIMATE FORECASTS FOR IMPROVING MANAGEMENT OF ENERGY AND HYDROPOWER RESOURCES IN THE WESTERN U.S.

Prepared for: California Energy Commission
Prepared by: University of California, Merced

JUNE 2008
CEC-500-2013-151

PREPARED BY:

Primary Author:
Anthony Westerling

University of California, Merced
Merced, CA, 95340

Contract Number: 500-04-002
Work Authorization No: MR 039

Prepared for:

California Energy Commission

Joseph O'Hagan
Contract Manager

Linda Spiegel
Office Manager
Energy Systems Research

Laurie ten Hope
Deputy Director
ENERGY RESEARCH AND DEVELOPMENT DIVISION

Robert P. Oglesby
Executive Director

ACKNOWLEDGEMENTS

Thanks are due to Mary Tyree for data handling and stimulating conversations; to Helene Margolis for enlightening discussions on the health effects of the California 2006 heat wave; to Pasha Groisman for up-to-date station data; to Alexey Kaplan for SST data; and to Xavier Rodó for thought-provoking conversations about climate and about health. Thanks to Connie Woodhouse and Dave Meko for assistance in obtaining stream flow reconstructions for the CRB and SSJ used in the analysis. Thanks also to Niklas Christensen for assistance with the CRSim reservoir model and in obtaining naturalized flows for the CRB. This work was supported by the National Oceanic and Atmospheric Administration, and the National Aeronautics and Space Administration. Special thanks to Naoko Kada for assistance with copy editing.

Please cite this report as follows: A. Westerling, T. Barnett, A. Gershunov, A. Hamlet, D. Lettenmaier, N. Lu, E. Rosenberg, A. Steinemann. 2009. *Climate Forecasts for Improving Management of Energy and Hydropower Resources in the Western U.S.* California Energy Commission, PIER Energy-Related Environmental Research Program. CEC-500-2013-151.

PREFACE

The California Energy Commission's Public Interest Energy Research (PIER) Program supports public interest energy research and development that will help improve the quality of life in California by bringing environmentally safe, affordable, and reliable energy services and products to the marketplace.

The PIER Program conducts public interest research, development, and demonstration (RD&D) projects to benefit California.

The PIER Program strives to conduct the most promising public interest energy research by partnering with RD&D entities, including individuals, businesses, utilities, and public or private research institutions.

PIER funding efforts focus on the following RD&D program areas:

- Buildings End-Use Energy Efficiency
- Energy Innovations Small Grants
- Energy-Related Environmental Research
- Energy Systems Integration
- Environmentally Preferred Advanced Generation
- Industrial/Agricultural/Water End-Use Energy Efficiency
- Renewable Energy Technologies
- Transportation

Climate Forecasts for Improving Management of Energy and Hydropower Resources in the Western U.S. is the final report for the Evaluation of Potential for Improved Co-Management of California and Pacific Northwest Water and Hydropower Resources project (contract number 500-02-004, work authorization 039) conducted by the University of California and the University of Washington. The information from this project contributes to PIER's Energy-Related Environmental Research Program.

When the source of a table, figure or photo is not otherwise credited, it is the work of the author of the report.

For more information about the PIER Program, please visit the Energy Commission's website at www.energy.ca.gov/pier or contact the Energy Commission at 916-327-1551.

TABLE OF CONTENTS

LIST OF FIGURES

LIST OF TABLES

ABSTRACT

This project addressed the feasibility of using climate information and seasonal climate forecasts to better manage the western regional electrical generating system. Several questions were addressed. Can temperature and temperature-related electrical energy demand be modeled and forecast with sufficient accuracy to support operational planning and scenario development with seasonal lead times? Can climatic patterns related to heat waves in California provide the basis for forecasts? Can hydropower resources be coordinated across the region's three major river basins to provide low-cost, reliable energy during peak demand periods?

Historical analyses of maximum temperatures, heat waves and stream flow indicated that large-scale climatic patterns could support conditional forecasts on seasonal time scales, as well as scenario analyses for regional planning. Since temperature affects electricity load, researchers demonstrated how energy loads can be modeled as a function of temperature with predictive accuracy and described tools available to construct probabilistic forecasts and scenarios. Modifications to Western Electricity Coordinating Council planning cases that model electricity generation in response to temperature and stream flow scenarios were also demonstrated.

The project described how patterns and trends in sea surface temperatures associated with heat waves could provide a basis for extended forecasts. Historical data, paleo-reconstructions and modeling suggested that a coherent climate signal in stream flow across the major river basins of the region may provide limited opportunities for sharing hydropower resources across those basins. A case study with the California Department of Water Resources demonstrated ways to confidently apply seasonal climate forecasts to water resource management.

Keywords: Temperature forecasts, Energy demand, Heat waves, Pacific Northwest, stream flow reconstructions, Columbia River basin, Sacramento San Joaquin basins, Colorado River basin, Climate variability, Hydropower production

EXECUTIVE SUMMARY

Introduction

Researchers have recently made substantial progress in developing models to forecast temperatures at seasonal lead times. These forecasts have been for specified temperatures (such as mean or maximum) sampled over some historical reference period. These forecasts are not well suited to energy system planning and management applications because they typically result in one number for an entire season. Making forecast data usable to energy systems that operate continuously requires daily, hourly and shorter decision times. A seasonal average must be "downscaled" into information about daily temperatures.

Hydropower is an important energy resource in the western United States. It provides a relatively inexpensive and renewable alternative to fossil fuel-based technologies such as natural gas turbines. Water managers in the western United States have long faced the challenge of meeting a variety of demands with limited and uncertain supplies. Seasonal climate outlooks offer the potential to improve decision making by extending the planning horizon for resource managers.

Project Purpose

This project explored the feasibility of using seasonal climate forecasts to help manage the western regional electrical generating system. This research attempted to answer several questions: Can temperature and the temperature-related variability in electrical energy demand be forecast with sufficient accuracy to support operational planning and scenario development with seasonal lead times? Can hydropower resources be coordinated across the region's three major river basins to provide low-cost reliable energy during peak demand periods? This project addressed these questions in three separate research efforts: (1) temperature sensitivity of energy load; (2) climate-driven variation in hydropower resources; and (3) a stakeholder partnership with the California Department of Water Resources.

The temperature sensitivity of energy load research attempted to forecast the parameters of maximum daily electricity load models by fitting statistical probability models to maximum daily temperature data. The researchers' hypothesis assumed that maximum daily electricity load varies because of temperature variability and calendar effects unrelated to climate, such as weekends and holidays. Researchers tested this hypothesis by estimating models for maximum daily electricity load as a function of these two factors in the Northwest, Northern California, Southern California, and Southwest regions. Developing estimating models for maximum daily electricity load posed a challenge because the relationship between load and temperature is nonlinear, and because the data used are not normally distributed. Parametric probability forecasts of maximum daily temperature are well suited to planning applications for energy management. Rather than yielding one statistic to describe temperature over an entire season, this approach allowed planners to generate daily maximum temperature samples for a coming season stochastically, and to assign probabilities to planning scenarios of interest.

The goal of the climate-driven variation in hydropower resources research was to improve the use of seasonal climate forecasts by water resource managers, who usually cite low levels of accuracy and difficulties with interpreting the data as reasons for not using climate forecasts. Many managers also say climate forecasts haven't demonstrated an application to their work. This research was intended to make such forecasts easier to use.

One goal of the stakeholder partnership with the California Department of Water Resources (DWR) was to make seasonal forecast information from the National Oceanic and Atmospheric Administration easier to understand and more widely used. Another goal was assessing how seasonal climate forecasts can improve seasonal stream flow forecasts and lead to more efficient water management, helping to reduce the state's vulnerability to drought. The project conducted a case study with DWR to accomplish these goals. DWR manages water for the nation's most populous state, which also includes the largest irrigated agricultural industry. California also arguably has the most publicized conflicts over water allocation in the country. This project focused on implementing existing products from previous and ongoing research funded by the National Oceanic and Atmospheric Administration, rather than developing new technologies.

Project Results

For the temperature sensitivity of energy loads research, the project team determined the correct specification for a model that estimated daily electricity load. They created regression models that accounted for 80 to 90 percent of the variability in maximum daily load in the Northwest, Northern California, Southern California, and Southwest regions. Because of the strong relationship between temperature and electrical load, forecasts of temperature may be useful for planning electricity generation and demand management.

The forecast distribution incorporated temperature statistics from past seasons with information about climate variability from year to year, such as temperature persistence, sea surface temperatures, and soil moisture. Establishing forecast parameters made it possible to predict the distribution of maximum daily temperature. Repeated random draws from these distributions can be used to generate temperature samples for scenario analysis. These distributions can also be used to generate a time series of probabilities that temperatures will exceed a certain threshold. Researchers calculated the probability per day of exceeding an arbitrary temperature threshold in Northern California (32 degrees Celsius) for each summer from 1950 to 2003 and then compared it to the observed frequency of temperature extremes.

Heat waves lasting several days can affect energy loads more than models of concurrent peak demand and peak temperature would predict. This report described relationships that could form the basis for more accurately forecasting heat waves in California. Observation showed that California heat waves are becoming more humid, with higher nighttime temperatures. The frequency and magnitude of nighttime heat waves has clearly and steadily been on the rise, and the trend appeared to be accelerating. Out of the largest six nighttime events occurring over almost six decades between 1948 and 2006, three have occurred in the last six years. The magnitude and timing of these changes impact both public health and energy demand.

Californians are less used to humid heat than dry heat, so they tend to use cooling more often at night and to set thermostats to lower temperatures during the day.

Recent research indicated that California heat waves vary from year to year and over even longer periods because of changing sea surface temperatures in the North Pacific, especially off the coast of Baja California. Whether a heat wave will produce high daytime or nighttime temperatures depends on the availability of an unusual upwind source of moisture. Warmer sea temperatures to the west of Baja California seem to make this moisture available. Global climate change models predict higher temperatures in the world's oceans, which poses another set of questions:

- How much of the warming of the sea near Baja is caused by global warming?
- Can forecasters skillfully predict heat wave activity in California based on surface temperatures of the Pacific Ocean?
- Can they expect the heat wave trends they have observed to continue?
- How much of the climb in high nighttime temperatures now being witnessed over California and Nevada is a regional expression of global warming?

Answering these questions unequivocally was beyond the scope of this study and requires an augmented set of tools, including dynamical modeling. The authors intended to address these questions in future studies. The results of this study were fully consistent with global warming. They provided a plausible scenario of a future California with more, hotter, more extensive and durable humid nighttime heat waves.

The climate-driven variation in hydropower resources project ran three reservoir simulation models for the Columbia River basin, Sacramento San Joaquin basins, and Colorado River basin. It used long-term temperature and precipitation data sets from 1916-2003 to drive the Variable Infiltration Capacity hydrologic simulation model, which simulated monthly stream flows over that 87-year period. While the three river basins examined varied in climate, water resource infrastructure and management policy, changes in their stream flows and hydroelectric output since the 1970s largely mirrored changes in their precipitation amounts during cool seasons.

In the western United States, hydropower resources were strongly coupled to variations in cool season precipitation, which accounted for approximately 85 percent of the variance in annual stream flow in the Columbia River basin, 90 percent in the Sacramento San Joaquin basins, and 55 percent in the Colorado River basin. Persistent changes in precipitation during the cool season have been observed since the mid-1970s. These changes have made the western U.S. more vulnerable to energy shortages because droughts during that time period tended to be longer, more intense, and similar from region to region. Conditions were also similar during times of high flows, when abundant hydropower resources were available throughout the West.

A study of historical climate records from 1858 to 1977 suggested that the pattern of variability observed from 1977 to 2003 is unusual when compared to events of the past 150 years or so.

Longer paleoclimatic records for the Sacramento San Joaquin basins and the Colorado River basin showed that similar patterns have occurred at most three times in the last 500 years at roughly 200-year intervals.

Variations in cool season precipitation, stream flow and hydropower resources coincided with predictions of global climate change. It was unclear whether these changes were related to global warming, or if they were simply temporary, natural variations in precipitation that were unusual in the earlier part of the 20th century. Planners may need to alter the way they manage energy and water systems if these changes were in fact natural and predictable in order to cope with the altered variability.

The stakeholder partnership with the DWR focused on two tasks. Statistical analysis established the accuracy of climate forecasts and correlated that data with existing water year information. Researchers then worked with DWR staff to identify decision makers who could benefit from these forecasts. Seasonal forecasts and historical data together can support integrated regional scenario analyses. Relating maximum temperatures, heat waves and stream data to climate can produce valuable planning and scenario analyses for the energy sector in the western United States.

The temperature sensitivity of energy loads research set the stage for future projects to test if accurate seasonal forecasts of heat wave activity in California can be based on nearby sea surface temperature patterns. Such forecasting could help determine if trends in heat wave activity will continue, which would have major implications on future electrical load. Such forecasts depend on predicting the long-term sea surface temperatures off the coast of Baja California and analyzing the impact of global warming through the use of dynamical modeling. This in turn will help clarify whether the climb in nocturnal heat waves now being witnessed over California and Nevada is a regional expression of a global process.

The climate-driven variation in hydropower resources research demonstrated the challenges of using climate forecasting to manage hydropower resources. Future research must clarify whether changes in cool season precipitation, stream flow and hydropower resources were related to global warming or were simply natural variations that have been unusual in the earlier parts of the 20th century. Changes in energy and water management may be needed to cope with the altered variability if these changes were systematic in nature.

The work with the DWR identified DWR decision makers that could benefit from the forecasts developed in this work. It is recommended that these forecasts be used to better manage water resources at the California DWR.

Project Benefits

This research developed models for predicting maximum daily electricity load as a function of (1) variability in temperature and (2) calendar effects unrelated to climate, such as weekends and holidays. This work will support energy system planning and management in regions including Northern California and Southern California. A second benefit of this work is the development of simulation models for the Columbia River basin, Sacramento San Joaquin

basins, and Colorado River basin, which will help improve decision making by water resource managers by extending their planning horizon. Comprehensive statistical analysis conducted with the DWR helped to correlate climate forecasts with water year classifications, as well as identifying key decision points and decision makers at DWR who could benefit from the research.

CHAPTER 1:
Introduction

This research analyzes several factors related to the feasibility of using seasonal climate forecasts to support management of the western regional electrical generating system. This research supports analyses of several questions: can temperature and temperature-related variability in electrical energy demand be forecast with sufficient skill to support operational planning and scenario development at seasonal lead times? Can hydropower resources be coordinated across the region's three major river basins to provide low-cost reliable energy during peak demand periods?

1.1 Energy Load Indices

Detailed electrical load data are generally proprietary and not publicly available. The studies described here required credible indices of western U.S. electricity demand that could be used to demonstrate the utility of climate applications. Four suitable indices were derived from FERC 714 reports for the Northwest, Northern California, Southern California and the Southwest. It was necessary to aggregate loads across utilities, because loads reported by one utility in one year's FERC 714 reporting can, and often are, shifted to another nearby utility's report in one or more subsequent years. A daily time series that could serve as an index of daily, seasonal, and interannual variability in load for each region was derived from the hourly data reported by selected utilities in each region for 1993-1999. Data from the year 2000 and immediately after were available, but were not used because of abrupt changes in reported loads due to the California energy crisis in 2000 and to industry-related demand in the Northwest. The daily maximum aggregate load for each region was detrended and scaled. Trends observed in the data were assumed to result from growth in demand due to changes in population, demography, development, and so forth. While there has been a pronounced trend in temperature in the western U.S. in recent decades, these were not likely to be large within the 1993 - 1999 sample. The result was four regional indices of daily peak energy loads that could then be related to variability in temperatures.

1.2 Temperature Sensitivity of Energy Load

The working hypothesis employed here is that variability in maximum daily electricity load is primarily driven by (1) variability in temperature and (2) calendar effects unrelated to climate (weekends and holidays). This hypothesis was tested by estimating models for maximum daily electricity load for each region defined above as functions of these two factors. These models are useful for motivating interest in temperature forecasts. This and other applications described here use a long-term daily-time-step gridded temperature data set. While only 7 years of load data were employed, using a long-term temperature data set to create four regional daily maximum temperature indices from 1950 – 2003 facilitated production of experimental temperature forecast products and models compatible with our load-temperature model.

Estimating models for maximum daily electricity load pose an interesting challenge because the relationship between load and temperature is nonlinear, and because the data used are not normally distributed. The correct specification was determined to be a nonlinear fit with semi-parametric smooth functions (piecewise polynomials) and skewed, leptokurtic residuals. Using just the polynomial transformation of daily maximum temperature and a factor for weekend versus workweek days, regression models were estimated that accounted for 80-90 percent of the variability in maximum daily load in each region. The strong relationship between temperature and electrical load indicates that skillful forecasts of temperature may be useful for planning related to electricity generation and demand management.

1.3 Parametric Temperature Forecasts

Recent research has made substantial progress in developing models capable of forecasting temperatures at seasonal lead times with significant skill. These forecasts have been for specified percentiles of temperature (such as, mean (50^{th} percentile), 90^{th} percentile, maximum (100^{th} percentile) and so forth.) sampled over some historical reference period. These forecasts can be spatially explicit for gridded or station temperatures, or aggregated over a region. The form of these forecasts is not well suited to energy system planning and management applications, however, because they result typically in one number for an entire season. A manager planning operations for a continuously operated system with daily, hourly and shorter decision time horizons may need some method to 'downscale' a seasonal average into useful information about daily temperatures to make practical use of such a forecast, which might prove as or more challenging a task than producing the original forecast in the first place.

This work examines the potential for fitting statistical probability models to maximum daily temperature data, and then forecasting the parameters that describe those models. Parametric probability forecasts for maximum daily temperature are well suited to planning applications for energy management. The basic approach is to fit an appropriate probability distribution to the temperature data to be forecast, and then to forecast the distribution parameters at seasonal lead times. Rather than yielding one statistic to describe temperature over an entire season, this approach allows planners to generate daily maximum temperature samples for a coming season stochastically, and to assign probabilities to planning scenarios of interest.

Like a climatology, the forecast distribution reflects knowledge about the statistical properties of temperatures observed in past seasons, while also incorporating a forecast reflecting available knowledge regarding expected interannual variability in climate (for example, a forecast based on persistence, sea surface temperatures, and soil moisture). The form of the forecast is also well suited to applications where knowledge of critical planning thresholds may be proprietary, since in many cases it does not require end users to specify a priori the temperature threshold of interest.

With the forecast parameters, it is possible to describe a forecast distribution of maximum daily temperature. Repeated random draws from these distributions can be used to generate temperature samples for scenario analysis. These distributions can also be used to generate a time series of probabilities of exceeding a temperature threshold of interest. For example, the

authors calculated the probability per day of exceeding an arbitrary temperature threshold in Northern California (32 degrees Celsius) for each summer from 1950 to 2003 and compared it to the observed frequency of temperature extremes. The R-squared and cross-validated R-squared for this time series were 0.36 and 0.32. Models like these can be a key ingredient for modeling the effects of climatic variations on the western energy grid.

1.4 Climatic Indicators for Humid Nighttime Heat Waves

Multi-day runs of high temperatures can have a greater impact on energy loads than would be predicted by models of concurrent peak demand and peak temperature. Initial work reported here describes relationships that could form the basis for forecasting heat waves in California. Observational work on heat wave activity in the California region shows that heat waves are becoming more humid and expressed more strongly in nighttime temperatures. These changes are undoubtedly having significant impacts on public health and energy demand, both its magnitude and timing, as cooling is required more often at night and also more intensely and at lower temperature thresholds during the day because people have less tolerance for (and, especially in California, acclimatization to) humid heat than dry heat. Both the interannual and long-term variability in California heat wave activity has been shown to be related to sea surface temperature in the North Pacific and, especially, off the coast of Baja California. Can skillful seasonal forecasts of heat wave activity in California be made based on Pacific sea surface temperature (SST) patterns? Can the observed trends in California heat wave activity be expected to continue? The main key to answering both questions appears to be in the interannual and long-term behavior of sea surface temperatures off the coast of Baja California.

The frequency and magnitude of nighttime heat waves has clearly and steadily been on the rise and the trend appears to be accelerating. Out of the largest 6 nighttime events occurring over almost six decades between 1948 and 2006, 3 have occurred in the last six years. The heat wave that spanned the second half of July 2006 reached a nighttime spatial extent of almost ¾ of the area, at its peak on July 23. Its overall nighttime magnitude was roughly twice that of the next largest recorded nighttime event (July 2003) and its overall daytime magnitude was also unprecedented, due particularly to the unusual combination of its duration and intensity.

The main factor that determines whether a heat wave will be primarily expressed in day or nighttime temperatures is the availability of an anomalous moisture source upwind of the synoptic circulation that converges hot surface air into the region. A warming SST trend east of Baja California appears to have been instrumental in making this moisture source more readily available. This SST trend is part of the global ocean surface and subsurface warming known to be due to anthropogenic climate change. Important questions to be addressed by future studies emerge. How much of the trend in BSST is caused by global warming? How strongly can it be expected to continue? How much of the climb in nocturnal heat wave activity that are being witnessed now over California and Nevada is a regional expression of a global process? Answering these questions unequivocally is beyond the scope of this study and requires an augmented set of tools including dynamical modeling. The authors intend to address these questions in future studies. For now, it should be simply noted that the results presented here are fully consistent with global warming and they do intuit a plausible scenario for future

summertime heat wave activity in California: more, hotter, more extensive and durable humid nighttime heat waves.

1.5 Climate-Driven Coherence in Interannual Variation in Hydropower Resources

Hydropower is an important energy resource in the western United States, providing a relatively inexpensive and renewable alternative to fossil fuel-based technologies such as natural gas turbines. Hydropower resources in the western United States are strongly coupled to cool season precipitation variability, which explains approximately 85 percent of the variance in annual stream flow in the Columbia River basin (PNW), 90 percent of the variance in the Sacramento San Joaquin (SSJ) basins, and 55 percent of the variance in the Colorado River basin (CRB). Persistent changes in cool season precipitation variability have been observed since the mid-1970s, and include increased variance, coefficient of variation, lag1 autocorrelation, and inter-regional covariation. Changes in warm season precipitation, by comparison, are most evident in increased lag1 autocorrelation since the mid-1970s.

Using long term temperature and precipitation data sets from 1916-2003 to drive the Variable Infiltration Capacity hydrologic simulation model, monthly stream flows from 1916-2003 were simulated at a number of river locations which in turn were used to drive three reservoir simulation models for the Columbia River basin, Sacramento San Joaquin basins, and Colorado River basin. Despite differences in climate and water resources infrastructure and management in the three regions examined, changes in stream flow and hydropower variability since the 1970s have largely mirrored changes in cool season precipitation variability. These changes have increased vulnerability to energy shortages in the western U.S. because droughts since the mid-1970s have tended to be longer and more intense, and more coincident from region to region. Similar changes are apparent for high flow conditions, when abundant hydropower resources have been available west-wide.

Paleoclimatic records from 1858-1977 suggests that the observed pattern of variability from 1977-2003 is unusual in the context of natural variability over the past 150 years or so. Longer paleoclimatic records for the Sacramento San Joaquin basins and Colorado River basin alone show that similar episodes have occurred at most three times in the last 500 years, at roughly 200 year intervals. The changes in cool season precipitation variability, stream flow and hydropower resources coincide with strong anthropogenically forced warming at the global scale, however it remains to be seen if these changes are systematic and physically related to global warming in some way, or if they are simply a temporary feature of natural variations in precipitation that have been unusual in the earlier parts of the 20th century record. If these changes are in fact systematic in nature, ongoing changes in energy and water management to cope with the altered variability may be needed.

1.6 Stakeholder Partnership: California Department of Water Resources

Water managers in the western United States have long faced the challenge of meeting a variety of demands with limited and uncertain supplies. Seasonal climate outlooks offer the potential to improve decision-making by extending the planning horizon for resource managers, yet the value of these forecasts is largely untapped. Among the most cited barriers to their use are low forecast skill, difficulties with interpretation, and lack of demonstrated application. This research is aimed at improving the use and usability of National Oceanic and Atmospheric Administration seasonal forecast information through a case study involving California's Department of Water Resources (DWR), managers of water for the most populous state, largest irrigated agricultural industry, and arguably, most publicized conflicts over water allocation in the country.

This project addressed the following science and applications questions:

- How can National Oceanic and Atmospheric Administration climate forecast products be effectively translated and integrated into decision-making to reduce the vulnerability and impacts of drought? How can seasonal climate forecasts result in improved seasonal stream flow forecasts and in turn more efficient water management?
- How can a process of working with stakeholders be developed that will help to promote the integration of forecast information into decision-making? How can the gap between forecasts and their potential beneficial uses be more effectively bridged through a process of understanding socio-organizational factors, opportunities and barriers?

Building upon previous and ongoing research funded by National Oceanic and Atmospheric Administration, this project focused on the transition of these products to operations, and the evaluation of their potential benefits in decision-making, rather than solely the development of new technologies.

This research produced results in two main categories. First, a comprehensive statistical analysis was conducted of climate forecast skill and correlation with water year classification systems. Second, collaborative relationships were established with DWR, and identified the types of decisions and decision-makers that could potentially benefit from these forecasts.

1.7 Summary

Seasonal forecasts and historical data can be used to support integrated regional scenario analyses. Analyses of historical experience with maximum temperatures, heat waves and stream flow indicate that relationships with climatic provide conditional forecasts on seasonal time scales that can support planning and scenario analyses for the energy sector in the western United States.

CHAPTER 2:
Compiling Regional Indices of Electricity Demand

Detailed electrical load data are generally proprietary and not publicly available. For the studies described herein, the authors needed credible indices of western U.S. electricity demand that could be used to demonstrate the utility of climate applications. In the following section the authors describe how suitable indices from FERC 714 reports were derived. The authors recognize that models based on more detailed, proprietary data may better suit the needs of individual energy utilities and others who may find the tools presented here of interest. Our intention here is to provide examples with publicly available data that could be adapted by utilities and other users to suit their individual needs, using their own proprietary data sources.

2.1 Data Sources and Limitations

FERC 714 data provide a publicly available source of hourly load data, but they are not without challenges. Large, discrete elements of electrical load can shift from one reporting area to another without documentation. In addition, the 2000 energy crisis in California led to changes that affected reporting in 2000 and subsequently. In order to get a "clean" data set that could be used to estimate load profiles and temperature sensitivity of load, the authors constrained our sample to FERC 714 reports from 1993 – 1999 (this dealt with the energy crisis effects by excluding them). Some utilities with problems apparent in their data or incomplete reporting were excluded. Hourly loads were aggregated by subregion (this dealt with localized shifts in loads across reporting areas). Utilities used in subregional aggregations are reported in Table 2.1.1.

A daily time series that could serve as an index of daily, seasonal, and interannual variability in load was derived from the hourly subregional data by taking the daily maximum aggregate load for each subregion and detrending and scaling it. Trends observed in the data were assumed to result from growth in demand due to changes in population, demography, development, and so forth. While there has been a pronounced trend in temperature in the western U.S. in recent decades, the authors did not think it was relevant within the 1993 - 1999 sample.

Table 2.1.1: WECC Utilities Used to Estimate Regional Electric Load Temperature Sensitivities

Northwest: Bonneville Power Administration British Columbia Hydro and Power Authority Public Utility District No 1 of Chelan County Public Utility District No 1 of Douglas County Eugene Water and Electric Board Public Utility District No 1 of Grant County Idaho Power Company Pacificorp Portland General Electric Seattle Department of Lighting
Northern CA: Northern California Power Agency Sacramento Municipal Water District Turlock Irrigation District Western Area Power Administration - SAC
Southern CA: City of Burbank Public Service Department City of Glendale Public Service Department Imperial Irrigation District Los Angeles Department of Water and Power Modesto Irrigation District Metropolitan Water District City of Pasadena Pacific Gas and Electric Southern California Edison San Diego Gas and Electric City of Vernon
Southwest: Arizona Electric Power Arizona Public Service Black Hills Power and Light Company Colorado Springs Utility Deseret Generation and Transmission Company El Paso Electric City of Farmington Montana Power Company Nevada Power Company Public Service Company New Mexico Sierra Pacific Power Company Salt River Project Tucson Electric Power Company Utah Association of Municipal Power Systems Utah Municipal Power Agency Western Area Power Administration West Plains Energy

Figure 2.1.1: Raw Maximum Daily Loads Aggregated by Subregion

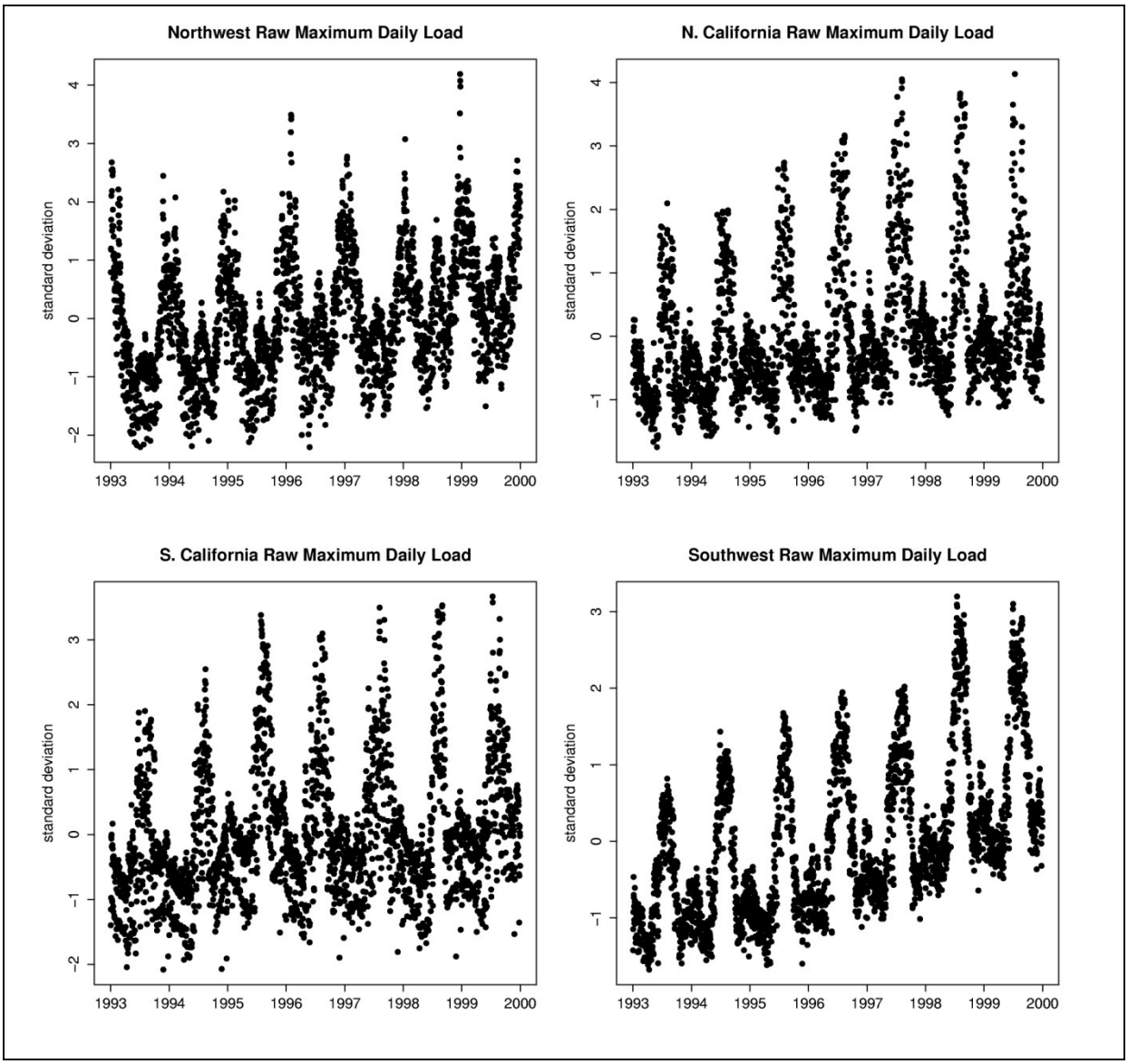

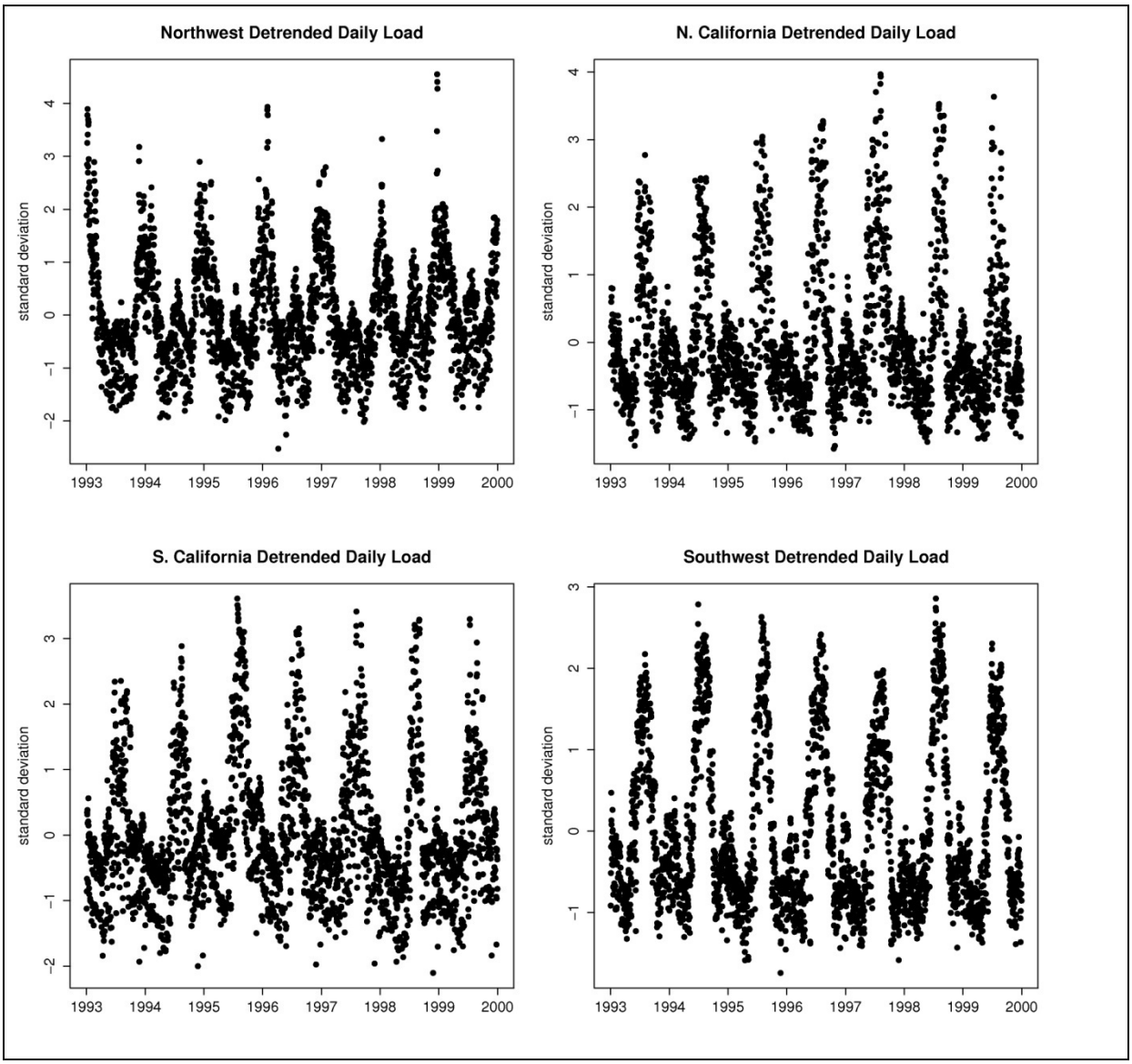

2.2 Spatial Domain and Imprecision

The four indices of electrical demand described here, for subregions loosely described as the Northwest, Northern California, Southern California, and the Southwest, are largely comprehensive for the regional energy grid that comprises the western United States and western Canada. While links to other regions exist, most of the energy consumed within this region is also generated within the region.

The Northwest region corresponds to Washington, Oregon, Idaho, and south-western Canada. The Northern California and Southern California regions split California at the northern Kern county line, at North latitude. The Southwest region includes the southwestern states of Arizona and New Mexico, as well as Nevada, Utah, Colorado, Wyoming, and Montana.

The FERC 714 data used here are aggregated by service area. These service areas can be quite large. Consequently, it is not feasible to use these data to describe electrical loads (or inferred electrical demand) at much higher spatial resolutions than the coarse scale of the four subregions used here. The 'Southwest' subregion could probably be broken up into two or more smaller subregions, but our analytical emphasis was on California and its interactions with the western grid, so the authors for greater simplicity and used four regions.

Furthermore, some service areas extend across two or more of our subregions. Even where individual service areas are well-defined and contained within one of our four subregions, they are linked to the western electricity grid. Electricity generated within a service area is not necessarily consumed within that service area, and vice versa. On the other hand, transmission capacity is, at key points, a binding constraint, limiting, for example, the current potential to transfer electricity generated in the Northwest to users in California. The researchers did not attempt to precisely define the effects of these transfers on the indices, but rather accept that they are approximate, imprecise indicators of both electrical load and, by inference, electrical demand in each subregion.

2.3 Temporal Coverage and Resolution

FERC 714 data provide hourly loads by service area. These were aggregated to provide daily maximum load time series for each subregion. The climatological data comparing these are mostly daily data, although some seasonal climatic indices are also employed.

As mentioned above, the FERC load data used here are for the seven years from 1993 to 1999. While it would be nice to have a longer load data time series to work with, there are some advantages to limiting ourselves to a shorter sample like this. To use a longer series, issues like the 2000 energy crisis, as well as more dramatic changes in demography, population, and end use technologies would have to be dealt with, and the authors would also need to disentangle effects of trends in these variables from possible trend effects due to climate.

2.4 Selecting Representative Series

Because load data for some service areas was not suitable for inclusion in the subregional aggregates due to data quality concerns or missing data, these indices do not yield the total actual electrical load for each region, but rather indices which are assumed to be highly correlated with variations in both actual electrical load and electricity demand. Thus they are suitable for climatological analysis, but additional data have to be employed to scale these indices to actual regional load or demand. Henceforth, references to electricity demand refer to these maximum daily load indices derived from FERC 714 reports. For example,, 'load' and 'demand' are in some cases used interchangeably, although, strictly speaking, the authors do not have any direct data on electricity demand.

2.5 Detrending and Scaling

Because trends in both mean and variance were identified, the authors detrended the daily maximum loads by dividing by the trend, rather than subtracting the trend (Figure 2.1.2). This served to effectively detrend both mean and variance. The resulting time series were subsequently scaled by subtracting the mean and dividing by the standard deviation to generate equivalent indices for each region, since the level of the load indicated by these indices is meaningless.

CHAPTER 3:
Modeling Load Sensitivity to Temperature

Our working hypothesis is that variability in maximum daily electricity load is primarily driven by (1) variability in temperature and (2) calendar effects unrelated to climate (weekends and holidays). In the following the authors estimate models for maximum daily electricity load for each subregion as functions of these two factors.

These models are useful for motivating interest in temperature forecasts. That is, if the relationship between temperature and electrical load can be shown to be strong, then skillful forecasts of temperature may be useful for planning related to electricity generation and demand management. In subsequent sections the authors address the skill and form of potentially useful temperature forecasts.

These models are also a key ingredient for modeling the effects of climatic variations on the western energy grid. In a subsequent section the authors describe modifications to the WECC electrical grid model for a 2004 summer planning scenario to allow analyses of the effects of various scenarios for both temperature and stream flow.

3.1 Max Daily Load Versus Max Temperature

For this and other applications described in this report, a long-term daily-time-step gridded temperature data set (Hamlet and Lettenmaier 2005) is used. While only 7 years of load data were employed, using a long-term temperature data set to create four subregional daily maximum temperature indices from 1950 – 2003 facilitated production of experimental temperature forecast products and models compatible with our load-temperature model.

Daily maximum temperature indices were constructed for each subregion by taking the average of gridded daily maximum temperatures over each subregion.

3.2 Weekend/Holiday Effects

Researchers created a dummy variable for weekends versus workweek days. No attempt was made to include holiday effects. Including holidays would likely marginally improve the fit of the model.

3.3 Non-Linearity

The relationship between temperature and electrical load is not linear. That is, load tends to increase with temperature above a certain threshold (for example, loads are higher on hot days), and to decrease with temperature below a certain threshold (loads are higher cold days), and the slope is not constant. Thus, there is a need to account for nonlinearity in our model.

3.4 Non-Normality

Standard ordinary least squares (OLS) regression model methods are not appropriate here because our data are not normally distributed. In particular, the standard assumption is that the errors (residuals) in an OLS regression model are normally distributed, whereas in this case they are highly skewed (the probability distribution describing the residuals is not symmetric about the mean) and leptokutic (the peak of the distribution is more acute and tails are fatter than in a normal distribution).

3.5 Estimating Nonlinear Regression with Skewed, Leptokurtic Residuals

The open source statistical package R (http://www.r-project.org) was used to estimate a nonlinear regression model with skewed, leptokurtic residuals. The authors use semi-parametric smooth functions (piecewise polynomials) available in the base statistical module in R to determine nonlinear basis functions for temperature. Once the basis functions are determined, any linear regression routine can be used because the regression model is linear in the new expanded temperature variable.

To fit a model with skewed, leptokurtic residuals, the authors used the sn ('skew-normal') library in R. The sn library has a module st.mle() that estimates linear regressions with skew-t distributed errors using maximum likelihood methods. The skew-t distribution is a student's t-distribution that has been extended by Azzalini and Capitanio (2003) via the introduction of a shape parameter which regulates skewness.

Using just the polynomial transformation of temperature and a factor for weekend versus workweek days, the authors estimated regression models that accounted for most of the variability in maximum daily load in each subregion:

Table 3.5.1: R-Squared for Maximum Daily Load Regressed on Maximum Daily Temperature and Weekday

	NW	NC	SC	SW
R2	0.9	0.8	0.82	0.9

All of these R2 values are highly significant with p-values < 0.001

3.6 Discussion

The skew-t error model is generally a good fit to these data (Figure 3.6.3). The right tail of the observed error distribution in Northern California appears to be somewhat fatter than the modeled distribution. This is also true, to a much lesser extent, in Southern California. This is due to the larger scatter in load apparent at high temperatures in Northern and Southern California.

The authors conjecture that this may be due to effects of power transfers on reported loads in California. For example,, accounting for constraints on cheaper power available for import to

Northern and Southern California on days with observed high temperatures might improve our model specification.

Other possible improvements include accounting for separately for holidays, and weighting temperatures by population. Currently, temperature indices equally weight each grid point within a subregion. If temperatures were instead weighted by the proportion of each subregion' s population located in each grid cell, the temperature indices might yield an improved fit with observed loads. However, holidays account for relatively few days, and temperatures are highly correlated across the spatial scales represented by one subregion, so these improvements would probably be marginal, while the models shown here are highly significant predictors of maximum daily load.

Figure 3.6.1: Load-Temperature Models-Points Show Maximum Daily Load Plotted Versus Maximum Daily Temperature

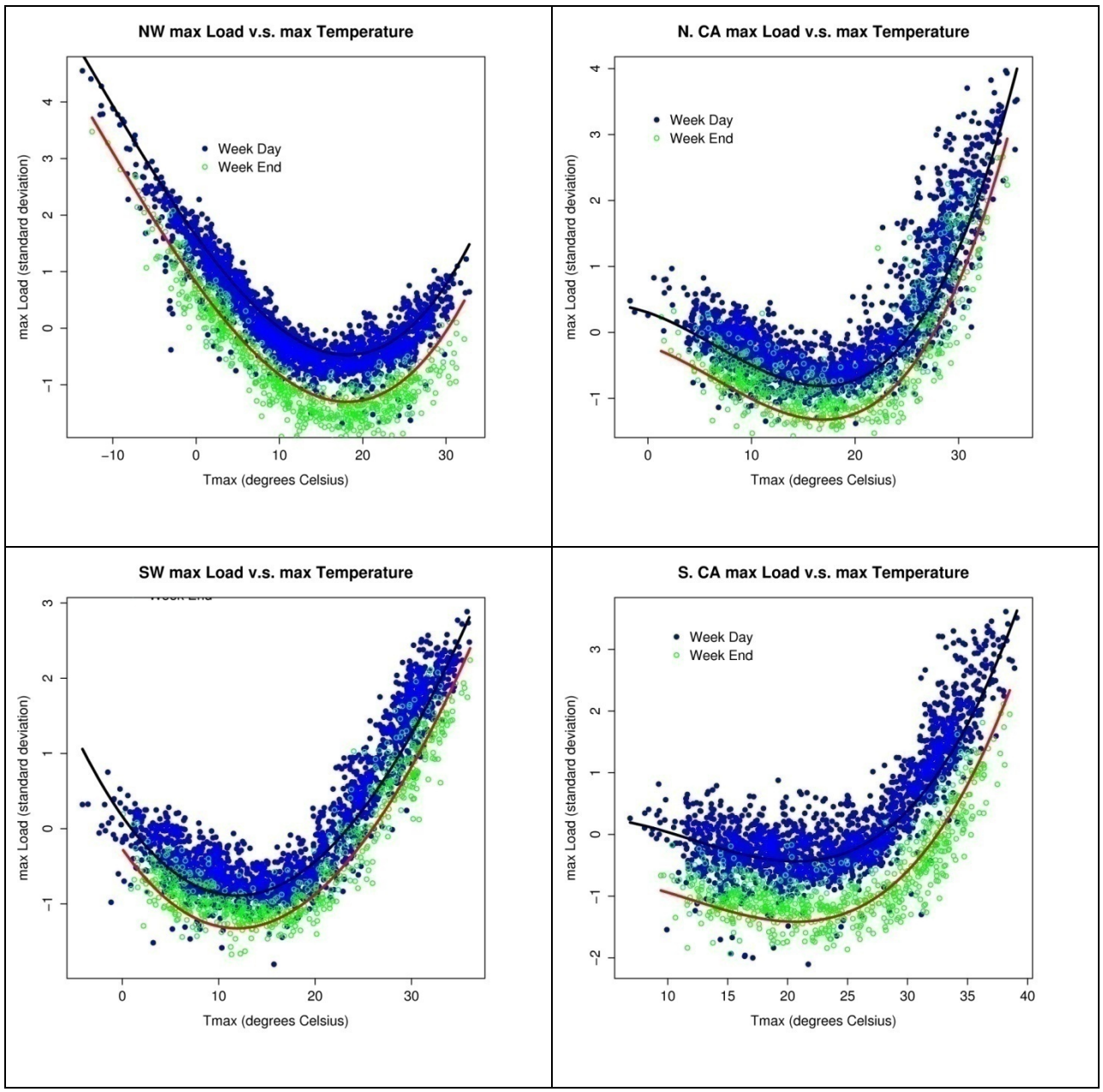

Blue are weekdays, green weekend days. Model fits are indicated with black (weekday) and red (weekend) lines.

Figure 3.6.2: Histograms of Residuals from Load-Temperature Regression Models

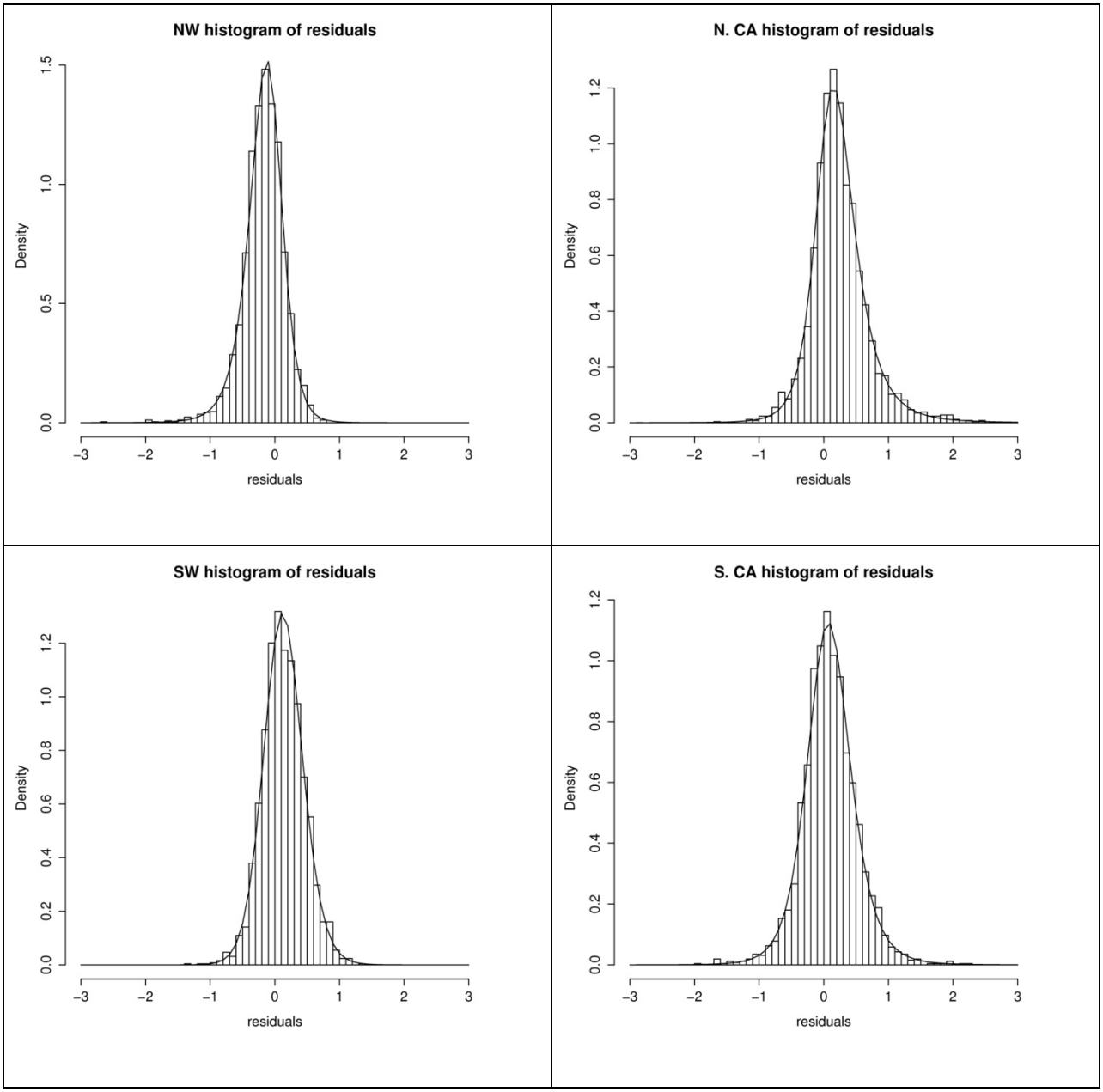

Plotted as Probability Densities

The superposed line indicates the skew-t fit to the residuals.

Figure 3.6.3: Q-Q Plots for Skew-T Regressions of Electrical Load on Temperature

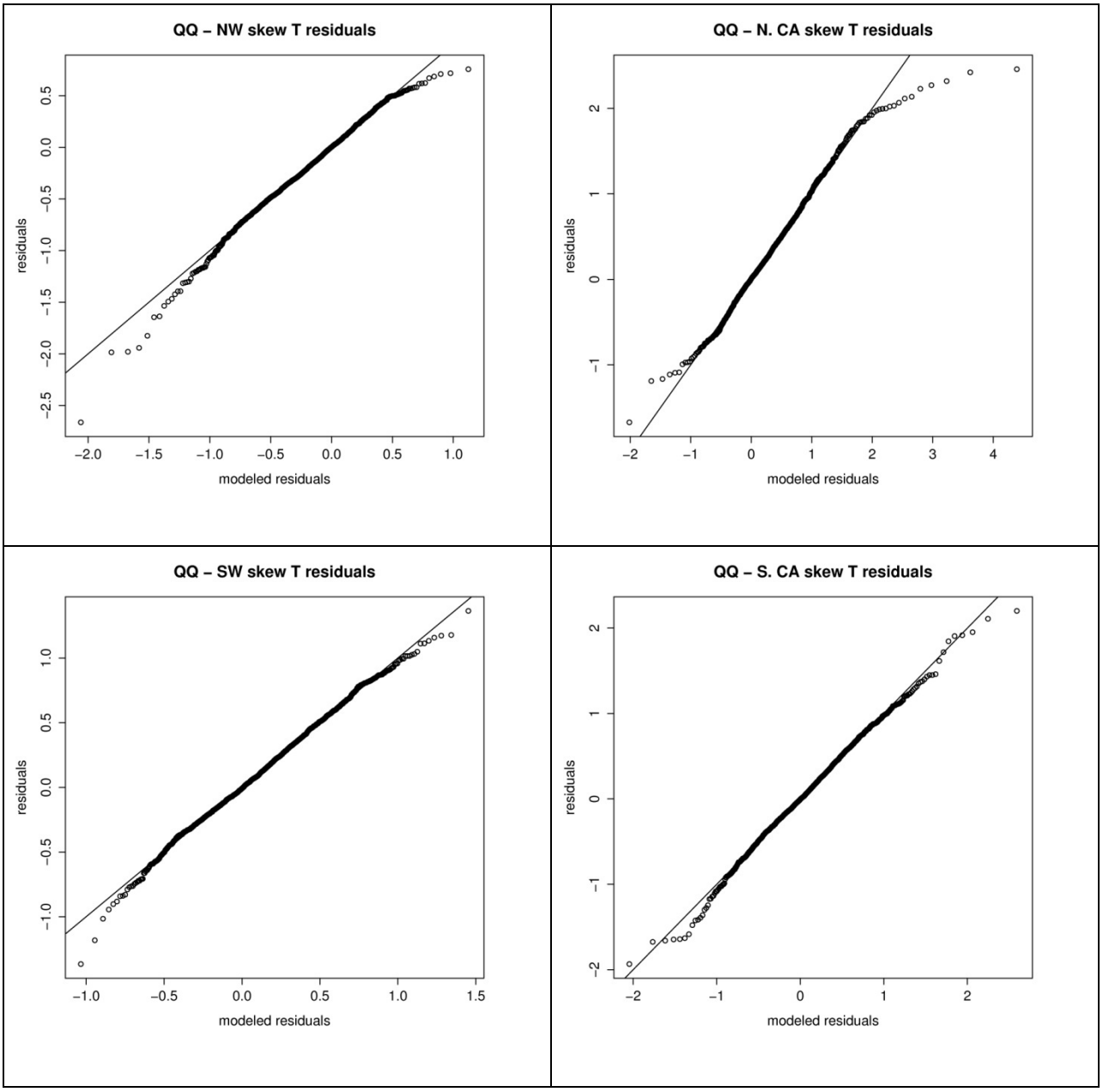

CHAPTER 4:
Forecasting Maximum Daily Temperature at Seasonal Lead Times

Recent research has made substantial progress in developing models capable of forecasting temperatures at seasonal lead times with significant skill. These forecasts have been for specified percentiles of temperature (such as mean (50th percentile), 90th percentile, maximum (100th percentile) and so forth) sampled over some historical reference period (see for example Alfaro et al 2004 and 2006). These forecasts can be spatially explicit (as in Alfaro et al) for gridded or station temperatures, or aggregated over a region.

The form of these forecasts is not well-suited to energy system planning and management applications, because they result typically in one number for an entire season. A manager planning operations for a continuously operated system with daily, hourly and shorter decision time horizons might need some method to 'downscale' a seasonal average into useful information about daily temperatures to make practical use of such a forecast, which might prove as or more challenging a task than producing the original forecast in the first place.

In this work, the authors examine the potential for fitting statistical probability models to maximum daily temperature data, and then forecasting the parameters that describe those models. If it is possible to forecast parameters describing daily maximum temperatures over a season, planners can use these forecasts to assign probabilities to any given temperature scenario of interest.

In the next sections the authors first review sources of statistical forecast skill and types of temperature forecast models. This background material was used to introduce statistical seasonal forecast, and then describe an example demonstrating a parametric approach to forecasting summer temperatures in Northern California.

4.1 Background: Sources of Statistical Forecast Skill

Statistical forecast models for temperature and other climatic variables typically rely on four sources of forecast skill: 'climatology' (descriptions of known past experience), persistence, observed Pacific sea surface temperatures, and simulated soil moistures. All four are briefly described in following sections. Researchers attempted to exploit all of these in designing this study's model specifications.

4.1.1 Climatology

A climate forecast usually provides a description of expected outcomes conditional on observations in the recent past. As an extreme case, a climatology can be thought of as a forecast of the future climate system based on all available past observations. Such a forecast might change gradually from year to year, as additional observations are incorporated into parameters like the mean and variance that describe some aspect of the climate system.

4.1.2 Persistence

A more useful forecast would be one that uses past associations between observations and subsequent outcomes. In modeling western U.S. temperatures, a climate forecast might take advantage of persistence in temperature trends; for example, warmer than average July's tend to be followed by warmer than average Augusts.

4.1.3 Pacific Sea Surface Temperatures

Pacific sea surface temperatures (SSTs) are useful for predicting temperature and precipitation in California—and more generally, in western North America—because the oceans store heat, and the pattern of surface temperature anomalies in the oceans influences subsequent weather patterns, providing some predictive skill on seasonal time scales. The El Nino/La Nina cycle (ENSO, for El Nino/Southern Oscillation) is an example of a well-known index describing patterns in the spatial distribution of SST anomalies in the Pacific that is associated with variability in climate in the western U.S. Scientists have observed that after an El Nino develops—signified by warmer than average sea surface temperatures in the eastern equatorial Pacific—above average rainfall and temperatures have often subsequently been experienced in the U.S. Southwest (Dettinger et al 1998, Gershunov et al 1999). A climate forecast might describe the likelihood of these outcomes conditional on an El Nino signal having been observed (or not) in the Pacific.

Similarly, an index of lower-frequency variability in North Pacific SSTs, sometimes called the Pacific Decadal Oscillation (PDO), is also associated with variability in precipitation and temperature in western North America. When the PDO is above its long run average, El Nino influences on climate in western North America tend to be stronger, and when the PDO is below average, La Nina influences tend to be strongest (Dettinger et al 1998, Gershunov et al 1999).

4.1.4 Soil Moisture

Soil moisture is useful as a predictor of temperature because "particularly for non-arid inland areas, a wet soil tends to depress the concurrent and subsequent monthly mean temperature, while a drier-than-normal soil is favorable for higher-than-expected monthly means…" (Durre et al 2000). Alfaro et al (2006) recently demonstrated that soil moistures are particularly useful in predicting summer temperatures in parts of Northern California and the interior western United States.

4.2 Background: Statistical Forecast Modeling Strategies

Statistical modeling methods for seasonal temperature and precipitation forecasts include composites, regressions, and models derived using Principle Components Analysis (PCA) and Canonical Correlation Analysis (CCA) (described below). The authors explored all three approaches in designing our forecast model. Composites based on SST indices did not demonstrate sufficient forecast skill. The CCA approach was productive, but required more complexity and expense, in terms of computing time, than needed for forecasting four subregional temperature indices. CCA models are best for forecasts with large numbers of predictors and predictands, as with high resolution gridded temperature forecasts. The best

approach was found to use regression models, with PCA analysis employed to summarize some of the explanatory variables.

4.2.1 Composites

A composite forecast of temperature or precipitation uses a sub-sample of outcomes, where the selection criterion is conditioned on antecedent observations. An example in Alfaro et al (2004) looks at summer temperature outcomes in California conditional on PDO being above or below normal. Typically, some aspect of the distribution of the variable of interest (such as mean, median, minimum, maximum temperature) is described statistically conditional on an index having observed values in an arbitrary range.

4.2.2 Regressions

The climatic variable of interest at a particular location can be modeled using some combination of locally observed antecedent climate variables as predictors (such as soil moisture), including leading values of the predictand (for a persistence or autoregressive model). In addition, indices of regional climatic influences such as El Nino/Southern Oscillation (ENSO) and PDO can also be included as predictors.

4.2.3 PCA and CCA

Because the climatic variables the authors wish to forecast—as well as the influences that provide forecast skill—tend to be highly correlated spatially, a useful modeling approach is to look for associations between persistent spatial patterns in the predictors and predictands. A PCA is a good way to summarize the important spatial patterns in a variable observed over many locations. It identifies a set of indices that when summed describe the variability in the data set as a whole. If each location varies independently of the others, then the analysis would produce a set of approximately equally significant indices that are equal in number to the number of locations. In practice, because of the spatial correlation for temperature and precipitation and related variables, a PCA for these typically produces just a few significant indices that together describe a majority of their variability over time. These are often associated with ENSO and PDO.

CCA provides a method for matching patterns in two data sets. It produces pairs of related indices, one from each data set, that are correlated with each other within a pair, and uncorrelated across pairs. A forecast can be constructed by first summarizing two large data sets like north Pacific SSTs and maximum summer temperatures over the western U.S. by using PCA on each data set to produce a small number of relevant indices for each, and then conducting a CCA to derive statistical relationships between the two sets of indices. Good examples of the application of this methodology to temperatures are Alfaro et al (2004 and 2006).

4.3 Background: Statistical Forecast Form

Temperature forecasts typically are for various arbitrary modes of the temperature probability distribution (for example, mean, median, 95 percentile, maximum, minimum, and so forth). These are non-parametric: the probability distribution function (PDF) is not parameterized and

estimated. The benefit of this approach is that it avoids introducing additional error from an imperfect model specification for the PDF. The drawbacks are primarily:

(1) The forecasts are not automatically probabilistic forecasts and researchers have to do some resampling of the observations, and so forth, to attempt to describe the range of likely outcomes given a particular forecast.

(2) For the part of the PDF that is of interest for a particular management application (for example, extremes), there may be insufficient data available to reliably describe the range of likely outcomes.

(3) Forecasting some arbitrary mode of the distribution is not as versatile as forecasting the entire distribution function.

Researchers tested parameterizations for temperature PDFs. For estimating maximum temperature PDFs at individual locations, skew normal specifications worked quite well. The benefit of estimating a PDF is that you then have a very powerful tool that allows you to precisely describe the probability of any outcome. The drawback of course is that if the functional form chosen for the parameterization is not a good specification for the part of the PDF that you care about for a management application, the precisely described probabilities may not be accurate. For individual locations or subregions on the scale of, say, Northern California, the work presented below indicates that the authors can specify a PDF and forecast the parameters of interest. It would also be of interest to jointly forecast the probability of extreme temperatures occurring simultaneously in different parts of the western U.S. as a whole, and that has so far proven more difficult to do accurately.

4.4 Background: Forecast Validation and Skill

Forecast models were tested using leave-one-out cross-validation. That is, for the period of record, a separate forecast model is estimated for each time step while withholding data from that time step, producing a retrospective forecast for each time step that is representative of the forecast accuracy that would pertain to an actual forecast for a future (not yet observed) time.

Forecast skill is described using both the cross-validated models' and the uncross-validated model results.

In general, it is often the case that seasonal forecasts for climatic variables like temperature and precipitation are better than climatology for high and low extreme forecasts, but not for forecasts of near-average conditions. That is because some climatic influences that are associated with the probability of extreme outcomes (such as specific combinations of ENSO and PDO phases, or very low or high soil moistures) are observable prior to the season you wish to forecast and tend to have strong persistence (depending on the season). In the absence of these influences, the historical range of outcomes can be quite broad, and highly variable.

It would appear that forecasts based on SSTs are not as good for Temperature as they are for Precipitation (see Gershunov et al 1999). SSTs seem to have the biggest influence on summer temperatures along the Pacific coast, as compared to the interior west (Alfaro et al 2004, 2006).

Within the interior west, the location where SSTs give you the most skill vary considerably for maximum versus minimum temperatures (Alfaro 2006).

ENSO/PDO have the largest, most consistent impact on precipitation in the extreme Southwest and Northwest, while the region in between is less predictable (Dettinger 1998, Gershunov et al 1999).

4.5 Parametric Probability Forecasts

Parametric probability forecasts for maximum daily temperature are well suited to planning applications for energy management. The basic approach is to fit an appropriate probability distribution to the temperature data being sought to forecast, and then to forecast the distribution parameters at seasonal lead times. Rather than yielding one statistic to describe temperature over an entire season, this approach allows planners to generate daily maximum temperature samples for a coming season stochastically, and to assign probabilities to planning scenarios of interest.

Like a climatology, the forecast distribution reflects our knowledge about the statistical properties of temperatures observed in past seasons, while also incorporating a forecast reflecting available knowledge regarding expected interannual variability in climate (for example, a forecast based on persistence, sea surface temperatures, and soil moisture). The form of the forecast is also well suited to applications where knowledge of critical planning thresholds may be proprietary, since in many cases it does not require end users to specify *a priori* the temperature threshold of interest.

4.6 Example: Northern California Summer Temperature

Northern California summer (June – July – August) daily maximum temperature is well-approximated by a skew-normal probability distribution. 1950 summer temperatures for Northern California, an arbitrarily selected example, demonstrate the point (Figures 4.6.1 through-4.6.3).

Figure 4.6.1: Example Skew-Normal Fit for 1950 June, July, August
Daily Maximum Temperature for Northern California

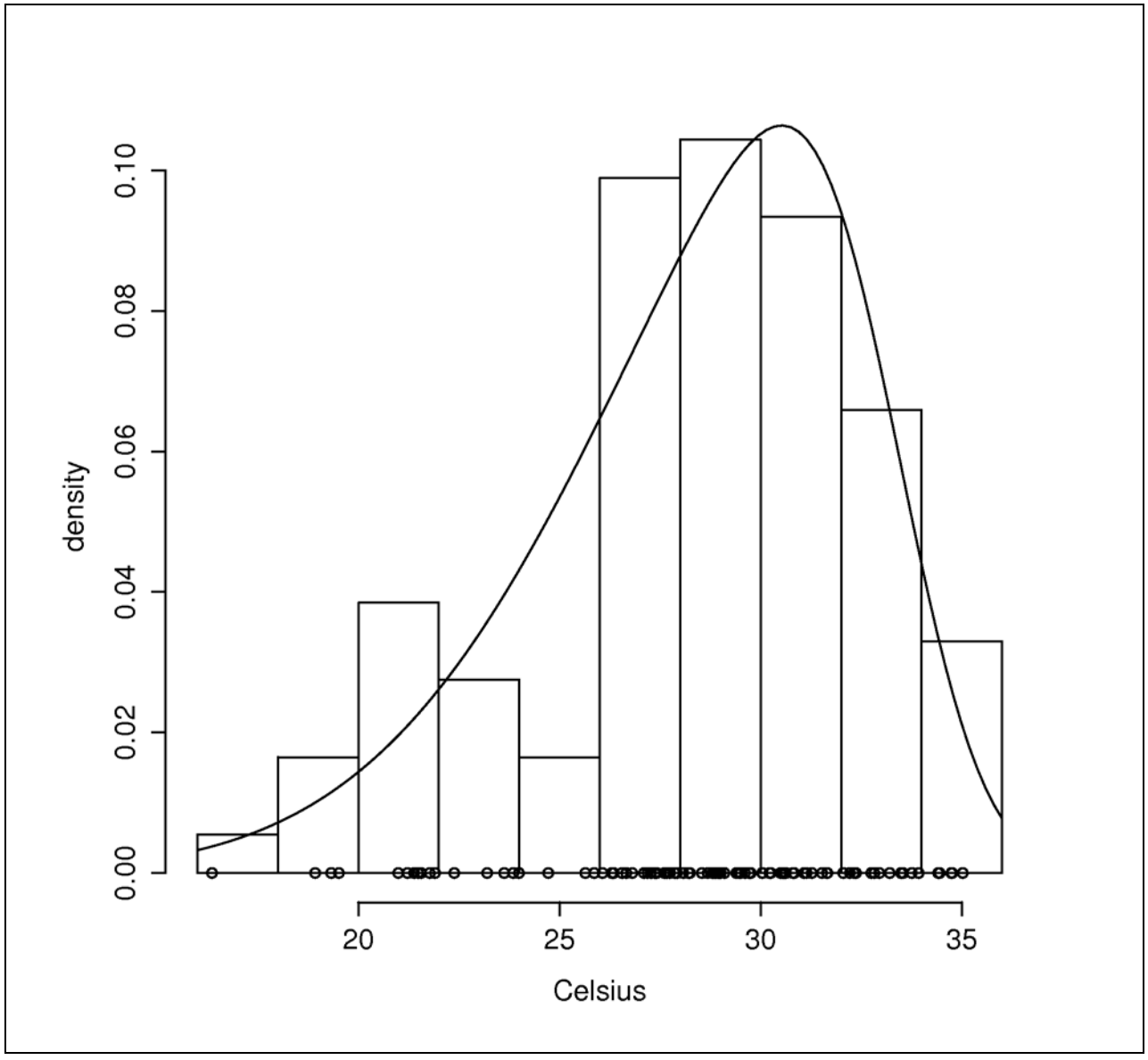

Figure 4.6.2: Q-Q Plots for Normal (Left) and Skew-Normal (Right) Fits to 1950 June, July, August Daily Maximum Temperature for Northern California

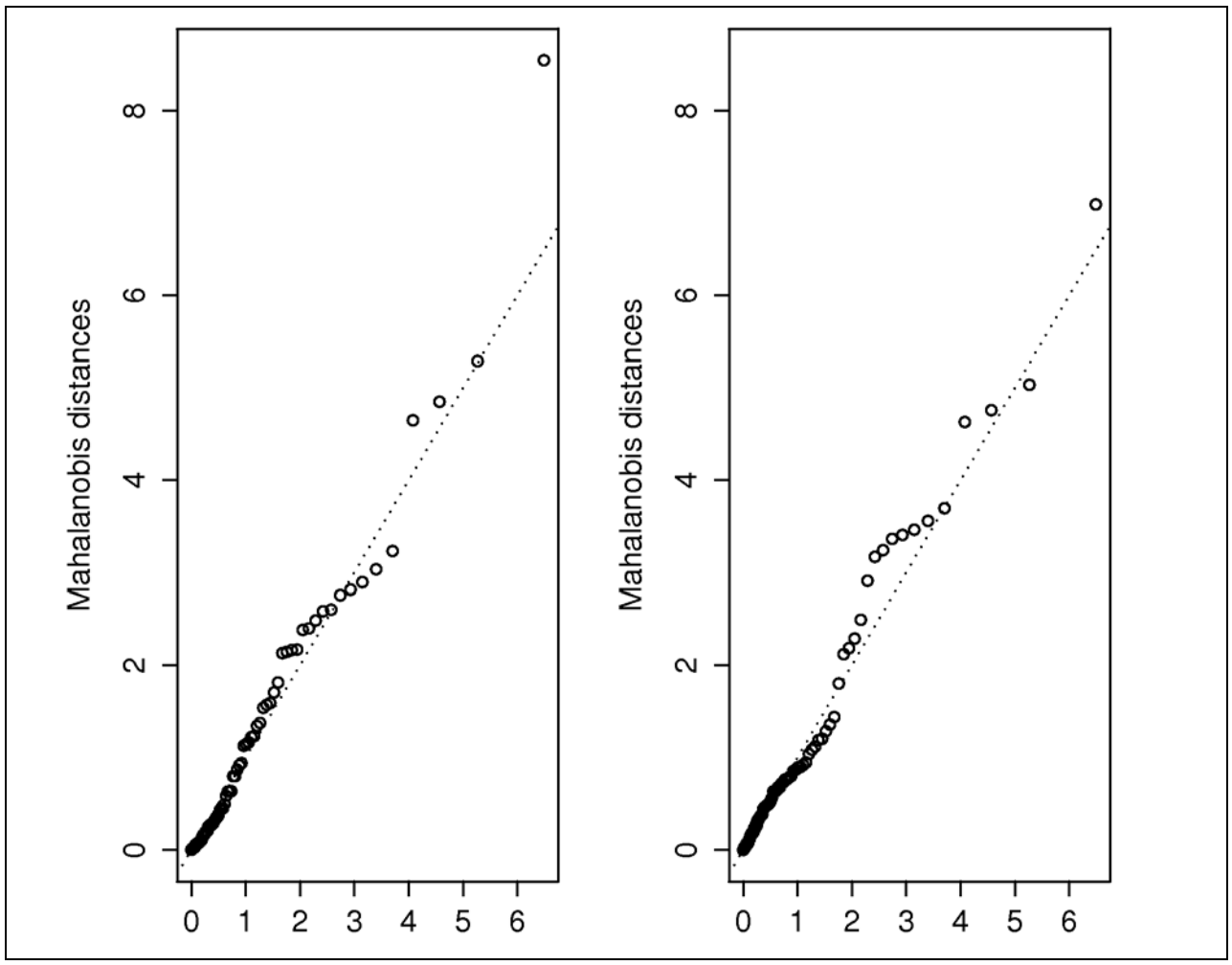

A skew-Normal distribution provides a better fit to the tails of the observed distribution than does a Normal distribution.

Figure 4.6.3: PP Plots for Normal (Left) and Skew-Normal (Right) Fits to 1950 Jun, July, August Daily Maximum Temperature for Northern California

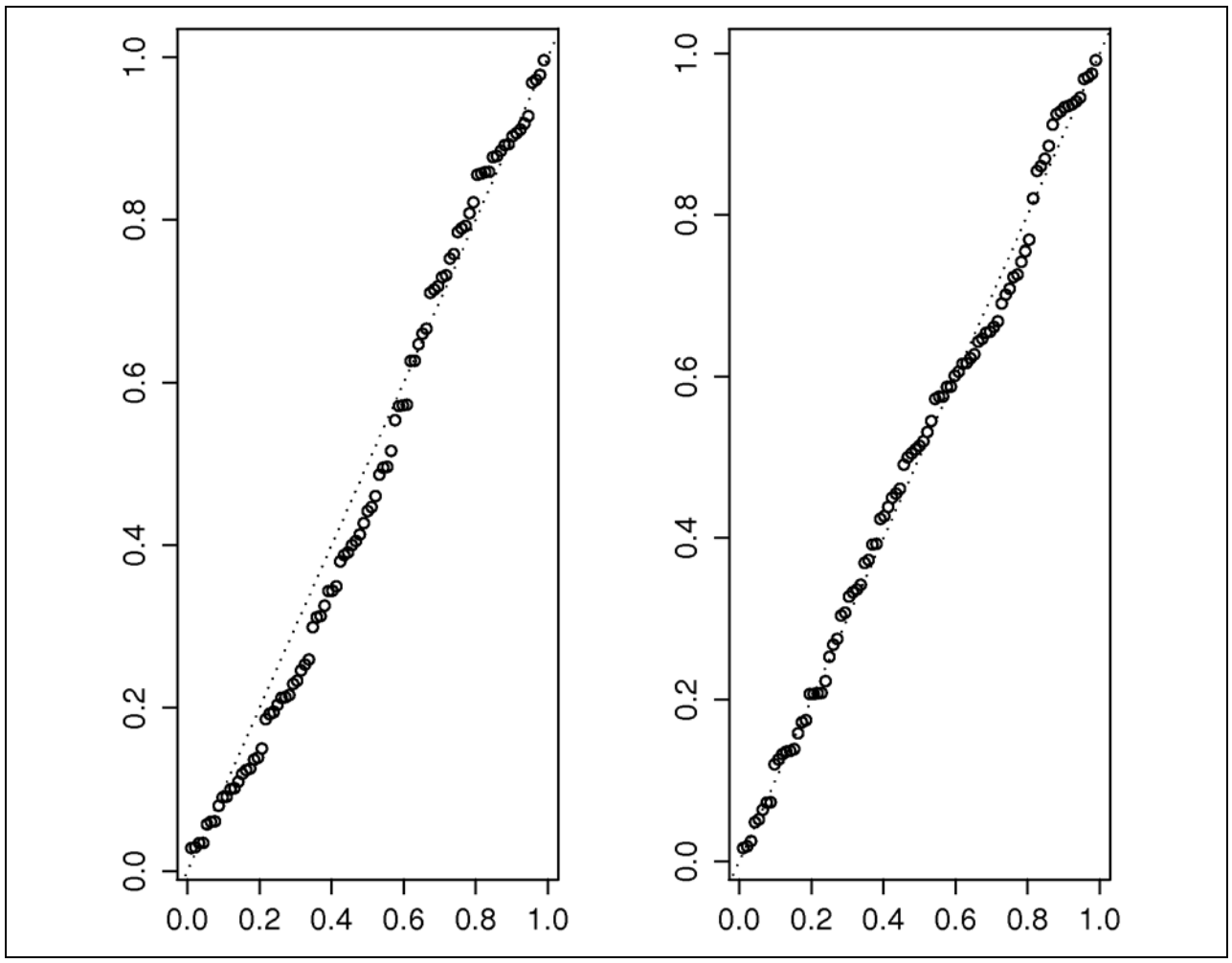

A skew-Normal distribution provides a better fit to the observed distribution than does a Normal distribution.

4.7 Skew-Normal Parameter Estimation and Forecasting

4.7.1 Data and Methods

A skew-normal distribution was fit to summer daily maximum temperatures in Northern California (from section two above) for each year in 1950 – 2003 using the sn.em() module in the sn library of the open-source R statistical project (accessed from the web via http://www.r-project.org. See Azzalini 1985 and Azzalini and Capitiano 1999). Distribution parameters controlling location, scale and shape (mean, standard deviation and skewness) were saved for each year, and forecast model specifications were then tested for the resulting time series of parameters.

Three sets of explanatory variables were tested. First, mean variance and skewness were calculated for May temperatures, to provide a means of testing persistence-based forecast model specifications.

A second set of explanatory variables consisted of North Pacific sea surface temperature indices for months prior to the summer being forecast, including the Nino 3.5 (N35) index and the Pacific Decadal Oscillation (PDO) index. Historical values of the indices were obtained from the National Oceanic and Atmospheric Administration (NOAA) Climate Prediction Center (information was accessed online at http:// www.cpc.ncep.noaa.gov/data/indices/).

A third set of explanatory variables tested consisted of cumulative moisture deficit for the water year through the end of April (for example, October – April) calculated on a 1/8 degree grid over the western U.S. using the VIC hydrologic model (Liang et al 1994) and the Penman-Montieth equation (Penman 1948 and Montieth 1965). Moisture deficit—the difference between potential and actual evapotranspiration—is a useful indicator of drought conditions. Annual regional drought indices were constructed from gridded cumulative moisture deficit time series using principle components. The authors used the prcomp() module in R to estimate the first five principle components for cumulative western U.S. moisture deficit.

Separate forecast models were estimated for location, scale and shape using ordinary linear regression functions in the R statistical package.

4.7.2 Results

Surprisingly, the persistence terms were not significant predictors for any of the parameters. The best model fit for the location parameter consisted of the first principle component of cumulative moisture deficit and an interaction term between May Nino 3.5 and average Dec-Feb PDO. The best fit was nonlinear in Nino 3.5, so the authors used a semi-parametric smooth function (a B-spline basis, degree 3) calculated with the bs() module in the splines library in R to transform the variable N35. The adjusted R-squared for this model was 0.42 and the cross-validated R-squared was 0.37. See Figure 4.7.1 for a graphical representation of both the regular and cross-validated regression models for the location parameter.

The authors did not identify any significant predictors for the scale parameter, so climatology was simply used. That is, the average scale parameter for the model estimation period was used as the best predictor of the scale parameter.

For the shape parameter, the best forecast model used the first and fifth principle components of the cumulative moisture deficit. The relationship between shape and the first principle component of moisture deficit was nonlinear, and the authors again used a semi-parametric smooth function (B-spline basis degree 2) to transform moisture deficit. Adjusted R-squared was 0.25 and the cross-validated R-squared was 0.19. The fit for the shape parameter (Figure 4.7.2) indicates that moisture deficit allows us to differentiate between high- and low- skew seasons, but not within those coarse categories.

For both location and shape, the models fit appeared to be robust in the sense that leave-one-out cross-validation did not appear to greatly change the estimated model parameters (Figures 4.7.1 through4.7.2).

4.7.3 Applications

With the forecast parameters, it is possible to describe a forecast distribution of maximum daily temperature. Figures 4.7.3 through 4.7.4 show two arbitrarily selected examples: 1955, a year with a highly skewed temperature distribution, and 2003, a year with a less skewed temperature distribution. Repeated random draws from these distributions can be used to generate temperature samples for scenario analysis.

These distributions can also be used to generate a time series of probabilities of exceeding a temperature threshold of interest. For example, the authors calculated the probability per day of exceeding an arbitrary temperature threshold in Northern California (32 degrees Celsius) for each summer from 1950 to 2003 and compared it to the observed frequency of temperature extremes (Figure 4.7.5). The R-squared and cross-validated R-squared for this time series were 0.36 and 0.32. Observed, estimated, forecast, and cross-validated forecast probabilities were all highly correlated (Table 3.7.1).

Table 4.7.1: Correlation Matrix for Probability Daily Max Temperatures Exceed 32 Degrees Celsius

	Observed	Estimated	Forecasted	CV-Forecasted
Observed	1.00	0.95	0.6	0.56
Estimated	0.95	1.00	0.67	0.64
Forecasted	0.6	0.67	1.00	1.00
CV-Fcasted	0.56	0.64	1.00	1.00

P-values all less than 0.001

Observed probabilities, probabilities estimated from skew-normal fits, probabilities estimated from forecast skew-normal fits, and probabilities estimated from cross-validated forecasted skew-normal fits

4.7.4 Discussion

This forecast method demonstrates a framework for estimating a forecast model that can be used by managers to build planning scenarios and assign probabilities to outcomes. Combined with the models demonstrated in Section 4.2 above, these scenarios can be translated into predicted electrical loads. As will be discussed in the sections below, these tools can be combined with generation and transmission models to test system robustness in extreme scenarios.

Furthermore, these forecast models can be estimated from publicly available temperature data without prior knowledge of critical management thresholds, and then customized by end users to fit their planning needs.

Figure 4.7.1: Observed Versus Forecast Location Parameter for Northern California Summer Daily Maximum Temperature

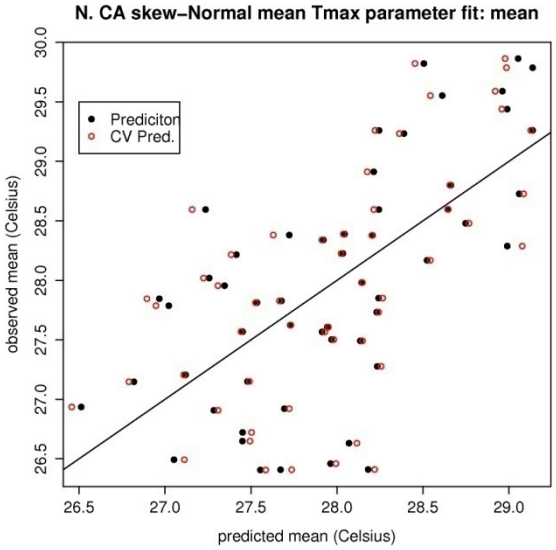

Figure 4.7.2: Observed Versus Forecast Shape Parameter for Northern California Summer Daily Maximum Temperature

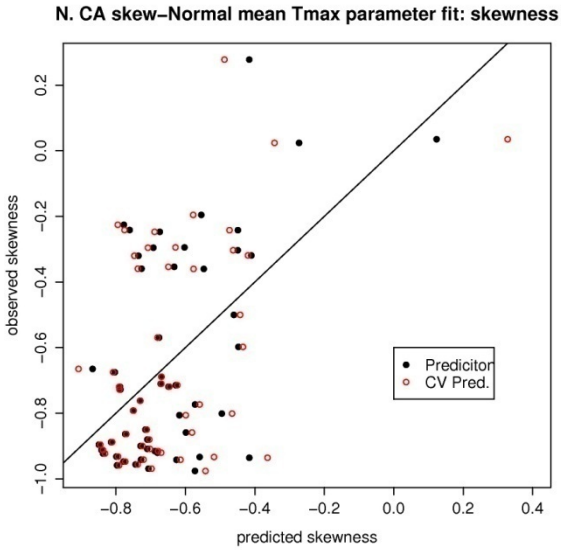

Figure 4.7.3: 1955 Summer Maximum Daily Temperatures and Estimated (Black) and Forecast (Green) Skew-Normal Distribution

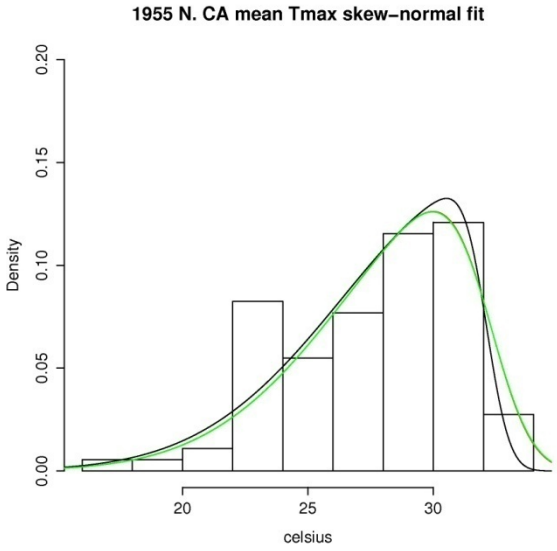

Figure 4.7.4: 2003 Summer Maximum Daily Temperatures and Estimated (Black) and Forecast (Green) Skew-Normal Distribution

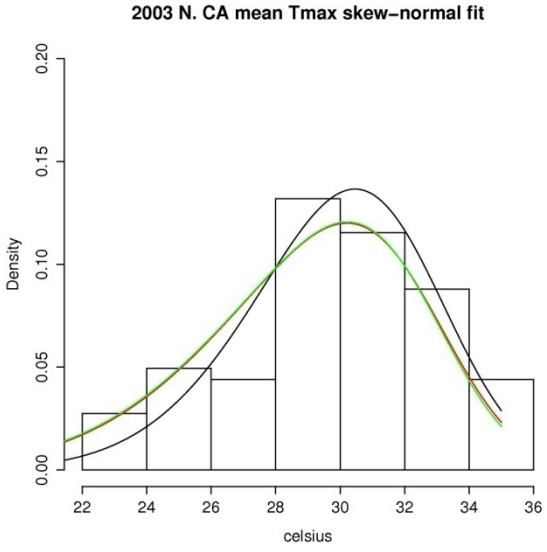

Figure 4.7.5: Forecast and Cross-Validated Forecast Probability of Exceeding 32 Degrees Celsius Maximum Daily Temperature

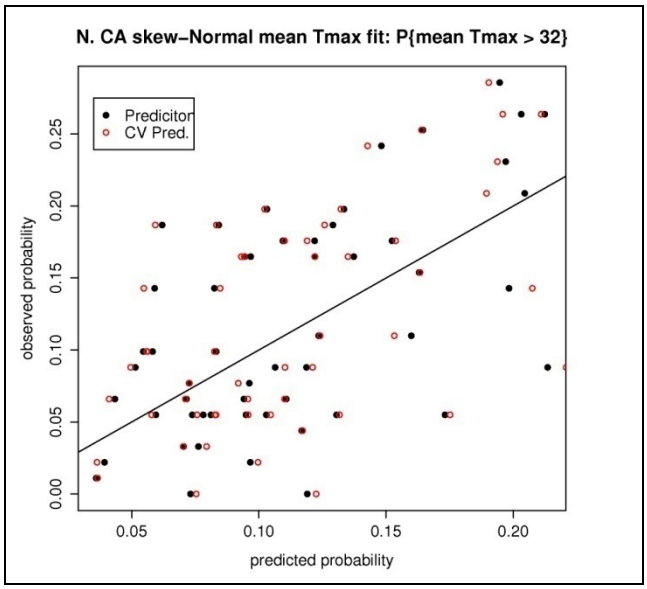

Averaged over Northern California) versus observed probability of exceeding 32 degrees Celsius, 1950 – 2003.

CHAPTER 5:
Modeling System Response to Temperature Driven Load with Constrained Hydropower

5.1 WECC Model

Project researchers use the WECC model to describe the impact of variability in temperature and in hydroelectric capacity (for example, the amount and timing of stream flow) on the types, amounts, and locations of power generation across the WECC region subject to generation and transmission capacity constraints.

The WECC model is a set of seasonal planning cases based on non-coincident peak electrical loads. So, for example, the 2004 summer case might incorporate a peak load for the Bonneville Power Administration's service area, and a peak load for El Paso Electric, but these peak loads might actually occur at very different times, or could even be negatively correlated.

Researchers adapted the WECC model to create a 24-hour model with coincident peaks. To do this, researchers created load profiles for each season for each utility's service area based hourly loads reported in FERC Form no. 714 for average weekend and weekday days. The peak weekday load for each utility in each seasonal planning case is matched to the peak in its hourly weekday load profile to create a 24-hour load model. Weekend loads are scaled relative to peak weekday loads; that is, based on the historical reports, weekend loads are assumed to be less than weekday loads.

To link the WECC model to temperature inputs, researchers derived weekday and weekend temperature sensitivity curves for maximum daily loads aggregated by subregion. They then used four subregions: the Northwest, Northern California, Southern California, and the Southwest/Interior West. It was necessary to aggregate loads across utilities, because loads reported by one utility in one year's FERC 714 reporting can, and often are, shifted to another nearby utility's report in one or more subsequent years. Each node in the WECC model is now associated with a maximum-load versus temperature relationship estimated from historical FERC 714 reported data and daily maximum temperatures averaged over the region. By inputting a temperature and weekday versus weekend, researchers can generate solutions that describe the sourcing and quantity of power generated and transmitted across the WECC region.

The WECC model represents internally the generating capacity of every power plant on the western grid and the transmission capacity throughout the grid, and can optimize the sourcing of electrical production to meet changes in load or in specified generating capacity subject to generating and transmission capacity constraints. While the transmission capacities are enumerated, information describing generating costs for each plant as a function of the quantity of generated power is proprietary. In order to use the WECC model to optimize generating solutions across the grid in response to changes in temperature or in generating capacity (for example, changes in potential hydropower generation), researchers ran the model in two

modes. In the first, researchers used generic cost curves for different types of generation (hydro, thermal, and so forth) that do not reflect idiosyncratic differences in power generation efficiency across plants within a type. In the second mode, researchers did not use economic criteria to assign generation to different nodes, but instead looked at demand within large geographic areas and assigned production arbitrarily according to the generation capacity and transmission constraints embodied in a WECC 2004 summer planning case.

The result of these adaptations is that researchers can model demand conditioned on variability in maximum temperature; researchers can model the amount, type and location of power generation to meet that demand using existing infrastructure; and observe when and where transmission constraints are binding on model solutions. This model as reconfigured is able to investigate economic tradeoffs between power generation sources in response to variations in temperature across subregions. So, for example, researchers could describe how the system responds to a case where Southern California experienced a heat wave and Northwest hydroelectric generating capacity was reduced due to drought. Greater specificity—for example, in accurately reflecting the generating costs of individual plants, or in relating temperature to demand aggregated over smaller subregions—would require utilities to use their own proprietary data. New data could be easily incorporated into this framework.

5.2 A Northwest Integrated Example: Meeting Summer Electricity Demand with Constrained Hydropower Resources

Researchers ran three test scenarios reducing Northwest hydropower production (at Grand Coulee) by 10 percent, 20 percent and 30 percent on a peak summer day hour (using a 2005 summer planning scenario) (Figure 5.2.1). Reduced hydropower generation was made up by thermal (coal) production at PGE plants. The cost curves used to value the change in generation type (Figure 5.2.2) were not specific to these plants. The result was a substantial net increase in hourly generating costs (Table 5.2.1).

Figure 5.2.1: Reduced Summer Hydropower Generation Test Scenario

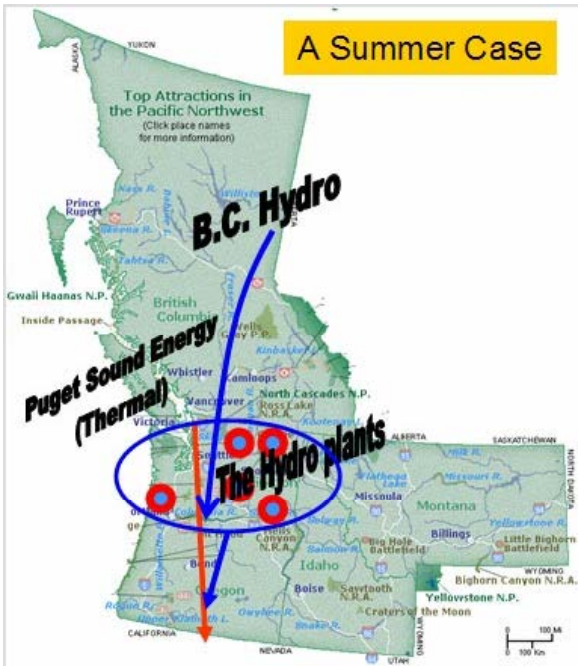

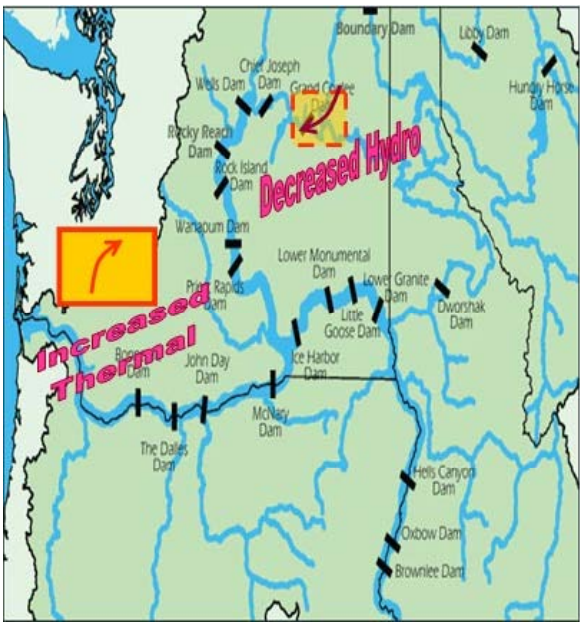

Figure 5.2.2: Generic Cost Curves in Test Scenario (Reduced Summer Hydropower)

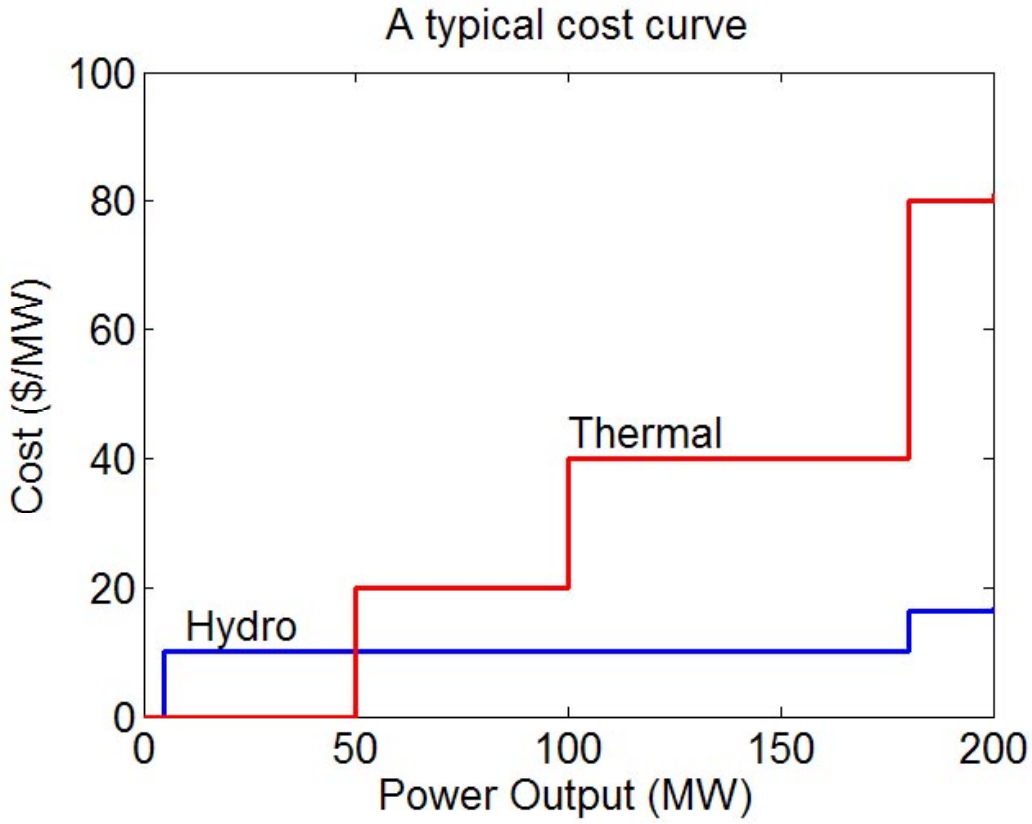

Table 5.2.1: Scenarios: Reduction in NW Hydropower Generation by 10, 20 and 30 Percent are Met by Increased Thermal Generation at PGE at an Increased Net Cost

Scenario	Hydro (Coulee)	Thermal (PGE)	Net Gain/Loss
Base	1800 MW	1443 MW	Na
- 10%	1620 MW	1614 MW	-$5,198
- 20%	1440 MW	1794 MW	-$13,670
- 30%	1260 MW	1974 MW	-$32,316

5.3 Test Application: Summer Weekday Peak Load Increase

This is an example of output from a test run of the PSLF software for the WECC model. We applied a large exogenous increase in load (75 percent) for the BPA service area to test the ability of the model to converge given a large increase in load. The increased load was allocated across a set of generation nodes, and increased generation costs were estimated using a typical peak load cost curve for thermal generators.

Example Output:

Step 1: When running a base operating case of a peak day in summer (2005), if the load is increased by a certain percentage because of the temperature change, as seen below, the resulting calculation will yield a total load increase of 433.66 MW.

---Starting compiling [load_chg.p] at Thu Jan 19 14:23:26 2006

== Starting load_chg.p ==

Note - PF case will not be updated

Note - Q change is based on Q

Note - Applying to area 40

Note - Using include owner list

dbg 105 - Including owner 29

== Change load level for case 05hs2a_test4.sav =

New total load for included owners is P: 2640.66/ Q: 1065.47

Old total load for included owners is P: 1588.96/ Q: 631.81

Difference is P: 1051.70/ Q: 433.66

== Finished load_chg.p - Changed 135 loads ==

Step 2: Researchers then adjust the generator output to pick up the load increases.

----Starting compiling [adjust_gen.p] at Thu Jan 19 14:23:37 2006

== Modify generation of the generators ==

--The generator is at Bus 246; it is owned by Owner: 76.

--The generator is at Bus 323; it is owned by Owner: 76.

--The generator is at Bus 482; it is owned by Owner: 76.

--The generator is at Bus 695; it is owned by Owner: 76.

--The generator is at Bus 873; it is owned by Owner: 76.

--The generator is at Bus 899; it is owned by Owner: 76.

--The generator is at Bus 989; it is owned by Owner: 76.

--The generator is at Bus 993; it is owned by Owner: 76.

--The generator is at Bus 994; it is owned by Owner: 76.

--The generator is at Bus 1064; it is owned by Owner: 76.

--The generator is at Bus 1068; it is owned by Owner: 76.

--The generator is at Bus 1109; it is owned by Owner: 76.

--The generator is at Bus 1658; it is owned by Owner: 80.

--The generator is at Bus 1659; it is owned by Owner: 80.

--The generator is at Bus 2028; it is owned by Owner: 10.

--The generator is at Bus 2296; it is owned by Owner: 10.

--The generator is at Bus 2297; it is owned by Owner: 10.

--The generator is at Bus 2298; it is owned by Owner: 10.

--The generator is at Bus 2299; it is owned by Owner: 10.

--The generator is at Bus 2300; it is owned by Owner: 10.

--The generator is at Bus 2301; it is owned by Owner: 10.

--The generator is at Bus 2302; it is owned by Owner: 10.

--The generator is at Bus 2371; it is owned by Owner: 10.

--The generator is at Bus 2372; it is owned by Owner: 10.

--The generator is at Bus 2373; it is owned by Owner: 10.

--The generator is at Bus 2374; it is owned by Owner: 10.

--The generator is at Bus 2499; it is owned by Owner: 10.

--The generator is at Bus 2500; it is owned by Owner: 10.

--The generator is at Bus 2501; it is owned by Owner: 10.

Note:Researchers have three tiers when choosing the generators to pick up the additional loads. In this case, the first tier generators can meet the needs.

--The current mismatch is: -8.3 (at a cost of $50 /MWH)

--The current mismatch is: -8.3 (at a cost of $60 /MWH)

--The current mismatch is: -8.3 (at a cost of $70 /MWH)

Step 3: Researchers then run the power flow to see if it converges.

If it converges, then it means the physical constraints such as the transmission line limitations have been met. If it does not converge, then generator outputs have to be manually adjusted. Binding transmission constraints can prevent convergence.

5.4 Test Application: Winter Weekday 24-Hour Load

This application tests the extension of the model from estimating non-coincident peak loads to estimating 24-hour loads, without any change in temperature or generating capacity. Using load profiles described above, researchers convert the winter 2004 peak planning case to a 24-hour case (Figure 5.4.1).

To plot the daily load by service area, researchers place specific areas on a grid (Figure 5.4.2). Figures 5.4.3 and 5.4.4 show the daily real and reactive load as a three-dimensional plot over this grid.

This case and the previous two Test Applications demonstrate our ability to use a reconfigured WECC model to analyze the impact of changes in temperature and hydropower generating capacity on the western electrical grid.

Figure 5.4.1: The Load Profiles of Each Region for the Base Case (2004 Low Winter)

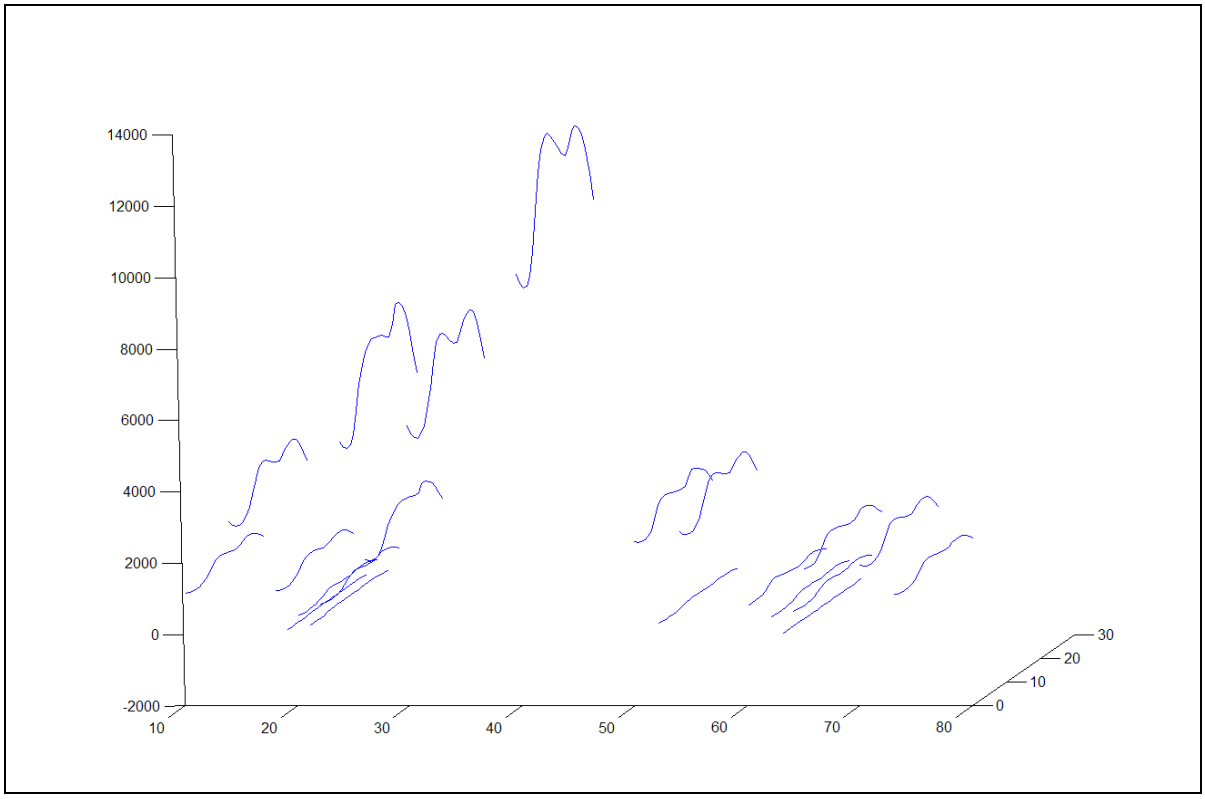

Figure 5.4.2: Gridded Representation of WECC Service Areas

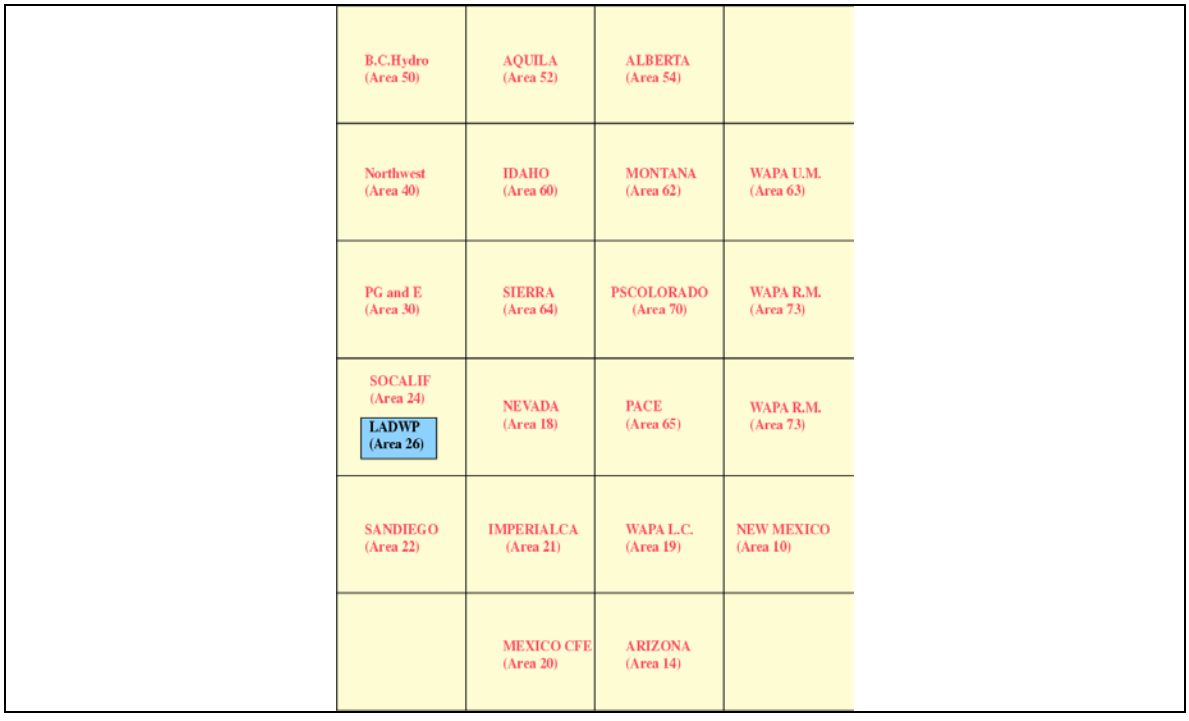

Figure 5.4.3: Real Power, 2004 Winter – Base Case Weekday Load from Hour 1 to Hour 24 for the 2004 Low Winter Planning Case

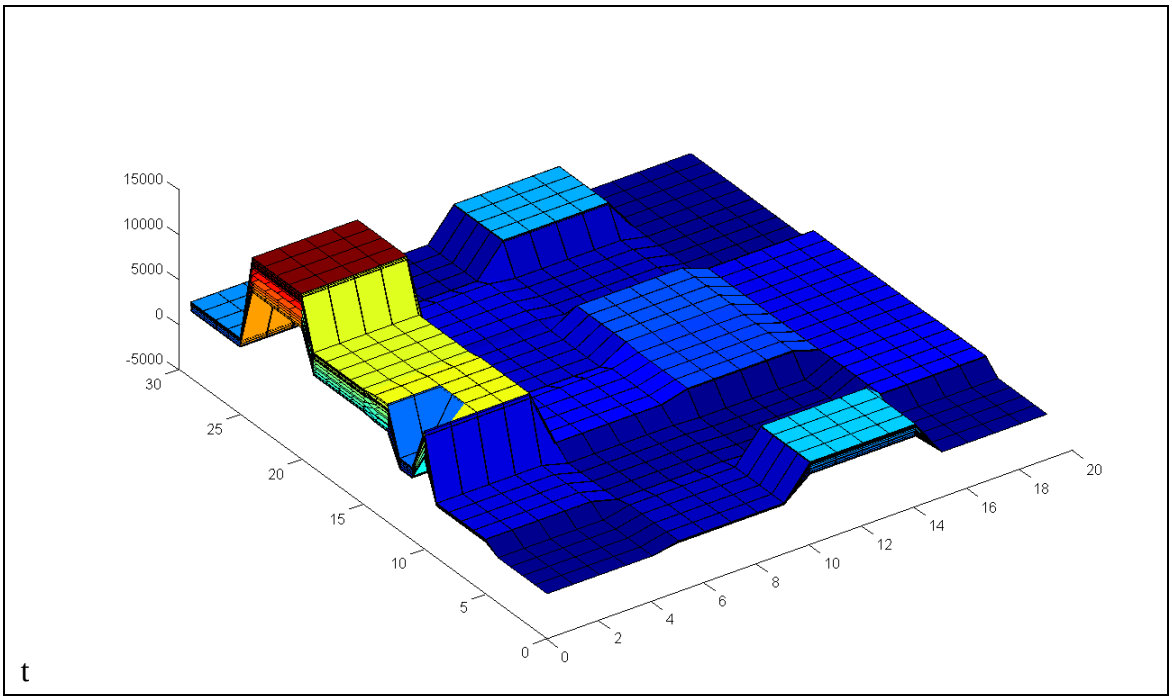

Figure 5.4.4: Reactive Power, 2004 Winter, Base Case Weekday Load from Hour 1 to Hour 24 for the 2004 Low Winter Planning Case

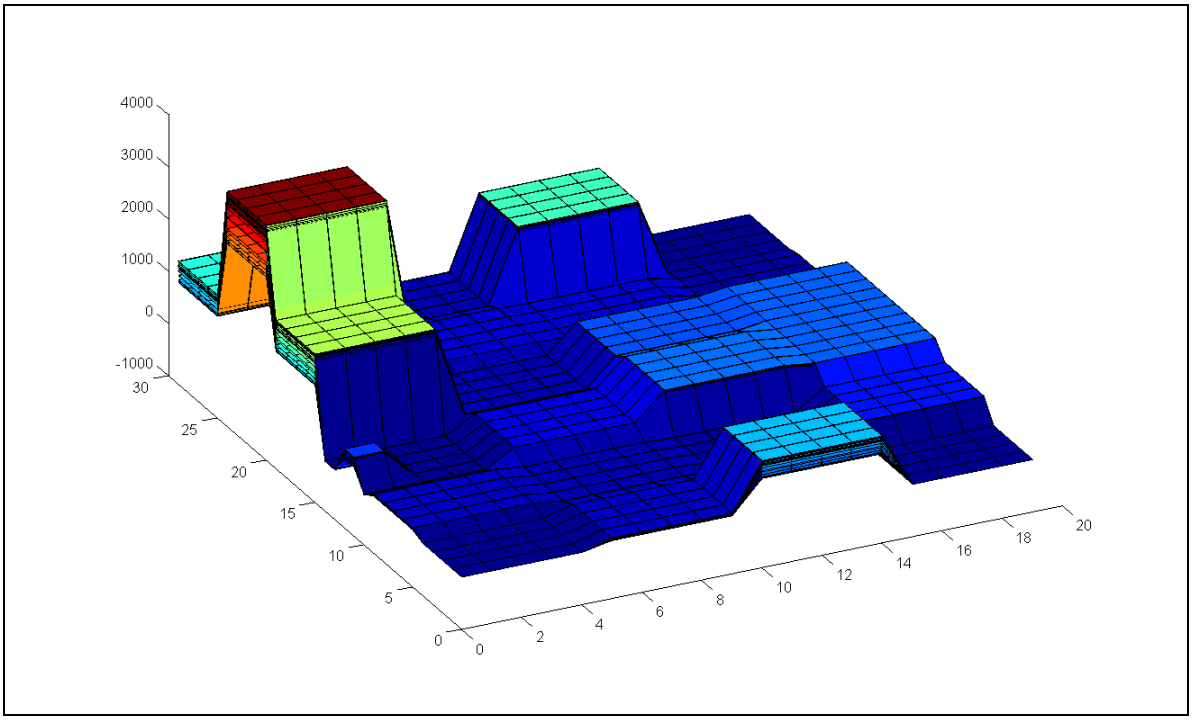

5.5 Adapting a Summer 2004 Planning Scenario

Load profiles were generated for weekdays and weekends for Winter (Dec-Feb), Spring (Mar-May), Summer (Jun-Aug), and Autumn (Sep-Nov) for each utility using FERC 714 hourly data for 1993-1999 (see Figures 5.5.1 through 5.5.123.

Peak loads in the 2004 summer planning case were assumed to occur on the day in 2004 with the highest daily maximum temperature, and to coincide with the peak hourly load for the weekday load profiles for service areas in that region.

Peak loads from the 2004 summer planning scenario and 2004 maximum daily temperatures were used to calibrate our load-temperature models from Section 5.2.. That is, the estimated relationships in Figure 5.2.1 were rescaled to match the loads reported in the 2004 planning scenario. Load profiles were used to estimate coincident loads based on the planning scenarios' non-coincident peaks.

Maximum daily loads by subregion were estimated for a range of regional temperature scenarios using the rescaled load-temperature model described above. The WECC model was used to allocate these loads to electrical generation nodes on the western regional grid. Since researchers assumed a common cost curve for thermal generation across nodes, the loads and generation vary by region, but do not vary meaningfully within regions that have the same temperature inputs to the model (for example, Northwest, Southwest, Northern CA, Southern CA). In this example (Figure 5.5.1), researchers compare a scenario where temperatures are at the 90th percentile across all four regions versus a scenario where temperatures are at the 100th percentile across all four regions. The additional demand in Southern California is met by increased production in the Northwest and Southwest.

These tools can be used with temperatures generated from conditional distributions to create probabilistic temperature-driven planning scenarios.

Figure 5.5 1: Use of the Modified WECC Model to Estimate Surplus Generation by Service Area (Represented by the Bubbles)

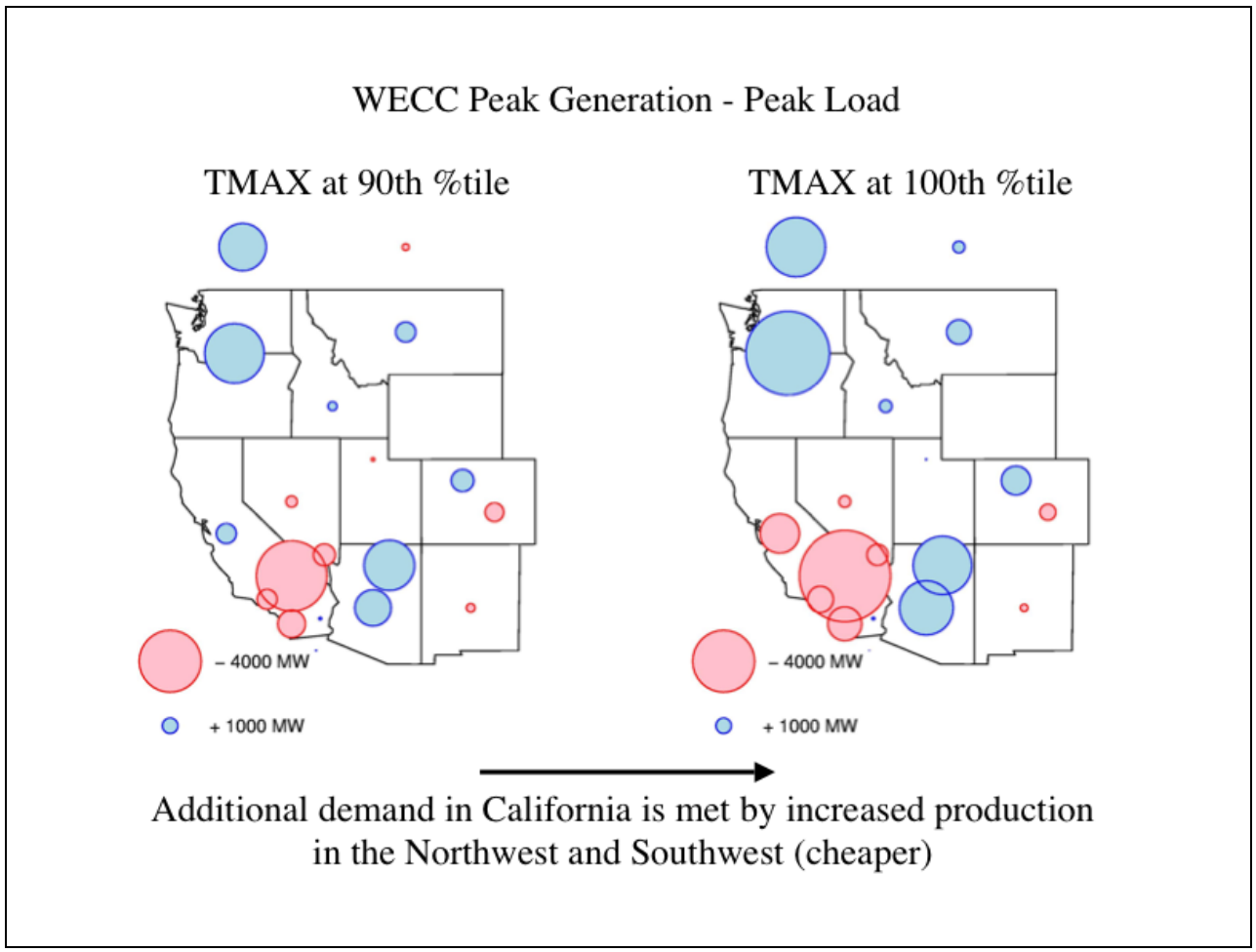

Left side all four western regions' TMAX at the 90th percentile versus all four regions' TMAX at the 100th percentile. Increased temperature increases demand everywhere, but especially in California and the Southwest. As demand increases, exports of power from the Northwest and Southwest to northern and southern CA increase. The price per kw/hour for peak power increases as well.

Figure 5.5.2: Northwest Hourly Load Profiles by Season, Weekday/Weekend, for BCHA, BPA, CHPD, DOPD

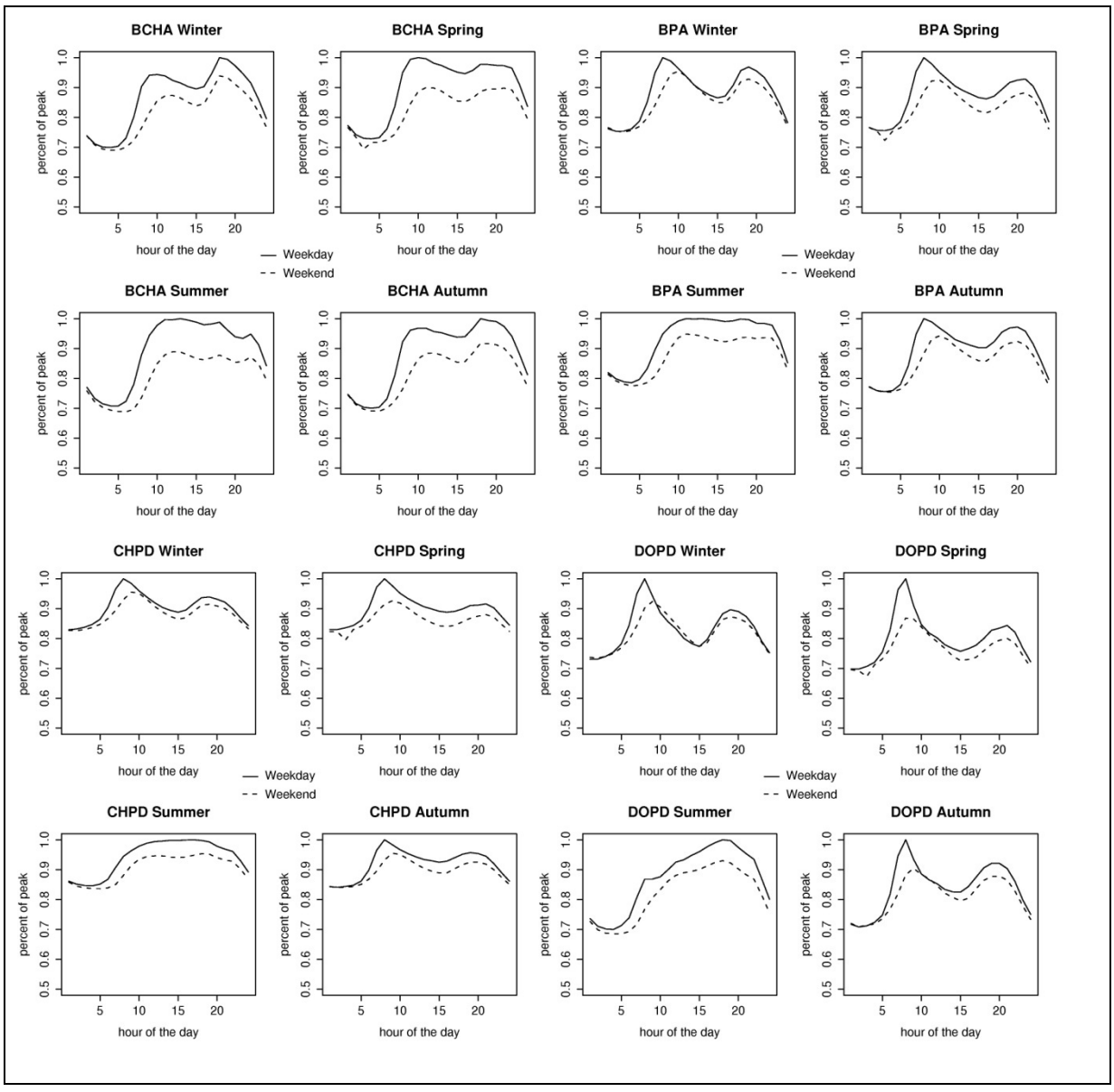

Figure 5.5.3: Northwest Hourly Load Profiles by Season, Weekday/Weekend, for EWEB, GCPD, IPC, PAC

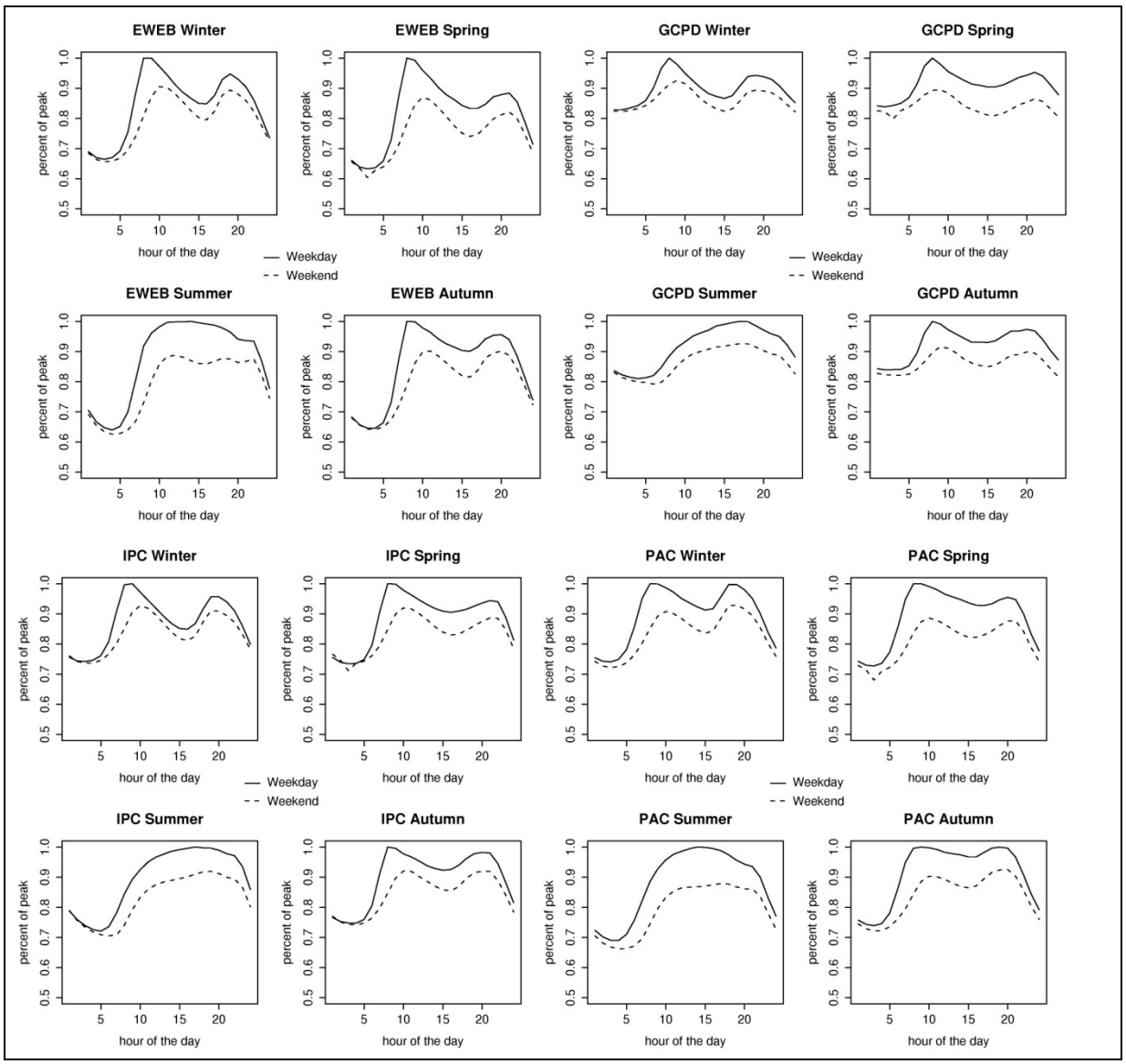

Figure 5.5.4: Northwest Hourly Load Profiles by Season, Weekday/Weekend, for PGE, SCL

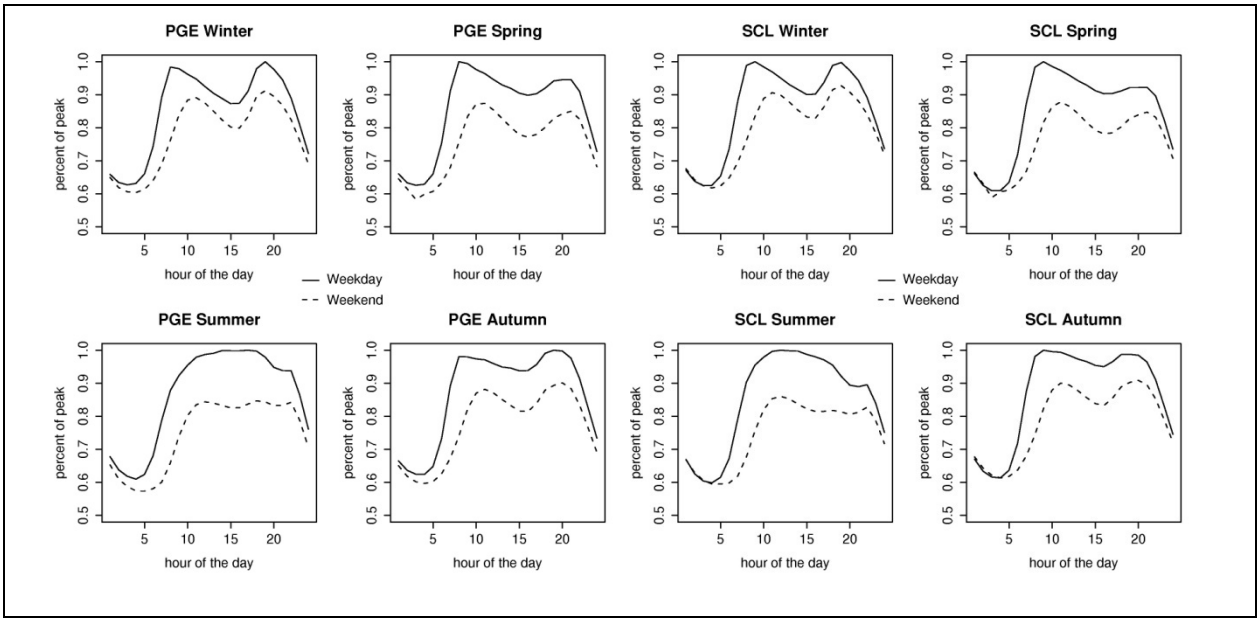

Figure 5.5.5: Northern California Hourly Load Profiles by Season, Weekday/Weekend, for NCPA, SMUD, TID, WAMP

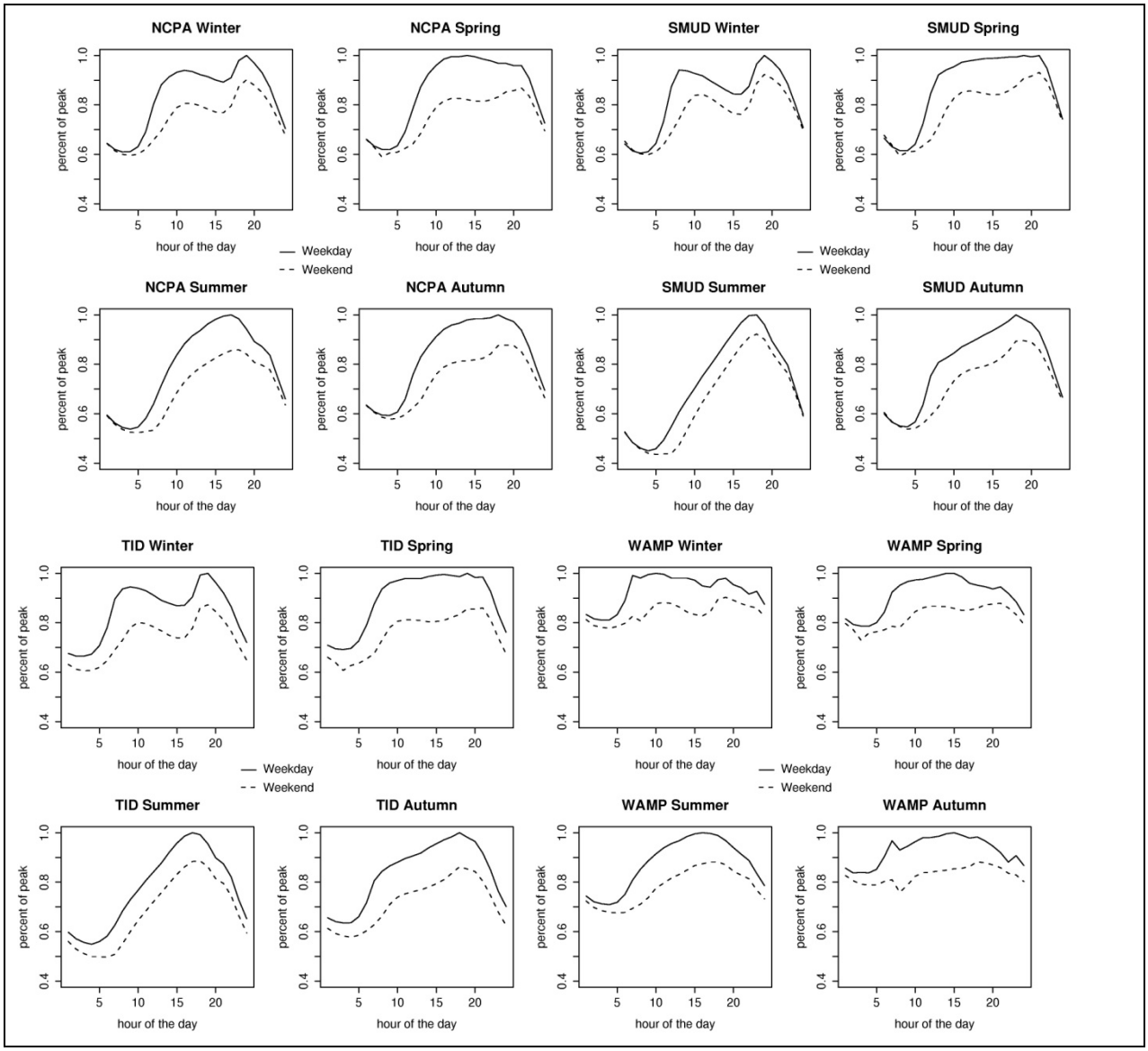

Figure 5.5.6: Southern California Hourly Load Profiles by Season, Weekday/Weekend, for BURB, GLEN, IID, LDWP

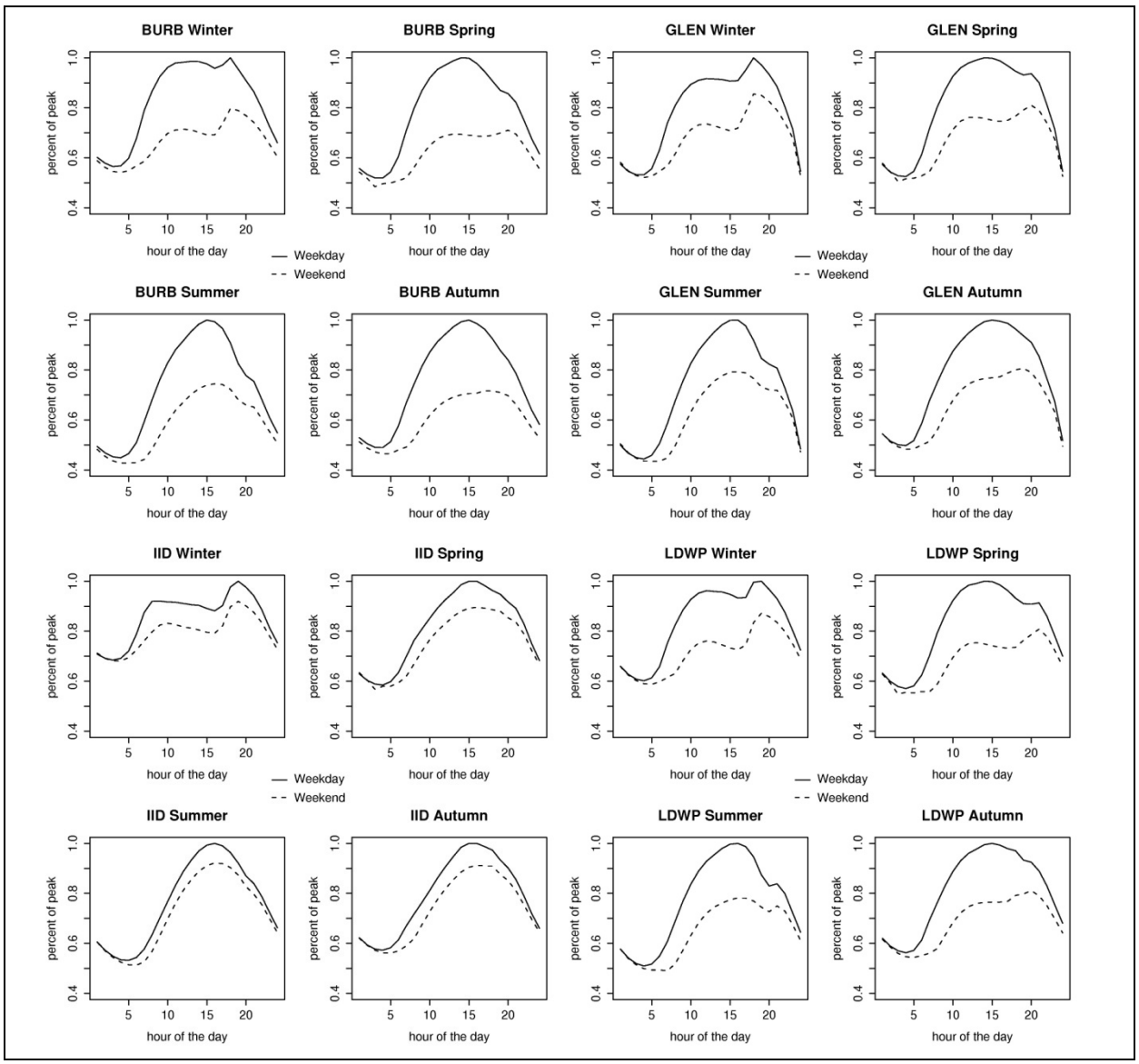

Figure 5.5.7: Southern California Hourly Load Profiles by Season, Weekday/Weekend, for MID, MWD, PASA, PGAE

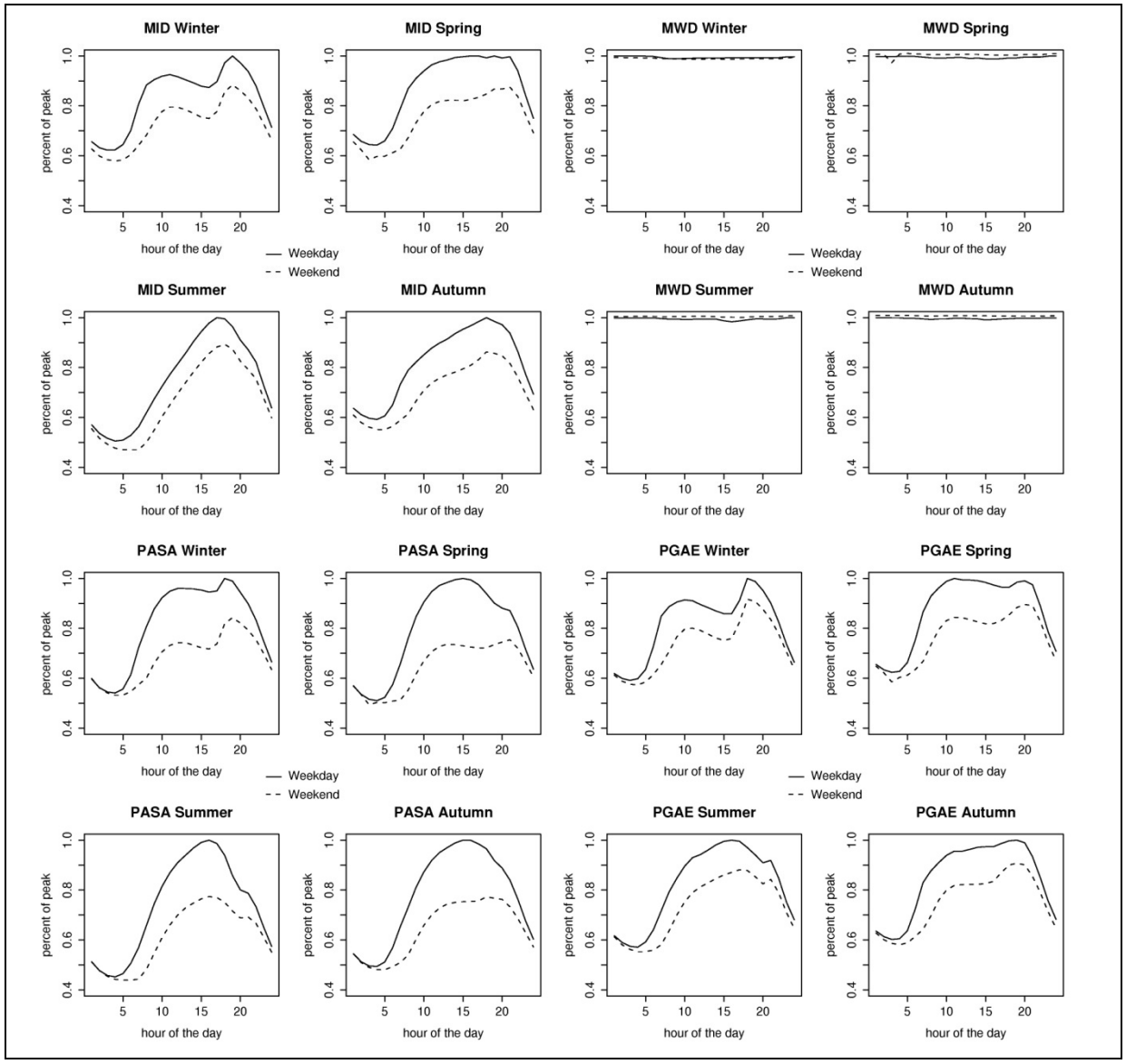

Figure 5.5.8: Southern California Hourly Load Profiles by Season, Weekday/Weekend, for SCE, SDGE, VERN

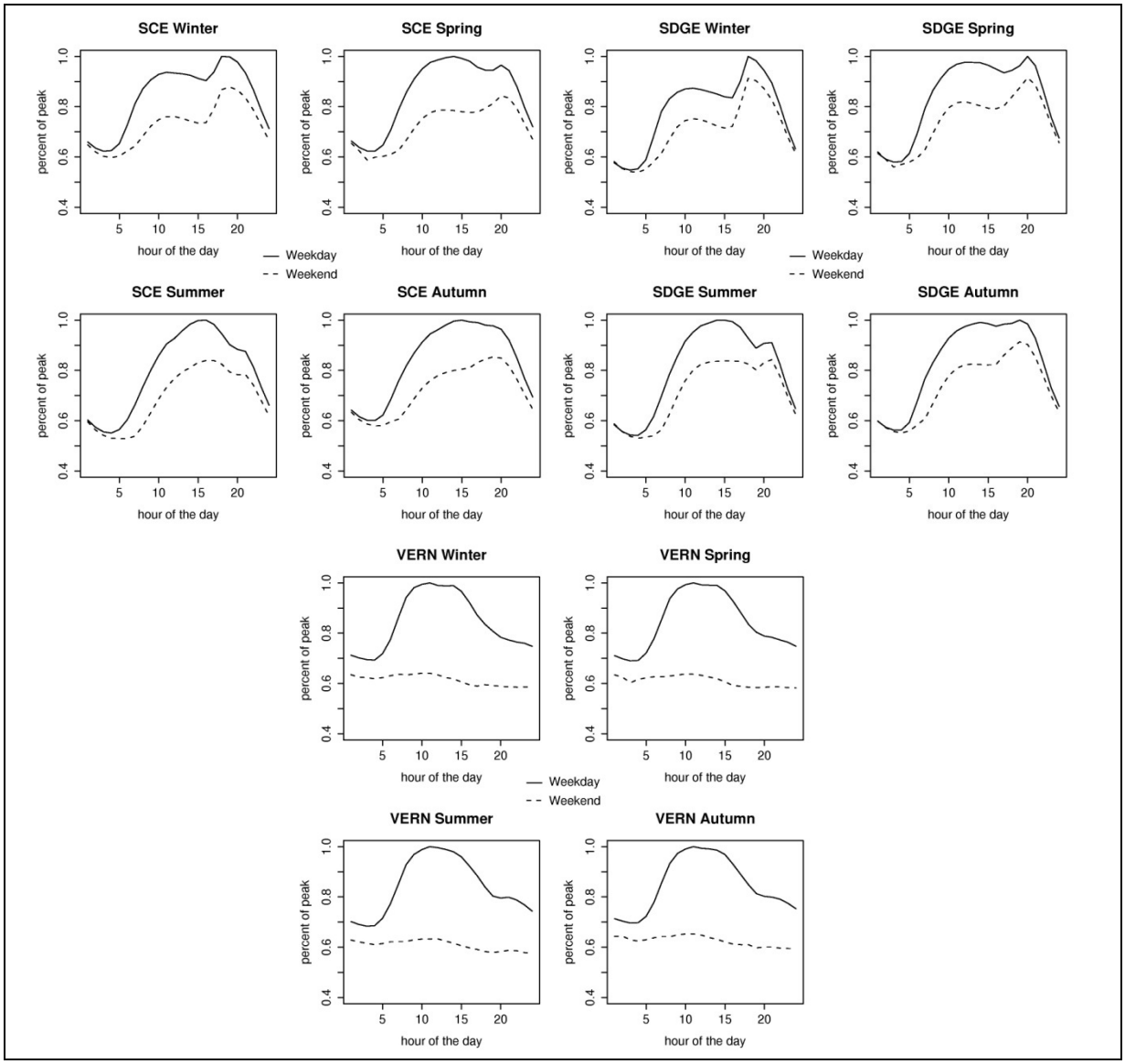

Figure 5.5.9: Southwest Hourly Load Profiles by Season, Weekday/Weekend, for AEPC, APS, BHPL, CSU

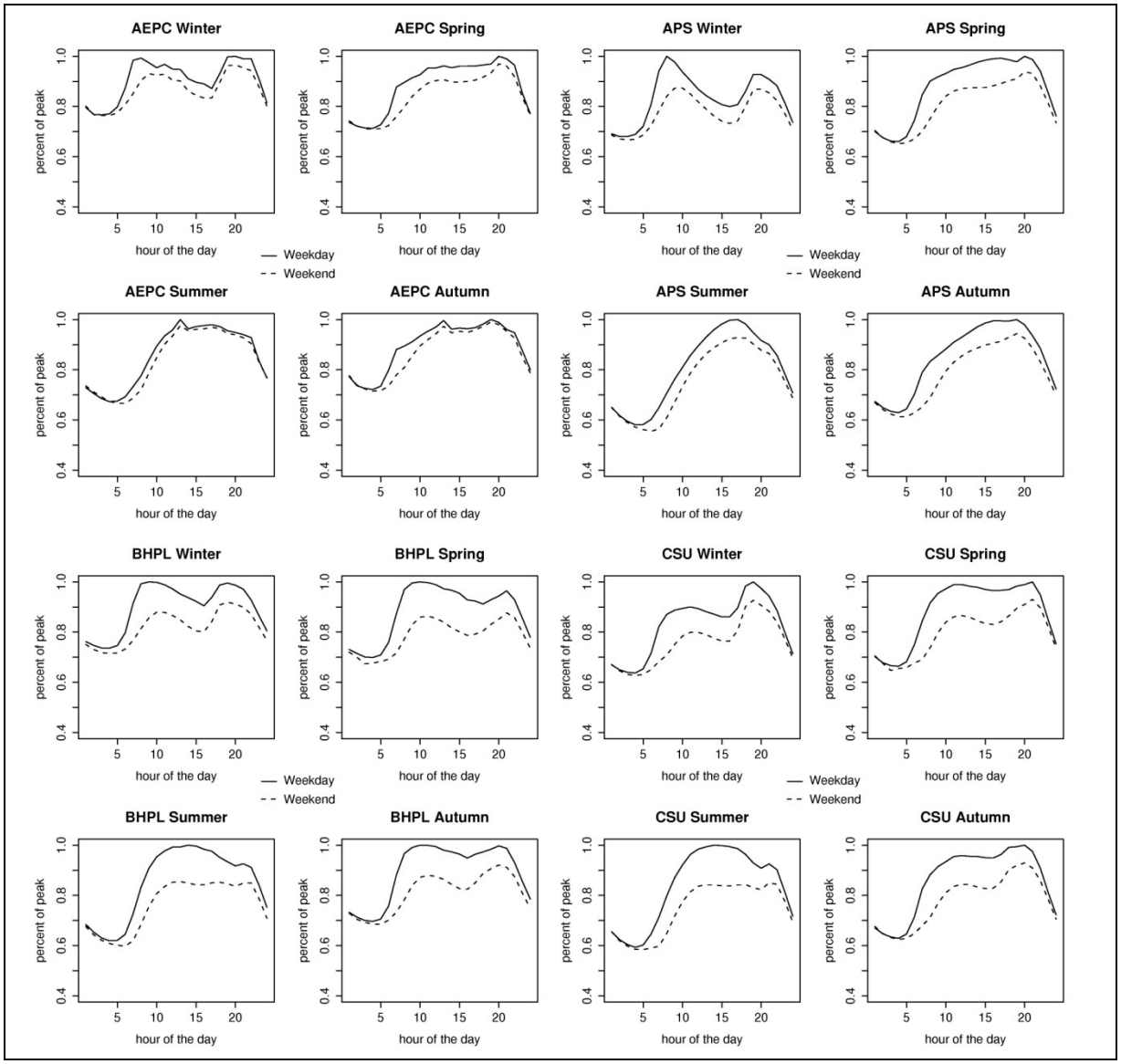

Figure 5.5.10: Southwest Hourly Load Profiles by Season, Weekday/Weekend, for DGT, EPE, FARM, MPC

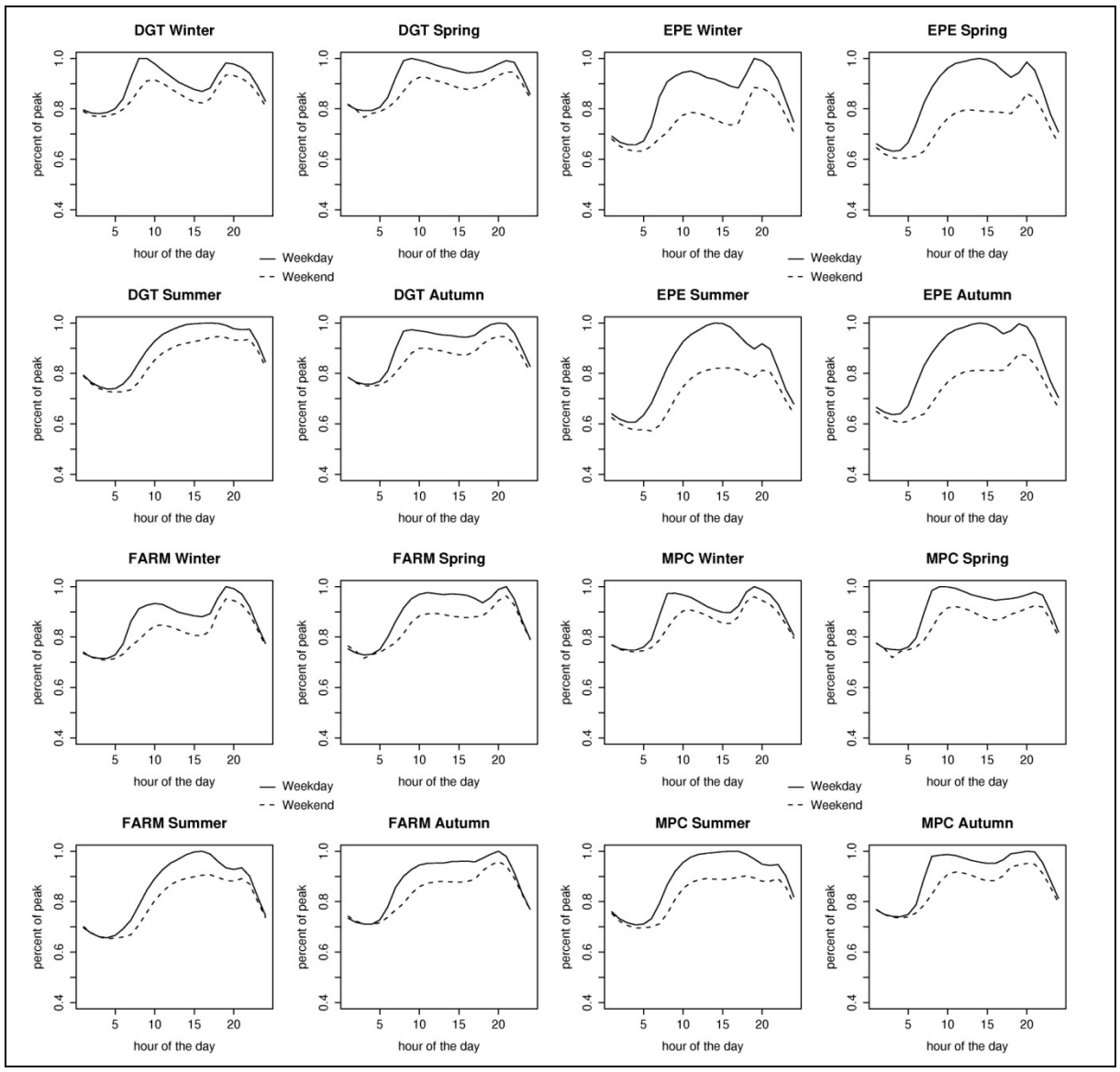

Figure 5.5.11: Southwest Hourly Load Profiles by Season, Weekday/Weekend, for NEVP, PNM, SPP, SRP

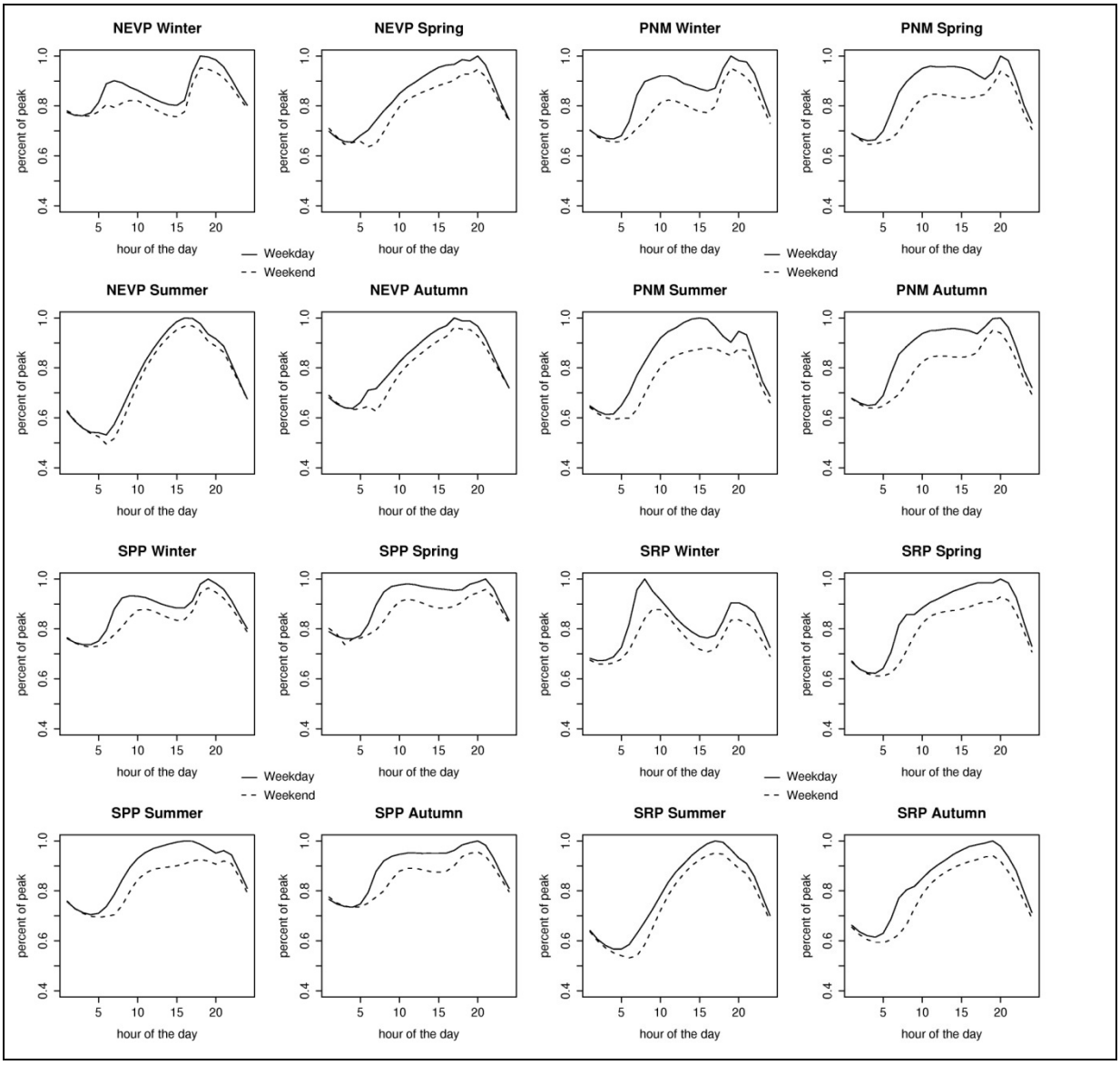

Figure 5.5.12: Southwest Hourly Load Profiles by Season, Weekday/Weekend, for TEP, UAMP, UMPA, WALC

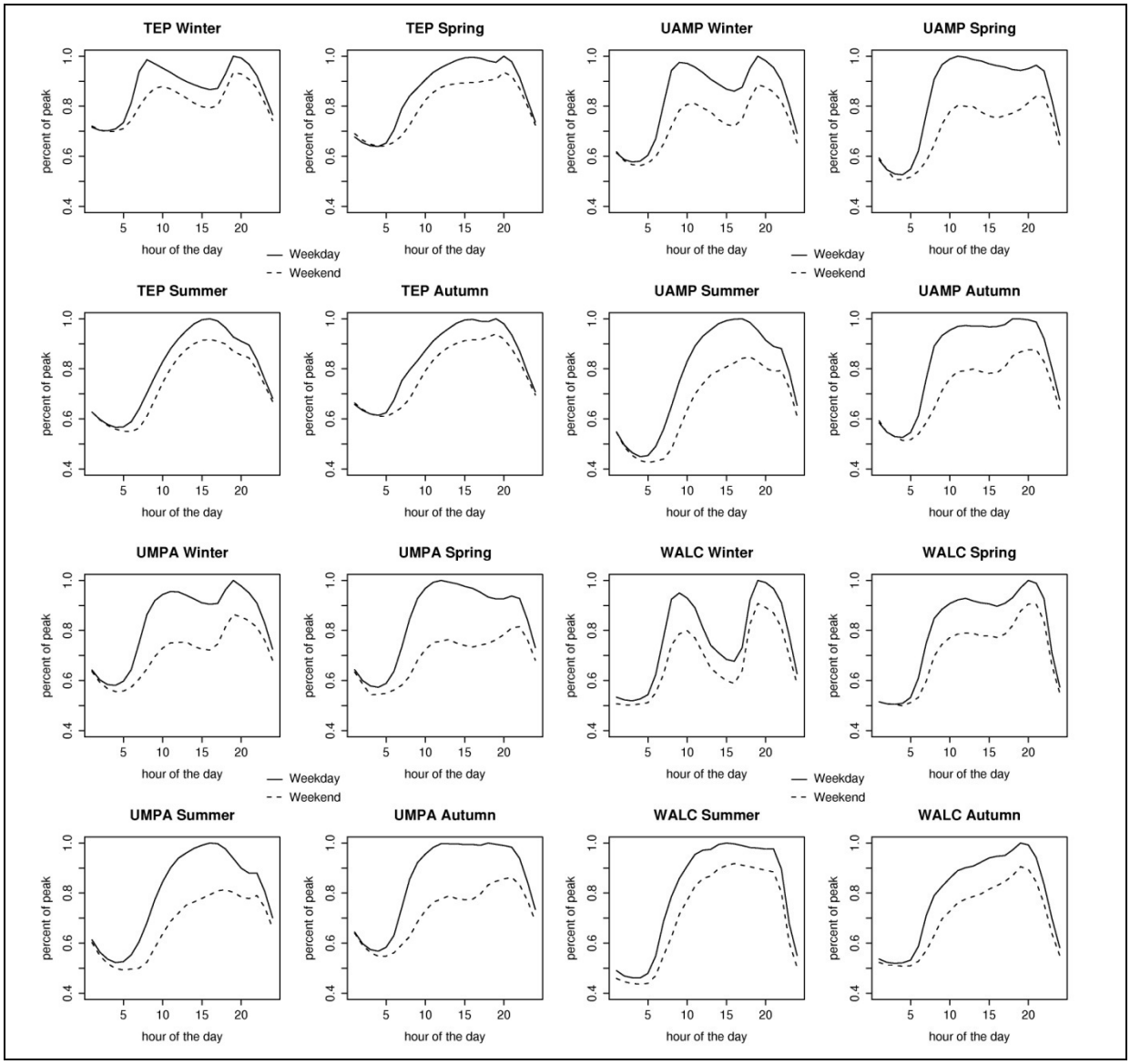

Figure 5.5.13: Southwest Hourly Load Profiles by Season, Weekday/Weekend, for WPE

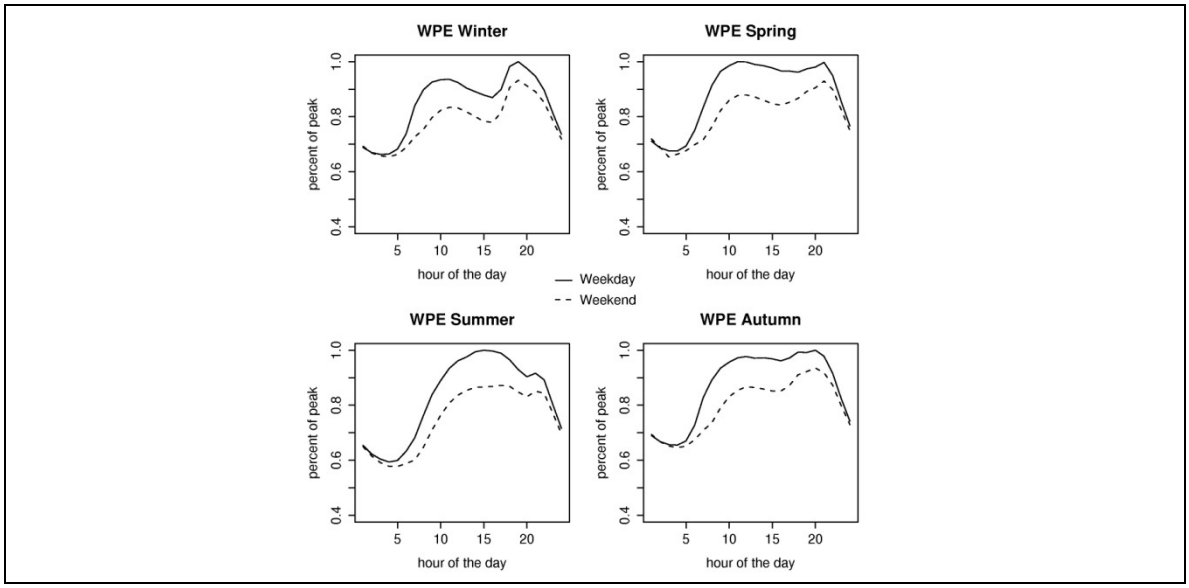

CHAPTER 6:
California Heat Waves: July 2006 and Recent History

Heat waves in the California region are recurring phenomena that occur mainly in June, July and August. Heat waves vary from event to event in their day and nighttime temperature expressions. Various factors including timing, synoptic circulation and humidity determine the magnitude (for example, intensity, duration and spatial extent) of any particular event. Atmospheric moisture availability determines a heat wave's day or nighttime preference. Most of the great California heat waves can be classified into primarily daytime or nighttime events depending on whether atmospheric conditions are dry or humid.

The July 2006 event was the largest heat wave on record (1948 through 2006). Although daytime temperatures during the July 2006 event were comparable to those in some prior great heat waves, the duration of the event was exceptionally long and its warm nighttime temperatures were unprecedented in records spanning almost six decades. The extreme intensity, duration and spatial extent were caused by a combination of factors, the most unusual of which was a very early and intense moisture anomaly advected into the region by a weaker heat wave circulation that preceded the development of the main event.

There is a positive trend in daytime heat wave activity over the entire region (part of which is a shift in the 1970s), but its magnitude varies spatially and in some places it is weak. Daytime heat wave activity is intensifying much more rapidly over the elevated interior compared to the lowland valleys. The occurrence of the unusually strong July 2006 event is consistent with a strong intensification of nocturnal heat wave activity since 2000. This intensification of nighttime heat wave activity appears to be part of a longer-term large-scale smooth and monotonically increasing trend that is fully consistent with the observed overall warming trend in minimum temperatures. Synoptic circulations associated with great regional heat waves advect hot air from the south. This air can be dry or moist, depending on whether an appropriately positioned moisture source is available. A particular source is a marine region east of Baja California that has been experiencing significant sea surface warming and moistening. The correlation between heat wave occurrences and the anomalous sea surface temperatures (SST) in the region west of Baja California is intriguing because the SST warming there appears to be part of a global pattern of SST warming during the last 6 decades.

6.1 Introduction

According to anecdotal evidence, the July 2006 California heat wave was unprecedented in several respects. Many local records for duration of above-threshold temperatures were broken. The heat wave affected Northern and Southern California simultaneously. Nightfall did not provide the expected relief from daytime heat. Unusually high humidity levels exacerbated the stressful effects and probably contributed to maintaining high nighttime temperatures (Los Angeles Times 2006). Enormous demands were placed on water and energy resources (Davis

2006). Californians, human and cattle alike, suffered, some expired[1], and most noticed that something highly unusual was underway. Now that weather data is available for most observing stations, researchers take a comprehensive retrospective look at the July 2006 California heat wave in the context of the region's climate over the past six decades: the temporal extent of sufficient data and the experience of a human lifetime.

Summertime heat waves top the list of stressful weather extremes that are most commonly linked with global anthropogenic climate change (Easterling et al. 2000a, Meehl and Tebaldi 2004, Tebaldi et al. 2006). Heat wave activity has received considerable attention lately, especially following the European heat waves in 2003 (Beniston and Diaz 2004, Schar 2004, Stott et al. 2004, Meehl and Tebaldi 2004, Gershunov and Douville 2007). Most studies have focused on local extreme temperature magnitudes and durations associated with heat waves (Beniston 2004, Beniston and Diaz 2004, Schar et al. 2004). Heat waves are inherently regional phenomena, however, with regional impacts. The spatial scale of heat waves amplifies the event's stressful effects by spreading them over broader sectors of ecosystems, society and infrastructure. Gershunov and Douville (2007) considered the spatial extent of summertime heat over Europe and North America in seasonal average temperature records and model projections. Although the increasing spatial scale of extreme continental summertime heat is obviously connected to heat-wave activity and clearly tied to global climate change, the explicit behavior of individual heat waves as well as their diurnal properties could not be considered in seasonally or daily averaged data.

A more precise and useful description of heat wave activity should include an explicit and separate quantification of daily and nightly temperature extremes. During a persistent daytime heat wave, cool nights provide respite from the stressful effects of heat on the health and general well-being of plants and animals, as well as for the energy sector, and prepare nature and society to face another day of scorching heat. Heat waves strongly manifested at night eliminate this badly needed opportunity for rejuvenation and increase the chances for catastrophic failure in natural and human systems. Extreme daytime heat is known to endanger health most directly via heat stroke as well as impact air pollution including ozone formation and thereby amplify heat wave related mortality (Fischer et al. 2004, Stedman 2004). Health impacts of nighttime heat are less well known, but there are indications that high minimum temperatures during heat waves enhance morbidity and mortality (Hemon and Jougla 2003, Grize et al. 2005). Analyzing excess mortality across Switzerland due to the June and August 2003 European heat waves, Grize et al. (2005) attributed local spikes in mortality to the compounding effect of elevated nighttime temperatures. During the July 2006 California event, a significant number of victims, most of whom were elderly and living alone, had not used their functioning air conditioning (Helene Margolis, personal communication). Perhaps they had turned off air conditioning in the evening expecting the strong nighttime cooling characteristic for this region, which did not materialize.

1. Over 140 human and 25000 cattle mortalities were attributed to the July heat wave in California (Munoz 2006, USAgNet 2006).

The physical mechanisms of day and nighttime heat waves may differ. Recent warming trends are known to have been stronger at night than during the day (Easterling et al. 1997, 2000b) resulting in a generally decreased diurnal temperature range. Stronger nighttime heating trends have been observed consistently at most locations around the globe and, in spite of modeling inconsistencies (Lobell et al. 2007), are among the most reliable and widespread expectations from anthropogenic global climate change (Tebaldi et al. 2006). In this regard, the California region is no exception as the observed summer warming here has been largely due to minimum temperatures (Figure 6.2.1). In this topographically, environmentally, economically and climatically complex region, global, regional and local, natural and anthropogenic effects abound (Duffy et al. 2007). Clear connections between regional extreme weather and global climate are generally elusive. Where they exist, they provide extremely useful opportunities to understand and skillfully anticipate the stressful local effects of global climate change. Weather extremes, however, must first be understood regionally, typically on the synoptic level.

The following sections describe the data including average summertime temperature variability and trends, as well as our approach to quantifying heat waves and their general behavior (section 6.2), illustrate the observed variability of regional day and nighttime heat waves (section 6.3), describe the synoptic dynamics leading to the greatest observed events in recent history (section 64), explain the 2006 event in that context (section 6.5), and finally focus on trends in day and nighttime heat waves (section 6.6). A section on forecasting heat waves follows (section 6.7). Summary and conclusions are presented in section 6.8.

6.2 Average Summer Temperature and Heat Wave Activity

There is no one objective and uniform definition of "heat wave". In the present study, researchers seek a regional measure that reflects an event's impacts (on regional health, infrastructure, economy, and so forth) and that can be easily quantified in indices that are clear and simply computed from the available data. We want these indices to plainly reflect important aspects of regional heat wave activity and to be straightforward, flexible and easily adaptable for relevant applications. The resulting heat wave indices should include components that add up to a heat wave's regional magnitude and result in numerous impacts on specific sectors of society and environment, and therefore, reflect and quantify an event's intensity, duration and spatial extent.

6.2.1 Observational Data

In order to describe the spatial extent of heat waves affecting the California region, their duration, and differential symptoms during day and night, researchers start with day- and night-time temperatures (Tmax and Tmin, respectively) recorded at ninety-five stations distributed more-or-less uniformly over the adjacent states of California and Nevada. These ninety-five stations (CA95) are a subset of a larger set of 141 stations with premium quality daily Tmin and Tmax records going back to at least January 1, 1948 and running through August 2006 (Figure 6.2.1.a and 6.2.1b, circles). The original set of 141 stations is characterized by a spatial weighting bias towards most populated areas (Figure 6.2.1.a and 6.2.1,b, black dots). The 95 core stations (CA95) were selected as representative of the region by keeping one best

quality station per locale of 30km radius and thereby removing the urban density bias[2]. Stations with the most complete records are typically found at lower elevations. To retain the effects of mountain climate diversity important in this topographically complex region, the highest elevation station, in addition to the best quality station, was retained wherever the elevation range exceeded 300m per locale. All stations were required to have at least 85 percent of the data present for the entire 59-year period. The sparsely populated and observed areas of the southeastern California and Nevada deserts are, by necessity, underrepresented and downplayed by subsequent analyses. All station data were selected from the updated National Climatic Data Center (NCDC) first order and cooperative observer summary of the day dataset, known as DSI-3200 (NCDC, 2003).

The seasonal focus here is on the summer period, June – August (JJA). The largest events tend to occur around the seasonal temperature maximum in mid-late July. Although intense heat waves occasionally occur in May and September, they tend to be localized resulting from rather different regional circulations than the extensive events considered here[3]. Including those months would not significantly influence our results, but concentrating on JJA sharpens our focus on the largest events. We further limit the temporal extent of this study to the 59 summers between 1948 and 2006. This choice was dictated by compromising record length for spatial completeness and detail.

6.2.2 Trends in Average Temperatures

As a prelude to studying heat wave activity, researchers first describe the observed trends in summer average temperature. Figure 6.2.1 shows local JJA Tmax and Tmin trends in addition to region-wide average temperatures and trends.

2 The analysis performed on the entire set of 141 stations predictably resulted in somewhat larger regional trends in both day and nighttime temperatures, but these differences were statistically insignificant.

3 The September 1978 daytime heat wave expressed along the south and central coast was one such example that resulted from an intense Santa Ana condition.

Figure 6.2.1: Linear Trend in Ambient JJA TMAX (a) and TMIN (b) by Station

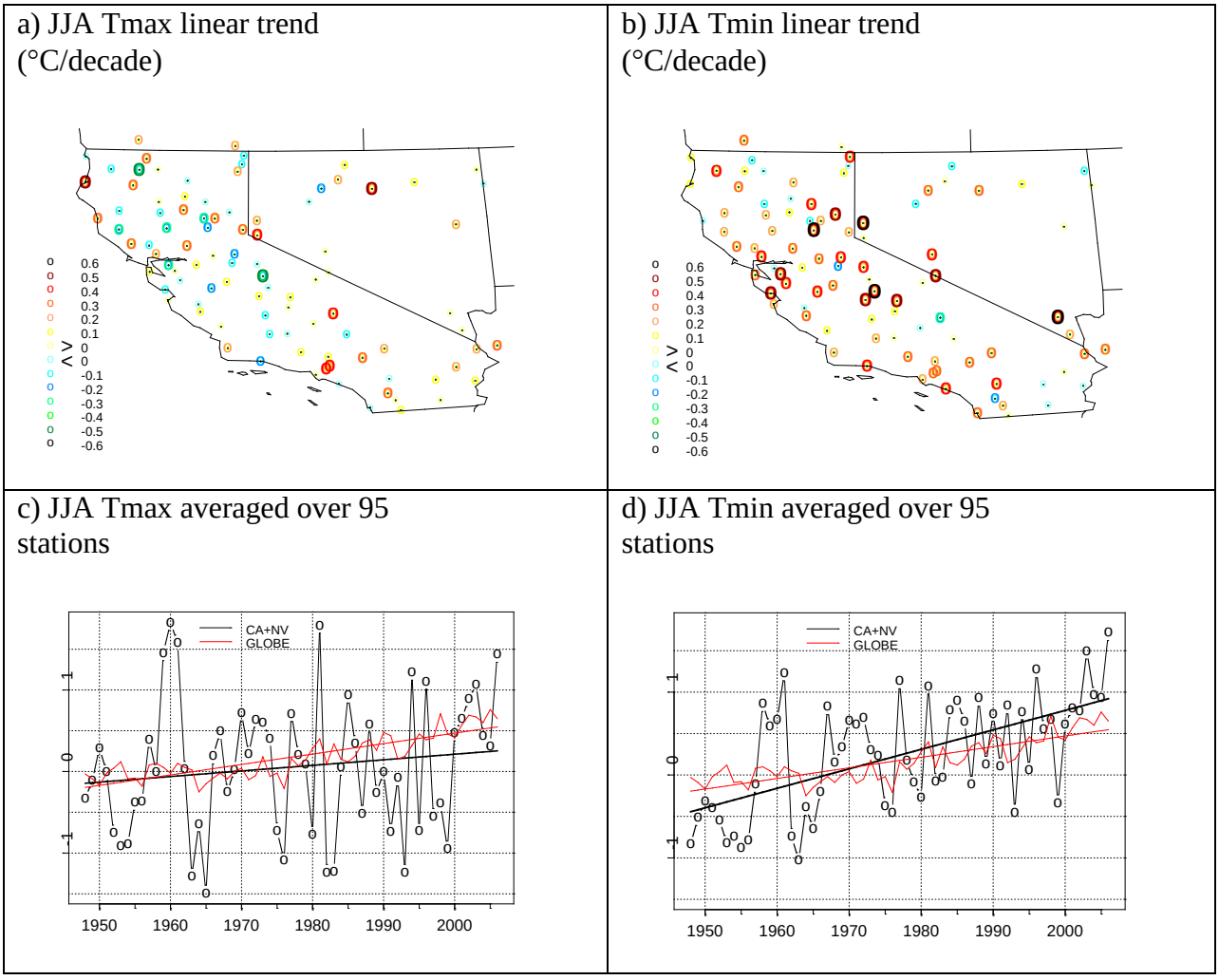

Red dots mark the 95 stations analyzed, while black dots mark urban-sprawl stations not used. Colored circles around the analyzed stations represent the sign and magnitude of local trends according to the legend in °C/decade. Larger circles depict greater trends. Panels (c) and (d) show regional anomalies and trends averaged over the 95 chosen stations and fitted regression line. Global *annual average mean* temperature anomalies and trend computed from the global meteorological station network updated from Hansen et al. (2001) are shown in red for reference. Anomalies are plotted with respect to the 1951-1980 period in this figure. Region-averaged Tmax/Tmin trend is 0.07/0.24°C per decade (0.4/1.4°C over the 59-yr record, compared to the global average of 0.13°C per decade or 0.76°C global warming recorded at land stations over the same period). The linear trends account for 2 percent and 35 percent of Tmax and Tmin variance, respectively.

Both daytime and nighttime temperatures have exhibited warming trends, but those for nighttime are considerably larger (Figures 6.2.1 a through d). Some stations showing the largest Tmin trends are urban (Reno WSFO Airport is second with a Tmin warming trend of 1.25∞C/decade, Las Vegas WSO Airport is fourth with 0.68∞C/decade). A priori, researchers expect the urban heat island effect to be especially strong for Tmin data (Cayan and Douglas 1984). Our data set includes a representative sample of urban points. These are, of course, also the places most at risk due to the compounded effects of heat waves on society, such as more people potentially exposed, power failure risk, and so forth. So, it is important to have the heat island effect represented here, but, as will be shown, it does not explain the bulk of the nighttime warming observed over the region. Rural stations are also warming considerably at night. Nevada City, a gold rush town in the low Sierra Nevada of California records the largest Tmin trend of 1.34∞C/decade and Auberry, California, located in the Sierra Nevada foothills between Fresno and South Yosemite Entrance comes in third with 0.99∞C/decade. Many other rural stations are warming at about 0.4∞C/decade at night and the average trend of 1.4 degrees over the 59-yr period of record is impressive. Maximum temperatures are not warming as much or as consistently throughout the state, but the overall trend of 0.4ºC/six decades is noteworthy. As noted by Alfaro et al., (2006), day-to-day, Tmax is more variable than Tmin. This intraseasonal observation obviously translates to interannual timescales further confounding trend detection in Tmax, especially at individual stations. Nevertheless, the summertime regional warming observed here over California and Nevada is fully consistent with the annual average global warming observed over land areas in worldwide station records (Figure 6.2.1 c and d). This is the average seasonal picture. Our primary interest below is to study the punctuation of the regional mean summer climate by outbreaks of extreme heat.

6.2.3 Quantifying Regional Summertime Heat Wave Activity

Daytime and nighttime heat-wave activity indices were derived to reflect the overall magnitude of extreme summertime (JJA) heat[4] consisting of intensity, frequency, duration and spatial extent of day and nighttime heat waves. At a particular station, a heat wave is defined to occur when temperature exceeds the 99th percentile of its local summertime climatology[5] (Figure 6.2.2). On days and nights when station temperatures exceeded these climatological values, researchers computed the local temperature excesses ($T_{i,j} - T_{99,j}$, i marks days/nights such that $T_{i,j} > T_{99,j}$, at station j) and summed them over each summer, obtaining the local summertime Degree Day index, $DD_{99}^{j,s} = \Sigma_i(Tmax_{i,j} - Tmax_{99,j})$, for *i* ranging from June 1 to August 31, the 92 days of summer, resulting in an annually resolved time series at each station. The Degree Night index (DN) is similarly defined for Tmin. By definition, $DD_{99}^{j,s}$ and $DN_{99}^{j,s}$ represent the intensity and frequency of intense (the hottest one percent of) local summer heat waves expressed during the day and night, respectively.

4 We consider individual events as well, below.

5 The 99th percentile of June through August daily Tmax and Tmin for the base period 1950 – 1999. By definition, only the 1 percent hottest days and nights exceed these values during the base period. We define these events as local heat waves.

Figure 6.2.2: 99th Percentile of Summer Daily and Nightly Temperatures

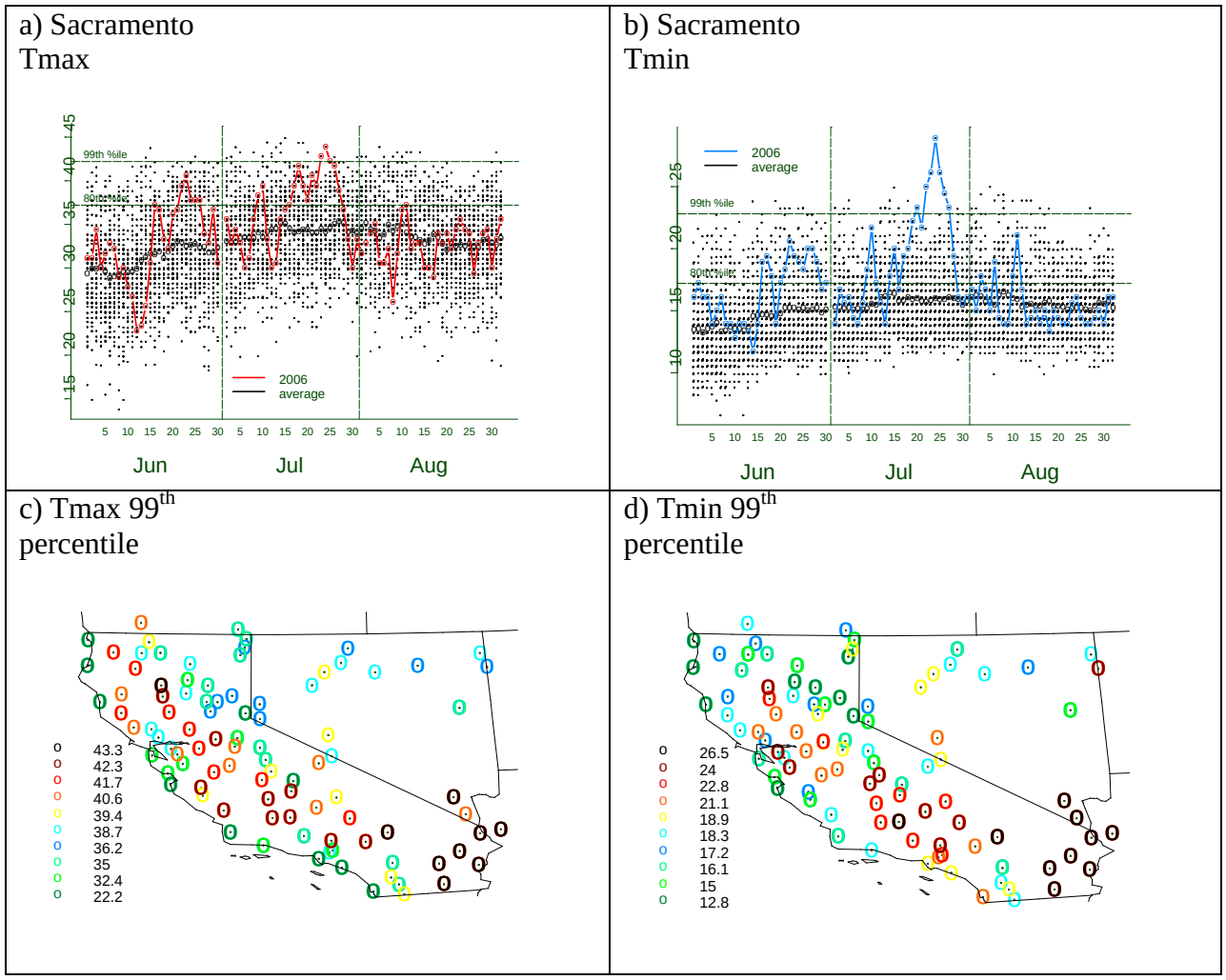

The spread of observed Tmax (a) and Tmin (b) plotted in °C in dots for every day of the summer with average (black circles) and 2006 observations (colored curve) as well as the 99th percentile (dashed line) computed over the 1950 – 1999 climatology for Sacramento (WSO City station). By definition, daytime or nighttime heat waves occur on days when Tmin or Tmax exceed this line. They are quantified locally as sums of exceedances over the 99th percentile. Panels (c) and (d) depict the approximate (in bins) 99th percentiles of summertime Tmax and Tmin, respectively, at all stations. Regional heat waves are quantified as exceedances over the local 99th percentile summed over all stations.

At Sacramento (WSO City station), the larger variance of summertime daily Tmax compared to Tmin variance is apparent in the different scales of Figure 6.2.2, panels a and b. The distribution of Tmin is skewed, having a sharp lower limit and a more volatile upper bound; the well-defined lower threshold indicates that nighttime cold extremes are limited, probably because radiative cooling is time-limited, while large extremes tend to occur on the hot side. Summer 2006, especially late July, featured an extremely intense and persistent heat wave and is used

here as an example. July 2006 featured warm Tmin excursions (5–10+ ∞C above the climatological mean) and cold extremes just 1-2 ∞C below the mean (Figure 6.2.3b). July 22-24 saw Tmin unprecedented on this record with 29∞C (84∞F). The 99th percentile of 22.8∞C (73∞F) was exceeded for seven (six consecutive) nights. Tmax, meanwhile, although not unprecedented, exceeded the 99th percentile (42.2∞C/108∞F) for two straight days (July 23-24) and generally varied more symmetrically around the climatological mean values.

To define heat wave activity and individual events over the region, researchers first compute the 99th percentiles at all stations (Figure 6.2.2 c and d). This result indicates that the highest temperature extremes during both day and night typically occur in the southeastern low deserts and interior valley regions, while the coolest hot extremes occur in the high Sierra Nevada and along the coast and coastal ranges. Extremes of both Tmax and Tmin display a very similar spatial distribution with few local exceptions, such as the southern California coast exhibits relatively hot extremes at night while the northern coastal hills are relatively more prone to intense daytime heat. These percentiles are used to quantify regional heat wave activity simply by summing threshold exceedances (departures over these local thresholds) over each summer and all stations (Figure 6.2.3).

Figure 6.2.3: Regional Daytime and Nighttime Heat Wave Indices DD and DN

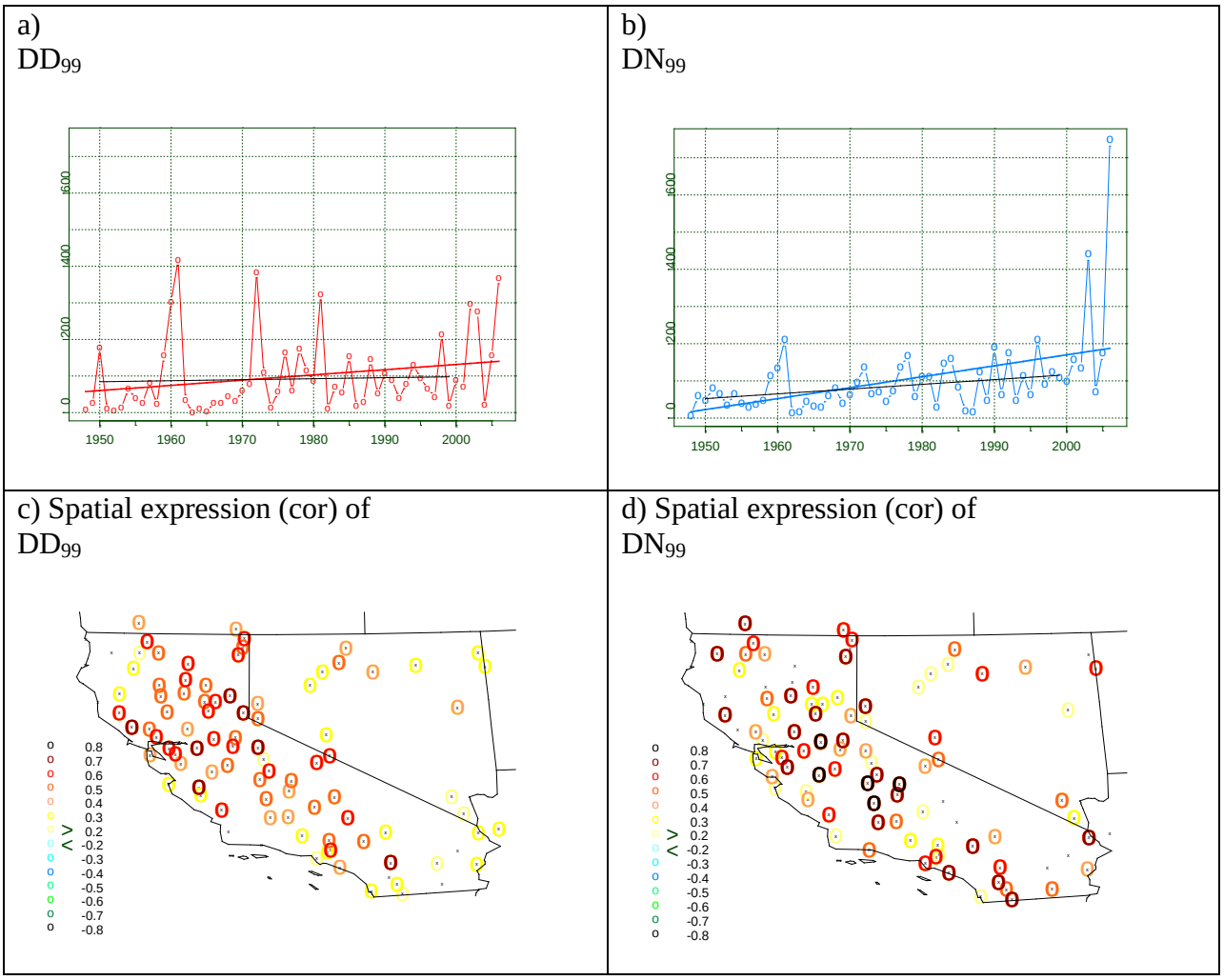

Degree days (DD_{99}, a) and degree nights (DN_{99}, b) are defined as exceedances over local climatological 99th percentiles summed over each summer and all stations, for example $DD_{99}=\Sigma_j(DD_{99}^{j,s})$, j = 1,…,95 stations. Linear regression lines are shown for the entire record (1948-2006, colors) and over the base period (1950-1999, black). The spatial expressions of these region-wide indices are shown as correlations with local DD_{99} (c) and DN_{99} (d).

These indices, DD_{99} and DN_{99} (ρ=.60), reflect region-wide summertime heat wave activity, for example intensity, frequency, duration, and spatial extent of individual heat waves aggregated over each summer (Figure 6.2.3a and b). Although the first half of the record saw intermittent intense *daytime* heat wave activity notably in the summers of 1960, 1961 and 1972, these occurred over a background of low activity (Figure 6.2.3a). There was a shift to generally higher activity in the mid 1970s that is consistent with warmer average temperatures (Figure 6.2.1c), that is in turn related to the North Pacific Decadal Oscillation (NPO) shift that is known to affect California summer temperature, including cooling degree days and frequencies of Tmax extremes (Alfaro et al. 2004). However, the slight trend in daytime heat wave activity is mostly

due to enhancement at the very end of the record. In contrast, the increasing trend in nighttime heat wave activity is a feature of the entire record that seems to have gotten a boost during the most recent summers 2003 and 2006, each unprecedented (Figure 6.2.3b).

The statewide nature of the most intense heat wave activity is apparent from the correlations of regional DD_{99} and DN_{99} with local values (Figure 6.2.3c and d). Principal components analysis (performed on the correlation matrix) reveals leading modes (PC1s) that are practically identical to region-wide DD_{99} (ρ=.954) and DN_{99} (ρ=.987). This is not surprising, given the large-scale nature of intense heat wave activity, and especially of the DN_{99} trend (Figure 6.2.3c and d). However, a strong and spatially coherent trend[6] is expressed in PC2 of DD_{99} (Figure 5.4a). This trend is towards a relative intensification of daytime heat wave activity in the elevated interior relative to the lowlands. The spatial pattern of this relative trend in daytime heat wave activity (Figure 5.4b) is strongly correlated with station elevation (ρ=.52). The elevational dependence of this relative trend is visually apparent to anyone familiar with the topography of the region by visual examination of Figure 4b. Although PC2 modifies the spatial footprint of large daytime heat waves, it is, by definition, uncorrelated with PC1 (Figure 6.2.3a) over the entire record. Rather, it shows that heat waves affected the 'heartland' valleys more than the interior hills in the earlier part of the record and the hills more than the valleys in the more recent summers, for example (anti-) correlated over the (early) late part of the record (compare Figures 6.2.4a and 6.2.3a). Moreover, the change from negative to positive correlations took place in the form of a clear linear trend in addition to a discrete shift in the late 1970s, indicating a progressive and coherent change in the spatial patterns of large daytime heat waves.

Although a detailed analysis of this geographic trend is beyond the scope and focus of this paper, it appears likely that the highlands, which are drying in summer due to progressively decreasing snow/rain ratio (Knowles et al. 2006), earlier spring snowmelt and runoff (Cayan et al. 2001, Stewart et al. 2005) and generally decreasing snowpack (Mote et al. 2005), are becoming relatively more prone to intensified daytime heat wave activity compared to the irrigated farmland of the Central Valley and the coastal valleys, such as the wine growing regions of Napa and Sonoma counties, where the trend in heat wave activity appears to have been progressively suppressed. Summertime Tmax, but not Tmin, is inversely related to natural soil moisture variability (Alfaro et al. 2006). Moreover, irrigation is known to suppress summertime daytime heat in California while leaving nighttime temperatures unaffected (Bonfils and Lobell 2007, Lobell and Bonfils 2007). Agricultural and urban aerosols, more concentrated in the valleys, may also be limiting lowland Tmax extremes. Low deserts circa southeastern California, evidently, are exempt from this daytime heat suppression (Figure 6.2.4b).

6 EOF2 (Figure 6.2.4b) reflects the trend pattern seen when trends are computed for each station's DD_{99} separately (not shown). The latter, of course, is noisier, while the former emerges because of the inherent spatial coherence in heat wave activity trends.

Figure 6.2.4: Second Principle Component of DD99 (PC2, a) and its Corresponding Spatial Pattern (EOF2) Expressed as Temporal Correlation Coefficient of PC2 with DD99 at Each Station (b)

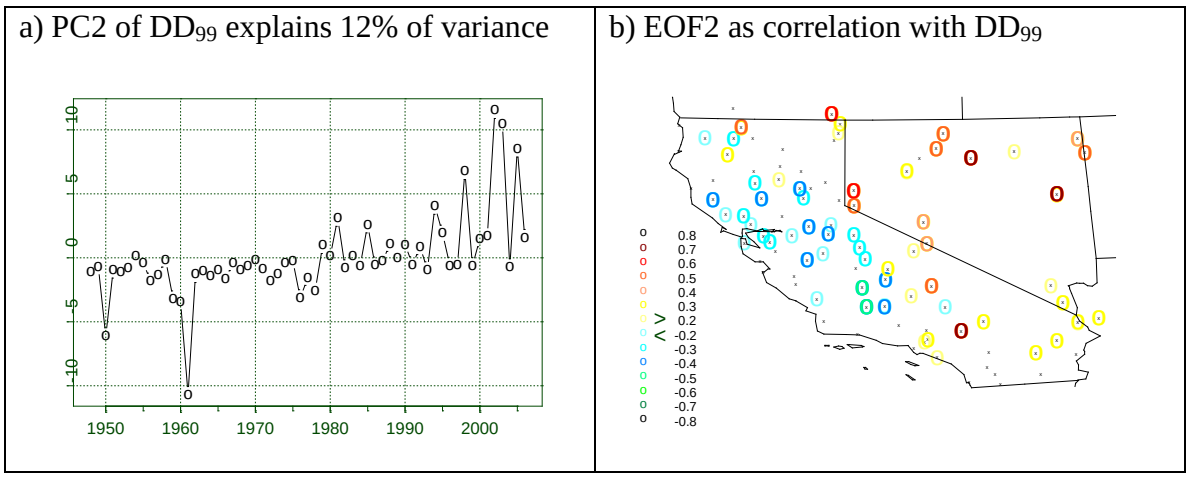

PC2 explains 12% of total variance in DD99, compared with 27% for PC1 (similar to DD99, Figure 6.2.3a and c). The spatial correlation of EOF2 with station elevation is 0.52.

In summary, regional heat wave activity is on the rise especially as expressed in Tmin and most prominently and increasingly since the 1970's. The observed trend is not explicitly focused on population centers and is apparently occurring on spatial scales involving at least California and Nevada. The early part of this rise is related to the mid-seventies NPO shift (Alfaro et al. 2004). This shift is best expressed in daytime heat waves, but the trend, especially in nighttime heat wave activity, continued and intensified since then in sync with regional average temperatures and observed large scale warming. Increasing daytime heat wave activity trend is strongest in the elevated interior of the region but suppressed in the lowland valleys. Following this general seasonal quantification and discussion of summertime heat wave activity, researchers focus on the magnitude of individual heat wave events and describe the intensity, spatial extent and duration of the largest observed extremes. We will then describe their synoptic causes.

6.2.4 Definitions

The terminology adapted in this article to describe heat wave magnitude should be clarified. Local and daily (or nightly) magnitudes are the Tmax (or Tmin) threshold exceedances recorded at a specific station on a specific day or night. These can be aggregated (summed) over space and time into seasonal regional magnitude (Figure 6.3.2); daily regional magnitude summed over all stations representing a region on a particular day or night (Figure 6.3.1); local heat wave magnitude at a single location summed over the duration of a heat wave (Figure 6.5.1). Local (or regional) heat wave duration is defined as the number of consecutive days when local threshold(s) is (are) exceeded, while spatial extent is defined as the percentage of representative stations where local thresholds are exceeded. Peak seasonal (or event) magnitude and spatial extent are defined as the maximum daily value over a season (or over the duration of a particular heat wave), for example, Figure 6.3.1. We sometimes apply the terms "total" or "overall" to mean aggregated measures over space and/or time (Figure 6.4.3).

6.3 Hot Summer Days and Nights

Researchers next examined the frequency and magnitude (such as, duration, intensity and spatial extent) of regional heat waves more closely at daily and nightly resolution. Figure 6.3.1a and b documents the magnitude of extreme ($T > T_{99}$) heat waves for each day and night on our 59-year record. Since spatial extent of heat waves strongly determines their regional magnitude, magnitude strongly reflects spatial extent (ρ=.95 for both day and nighttime events). Individual heat waves are visible on these plots. In general,

- heat waves tend to occur between late June and mid-August,
- heat waves tend to last for a few to several consecutive days,
- daytime heat waves occurred sporadically throughout the 59-yr period,
- nighttime heat waves have markedly increased in occurrence since the 1970's,
- heat wave activity during both day and night has been remarkable since 2000.

Detailed comparisons between the two panels of Figure 6.3.1, as well as intraseasonal temporal correlations (Table 6.3.1) of DD_{99} and DN_{99} regional magnitude and spatial extent (Figure 6.3.2), suggest that day and nighttime events are often, but not nearly always, coincidental. However, also from close examination of Figure 6.3.1, and as researchers shall see below, the largest Tmax events nearly always have some expression in Tmin and vice versa. Summers with notable types of extensive heat-wave activity can be identified, such as: 1960 with extensive and durable daytime heat wave in mid-July; 1961 with two separate large primarily daytime events in June and July; 1972 with a short and intense heat wave in mid-July primarily extensive during the day and a couple of separate minor episodes; 1981 with an extensive daytime event in early August; 2001 with a large nighttime event in early July and modest daytime expression; 2002 with a short and extensive primarily daytime event in early July; 2003 with a durable heat wave spanning a large portion of July during night and day; 2005 had a less extensive but durable day and nighttime event in the middle of July; 2006 with a durable and tremendously extensive July heat wave. In terms of the overall nightly magnitude the most recent period (since 2000) appears to have been without precedent on this record and July 2006 stands far out from even the enhanced nighttime heat wave activity of this most recent period.

Figure 6.3.1: The Daily-Level Magnitude of Heat Wave Activity Defined by DD_{99} (a) and DN_{99} (b) Summed Over All Stations on the Record

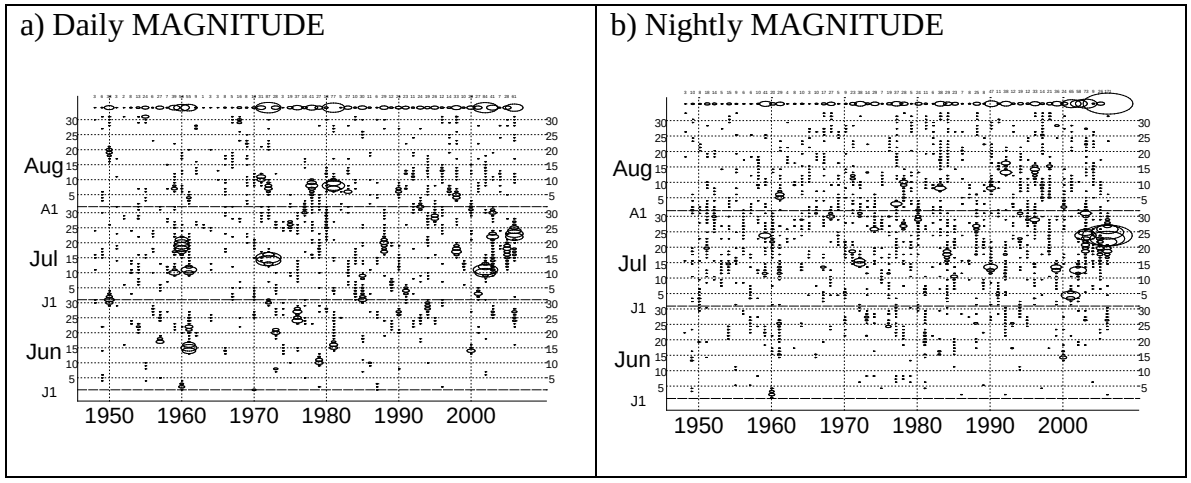

The x-axis corresponds to each year on record, while the y-axis corresponds to each summer day (a) and night (b). The scale is given by the maximum magnitude recorded each summer shown at the top of the plot and again in Figure 6.3.3a and b. The overall magnitude for each summer is shown in Figure 6.2.4a and b.

While overall summertime magnitude of heat wave activity was summarized in Figure 6.2.3, each summer's peak regional heat waves can be summarized, by their maximum intensity (Figure 6.3.2a and b), spatial extent (Figure 6.3.2c and d) and duration (Figure 6.3.2e and f).

6.3.1 Peak Magnitude, Spatial Extent and Maximum Duration: Co-Variability and Trends

Both the mean summer (Figure 6.2.3) and maximum daily spatial extent of heat-wave activity summarized for each summer on record (Figure 6.3.1a and b) suggest that, occasionally large heat waves notwithstanding, the general (background) level of heat-wave activity has increased as a step-function (a shift) in the 1970s for daytime heat waves, reflecting the known relationship between springtime NPO and JJA temperatures over the region (Alfaro et al. 2004). The same cannot be said for nighttime heat waves, which show a rather continuously accelerating increasing trend. When diurnal mean (Tmin + Tmax) regional heat waves are considered, the distinction between climate shift and trend could be more difficult to make out. The same can be said for peak spatial extent and duration.

Figure 6.3.2: Seasonal Maxima of Heat Wave Components

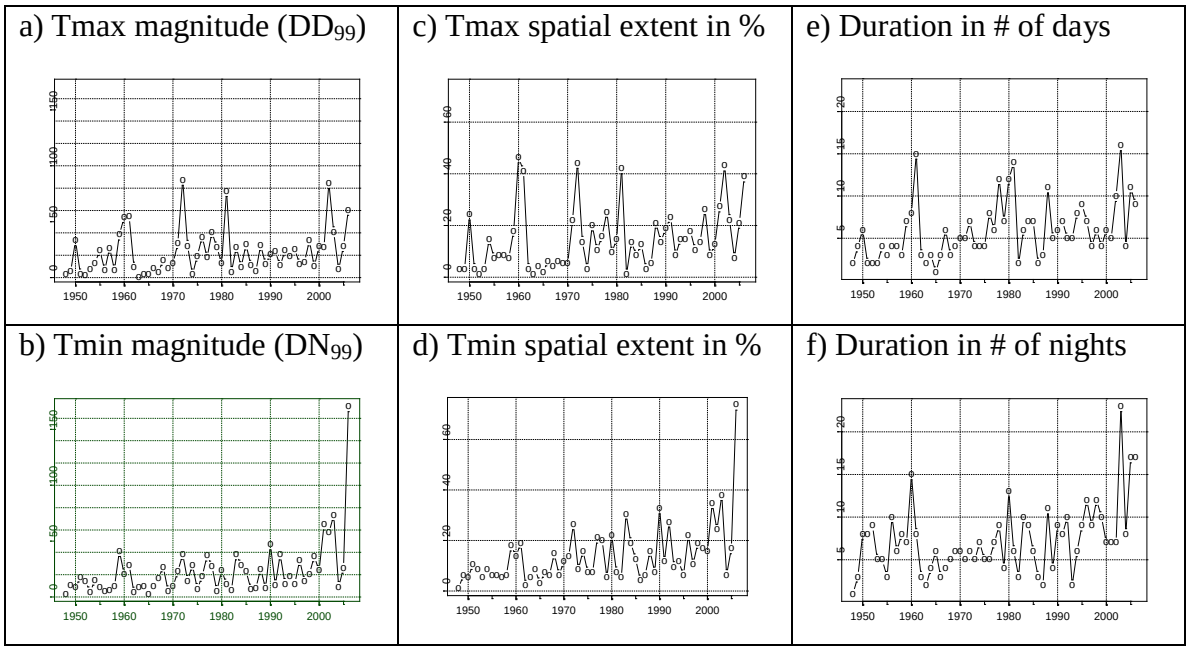

Total regional magnitude on the peak day (a) and night (b) of the greatest events, maximum spatial extent in % of stations by day (c) and night (d); and maximum continuous duration of daytime (e) and nighttime (f) heat waves.

All variables were computed for each summer on record from data presented in Figure 6.3.1. Note that the maximal components of day and nighttime heat wave activity do not always refer to the same events. Also, the greatest one-day (or night) magnitude or spatial extent is not always, for example not in every summer, associated with the longest duration. Correlations between these indices are given in Table 6.3.1.

Table 6.3.1: Correlation Between Maximal Heat Wave Components

Maximal components	MAGNITUDE	SP EXTENT	DURATION
MAGNITUDE	**0.46**	**0.96**	**0.58**
SP EXTENT	**0.91**	**0.46**	**0.65**
DURATION	**0.67**	**0.70**	**0.60**
TRENDS 1948:2006	**3.0* : 6.6*** **	**2.1** : 3.4*** **	**0.8*** : 1.0*** **
TRENDS 1950:1999	**0.7 : 2.5** **	**0.9 : 1.9*** **	**0.6** : 0.4**

This table shows correlation coefficient between, and trends within, the heat wave component indices displayed in Figure 6.3.1 for regional daytime (red) and nighttime (blue) heat waves. Correlations between daytime and nighttime heat wave components are displayed along the

main diagonal. All correlations of 0.4 and above are significant at the 99.9 percent level. Trends in appropriate units per decade (degree days for magnitude, percent stations for spatial extent, days for duration) are displayed along the bottom row with significance (*90 percent, **95 percent, ***99 percent). Table 6.3.1 confirms that peak spatial extent and magnitude are very closely correlated for both daytime and nocturnal events. They almost always refer to the same extreme days or nights. Duration and peak spatial extent are also closely related for both types of heat waves, although there are exceptionally active summers when the most extensive event is not the most durable (such as 1981). The somewhat weaker positive correlations between duration and peak magnitude suggest that heat wave duration is related to peak magnitude via a more direct relationship with spatial extent. Peak spatial extent (and magnitude) of daytime and nighttime heat wave activity are weakly (although, at ρ=0.46, certainly significantly) related; seasonal maximum duration of the two types of events is more strongly related (36 percent of interannual variance in common). It is likely that the more durable events tend to be those expressed robustly during day and night. Ranked (Spearman) correlations between daily-scale DD_{99} and DN_{99} (Figure 6.3.3) are highly variable from summer-to-summer but always positive and notably strong in years with strong heat wave activity during day and/or night (Figures 6.2.3 a and b and 6.3.1). This coupling between day and nighttime heat wave timing has been persistently strong during the recent summers of enhanced heat wave activity.

Figure 6.3.3: Ranked (Spearman's) Correlations Between Each Summer's Daily and Nightly Heat Wave Magnitude

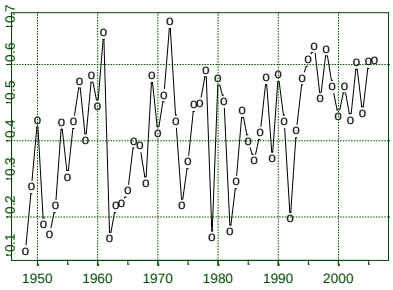

This reflects the degree to which day- and nighttime heat waves are coincident.

These observations reflect the fact that the timing of regional daytime and nighttime heat waves is usually coincidental; as seen below, they are nearly always produced by the same or similar synoptic atmospheric circulation features. However, their relative intensities as expressed during night and day vary a great deal. The most intense and extensive heat waves expressed primarily in Tmin or Tmax may therefore respond to profoundly different synoptic forcing features. This is addressed below. We will also see more clearly that the July 2006 heat wave, although consistent with increasing heat wave activity trends and shifts, cannot be entirely explained by these factors, especially where night-time temperatures are concerned. A closer look at the synoptic setting is required.

6.4 Anatomy of Great Heat Waves

Before considering synoptic causes of July 2006 compared to other large events, researchers describe the timing and canonical features of a handful of the largest day and nighttime events on record.

To illustrate the general appearance of and concurrence between great day- and nighttime heat waves, researchers identify these most extensive and intense day and nighttime heat wave episodes on record. Figure 6.4.1 presents the largest events for five most active summers, besides 2006, ranked according to results presented in Figures 6.2.4 and 6.3.1 and emphasizing instantaneously the largest (for example greatest peak magnitude), not necessarily the most durable, events.

Figure 6.4.1: Regional Degree Days (DD_{99}: a,b) and Nights (DN_{99}: c,d) Associated with the Greatest Daytime (a,c) and Nighttime (b,d) Heat Waves

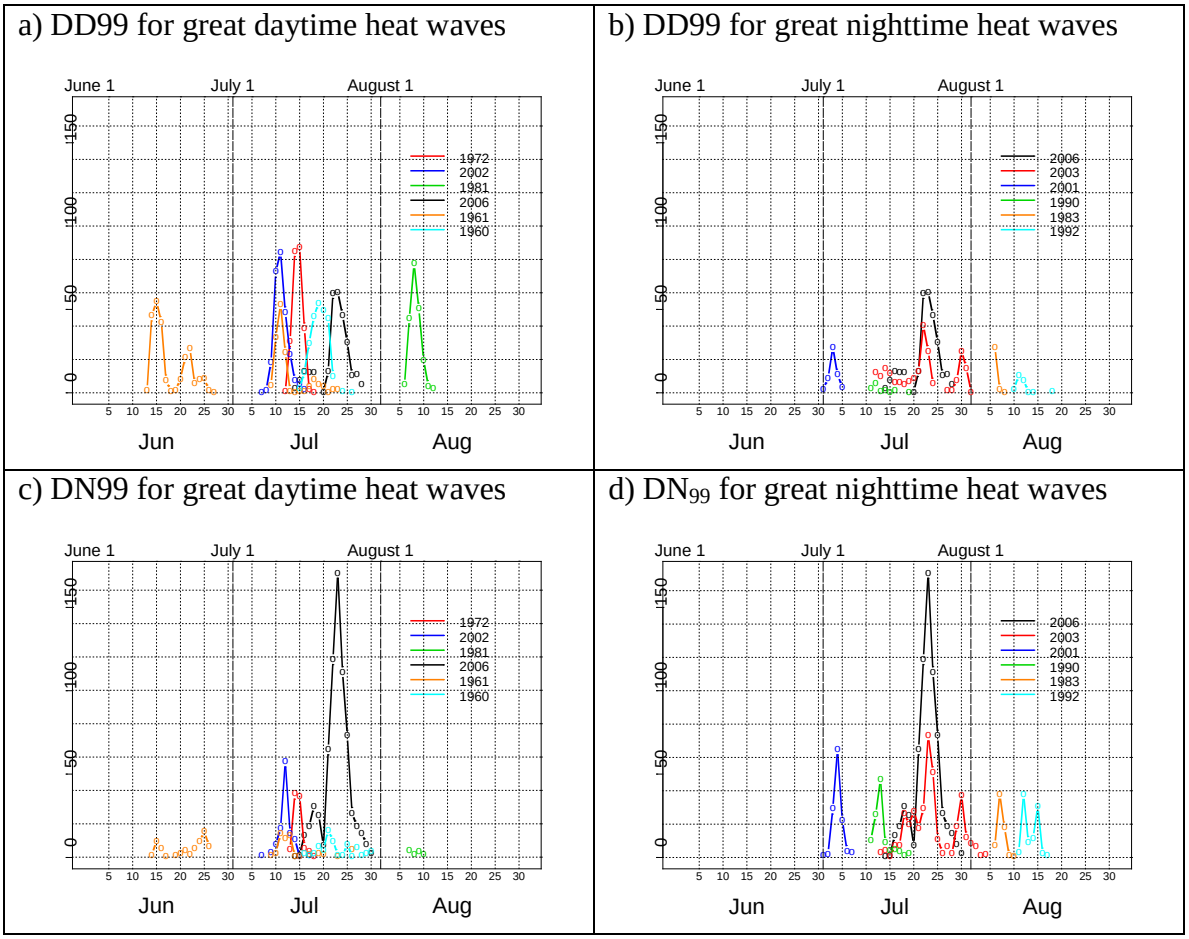

Figure 6.4.1 shows the magnitude of the largest events, which is closely related to spatial extent (Table 6.3.1). Events (colors) are arranged of decreasing peak magnitude. Only the main events for each of the chosen summers are shown. Note that the same colors refer to the same (different) events on the vertical (horizontal) panels.

The entire seasons' activity can be seen on Figure 6.3.1. Statistics for these events, moreover, are presented in Table 6.4.1 and discussed below. With the exception of July 2006, the largest daytime heat waves have been more extensive than the largest nighttime events (Table 6.4.1). Extreme nighttime heat accompanied the greatest and most extensive daytime heat waves to some degree (Figure 6.4.1a and c) and vice versa (Figure 6.4.1d,b); thus the moderate temporal correlations observed in Figure 6.3.3. Durations are generally about a week for most great heat waves, but can drag on for 2-3 weeks as occurred in 1961 and also in 2003 and 2006. Each great event has a well-defined peak date or two. Nighttime heat waves display a stronger preference for July than do their daytime counterparts (this is also confirmed by Figure 6.3.1 as well as other results based on lower thresholds, not shown). As far as spatial extent (Table 6.4.1), all six

of the great heat waves were of comparable scale, with about 40 percent of the stations registering extreme Tmax on the peak day. *In contrast, during the great nocturnal heat wave of 2006, 74 percent of our stations recorded extreme Tmin values on July 23, 2006, an event without recorded parallel on the 59-year record (Table 6.4.1)*. Notably, a hot prelude preceded the peak night (and day) of the event on July 23.

Table 6.4.1: Peak Dates of the Greatest Regional Heat Waves on Record Listed in Order of Largest One-Day and One-Night Magnitude (See Figure 5.5)

GREAT DAYTIME HEAT WAVES

Peak Date	Total Magnitude	Peak Sp Extent	Duration
1972, 7, 14	**273/120**	**44/26**	**7/6**
2002, 7, 11*	264/115	43/24	10/7
1960, 7, 19*	251/72	46/14	9/15
1961, 6, 15*	236/65	41/12	15/8
1981, 8, 8*	204/12	42/7	7/4
1961, 7, 11*	145/58	40/14	15/8

GREAT NIGHTTIME HEAT WAVES

Peak Date	Total Magnitude	Peak Sp Extent	Duration
2006, 7, 23	**709/286**	**74/39**	**17/9**
2003, 7, 23*	384/249	38/22	23/16
2001, 7, 4*	128/54	35/27	7 /5
1990, 7, 13*	116/14	33/19	9 /6
1983, 8, 7*	103/44	31/14	5/3
1992, 8, 12*	100/27	27/8	7/5

The events marked by an asterisk (*) are used for composite results in Figure 6.5.1. The great 2006 and 1972 events (bold) are treated separately. Overall magnitude, defined as the sum of DD_{99} and DN_{99} over the entire duration of the event and over all stations, associated with each event is given in red and blue font, as are peak spatial extent and duration. The station-by-station values of DD_{99} and DN_{99} anomalies are plotted for the 3 largest overall events (2006, 2003, and 1972) in Figure 6.4.3. The overall daytime and nighttime magnitudes are plotted in Figure 6.4.2.

Figure 6.4.2: Table 6.4.1: In Pictorial Form

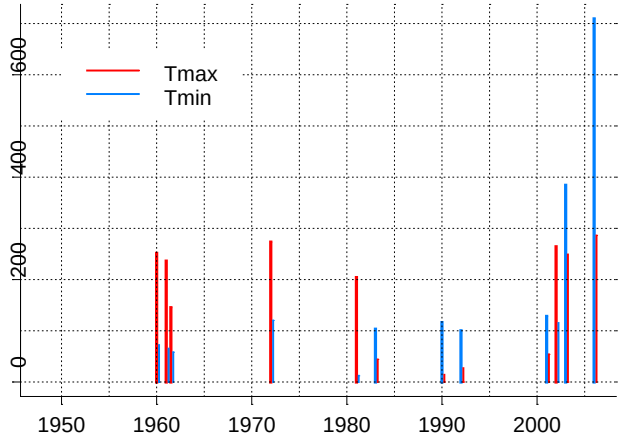

Overall magnitude is plotted. Thick (thin) lines delineate the heat wave's primary (secondary) expression, i.e. daytime or nighttime.

Overall heat-wave magnitude (Figure 6.4.2) better separates the largest events than duration or spatial extent alone. Nighttime heat waves used to be of smaller magnitude than daytime events, but this has lately changed. Nighttime events of 2001, 2003 and 2006 have each set successive magnitude records. Daytime heat wave activity is changing, not in magnitude but in the fact that the most recent great daytime heat waves were daytime components of even greater nighttime events, such as 2003, 2006. The order of the most intense heat waves is modified somewhat with respect to the merely most spatially extensive with the greatest events tending to occur towards the latter part of the record, especially at night (Figure 6.4.2). The 2006 event was by a large measure unprecedented in overall magnitude, again, specifically at night. During the day, July 2006 is fourth in terms of daytime peak intensity, but its rather impressive duration makes it number 1 among *daytime* events in terms of overall magnitude.

The spatial patterns of overall day and nighttime magnitude are shown for three of the largest events on record (2006, 2003 and 1972) in Figure 6.4.3.

Figure 6.4.3: Overall Magnitude for the Three Largest Heat Waves

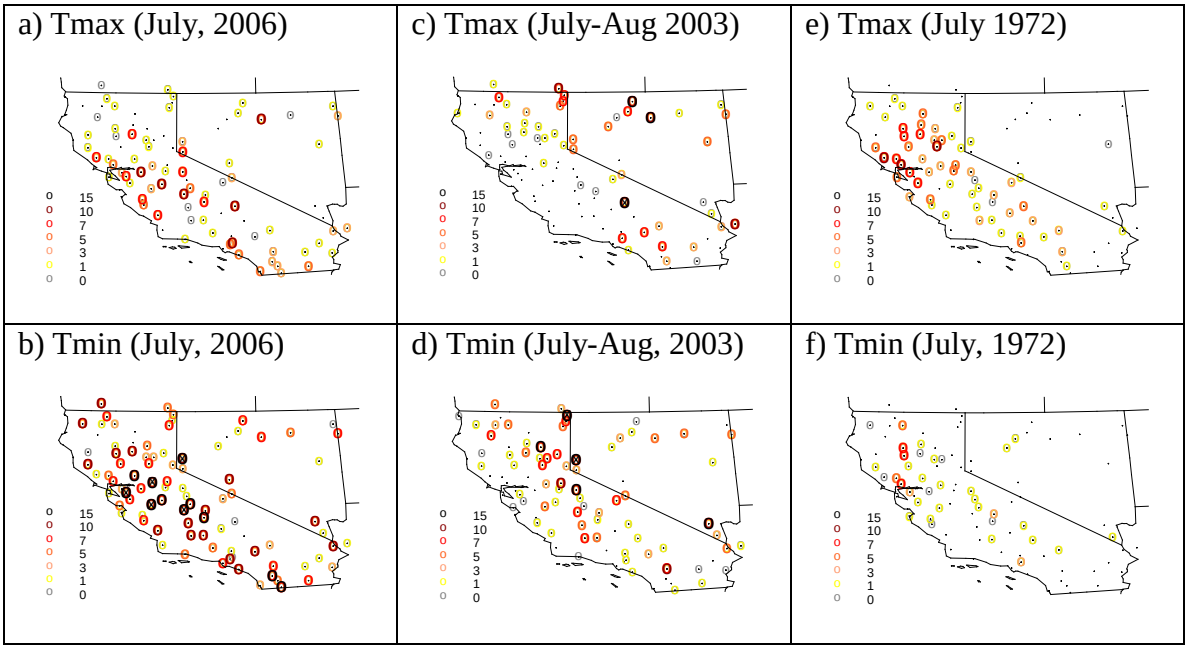

Local overall daytime (top panels) and nighttime (bottom panels) magnitude of the July 2006 event and the two next largest events. Station-level Degree Days (DD_{99}: a) and Nights (DN_{99}: b) are integrated over the duration of the 2006 event (July 15-30). Comparable results for July 12-August 4, 2003 (c and d) and July 12-18, 1972 (e and f). Black dots are the 95 core stations. Colored circles correspond to values exceeding those given in the legend, black "X"s mark values in excess of 20 degrees. Overall magnitude for each event is given in Table 6.4.1 and Figure 6.4.2.

6.5 Synoptic Aspects of Great Daytime and Nighttime Heat Waves

6.5.1 A Canonical View

We next describe mechanistic causes of great heat waves by compositing circulation anomalies at the surface (mean sea level pressure or MSLP and wind at sigma level 995) and the free atmosphere (500mb geopotential height) as well as precipitable water (PRWTR) on the peak day of the five largest daytime and nighttime events (Figure 6.5.1). These dates are marked with asterisks in Table 6.4.1. The two largest day and nighttime events (July 1972 and 2006) are treated separately below. Although including these events would not noticeably change the composites presented in Figure 6.5.1, these two events were rather different from the other great day and nighttime heat waves in several various and important aspects.

Figure 6.5.1: Composite Anomaly Maps

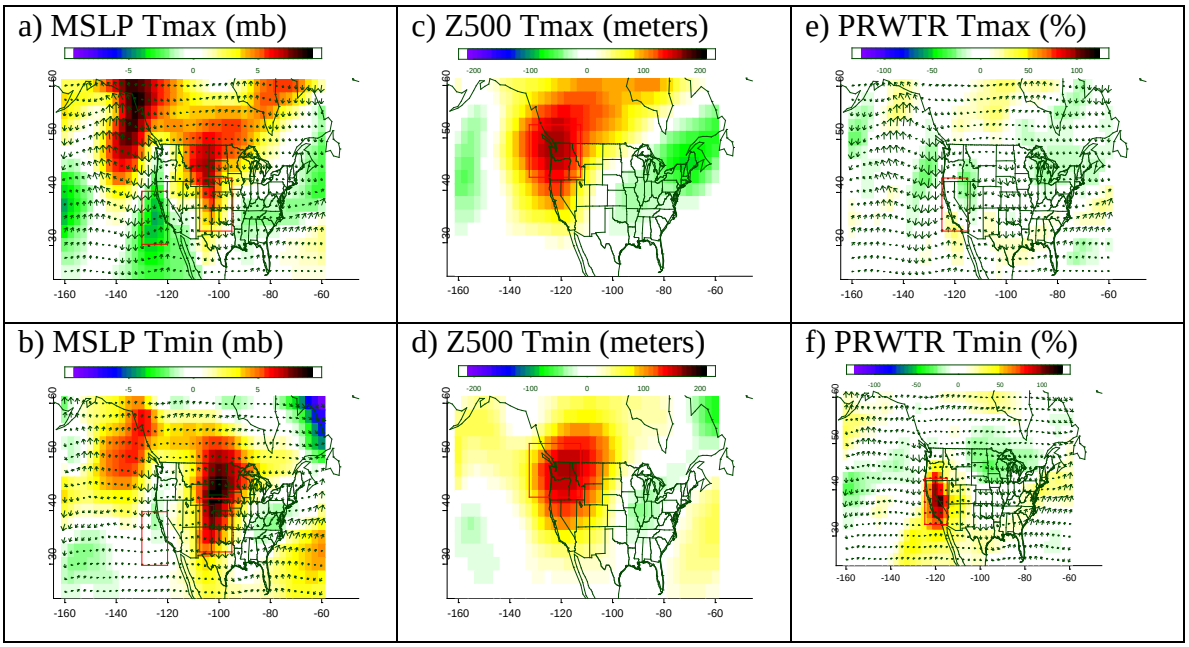

Figure 6.5.1 shows surface circulation (wind at sigma level 995) and mean sea level pressure in millibars (a and b), 500mb geopotential height in meters (c and d), and precipitable water in percent of normal content (e and f) anomalies with respect to JJA mean. Anomalies are composited for the peak days of the largest five daytime events (a and c and e) and the largest five nighttime events (b,d and f) excluding 2006 and 1972 (see Table 6.4.1 for exact dates). The data are from the NCEP/NCAR Reanalysis I (Kistler et al. 2001). Red rectangles outline regions used for evolution plots presented in Figure 6.5.4.

Great heat waves are set up by a layered structure in the atmospheric circulation involving horizontal and vertical motions conducive to hot regional weather (Figure 6.5.1a through d). The day and nighttime heat wave surface circulation composites (Figure 6.5.1a and b) show an anomalous surface pressure gradient sloping southwestward from the Great Plains to the Pacific Coast causing anomalous surface convergence into California. Regional circulation during the peak day in daytime events is characterized by an anomalous surface High that has moved[7] southward along the Front Range of the Rockies into the central and southern Great Plains, a surface Low off the California coast and a broad High several degrees longitude west of Washington coast. During peak daytime events, these features bring strong convergent surface winds into California from practically all directions. During peak nighttime events, the Great Plains High tends to be stronger and more extensive while the other features, including the California Coastal Low, are weaker making for a reduced anomalous convergence, especially from the Great Basin, for example, from the high Nevada desert. The circulation aloft

7 Dynamic cartoons of these maps spanning the evolution of events clearly show this development but cannot be fully reproduced in this static format.

(Figure 6.5.1c and d) consists of a broad and intense High centered above Washington State. During the two types of events, the anomalous high intensity is similar (about 160 geopotential meters), but the center of the High tends to be displaced zonally by a couple of degrees so that during daytime (nighttime) events it is centered over western (eastern) Washington. It is difficult to assess the absolute significance of these slight differences since they may be due to small sample size as well as to differences in the timing with respect to circulation of the most intense day and nighttime events. These differences between the two types of canonical events are certainly within the range of variability of the two five-day samples. In any case, the circulation at the surface as well as aloft appears rather similar for both day and nighttime event peaks.

The observations indicate that it is the atmospheric moisture content, rather than circulation that determines whether a heat wave is predominantly a daytime or nighttime event (Figure 6.5.1e and f). Nocturnal events are about twice as moist (PRWTR anomaly of more than twice the normal ~18 kg/m2 for JJA averaged over this arid region). For daytime events, the anomaly is slightly drier than normal over California and Nevada. It is not generally cloudy and, aside from occasional mountain and desert thunderstorms, does not rain over this arid region in summer even during the hot spells of the humid nocturnal variety. It seems clear that the enhanced greenhouse effect of water vapor is what mainly elevates nighttime temperatures during nocturnal heat waves. This regionally enhanced greenhouse operates during the day as well, to be sure, but the moisture also tends to reduce somewhat the incident solar radiation, particularly over topography where convective cloudiness develops in hot moist conditions. Compared to humid heat waves, in dry heat waves the daytime temperatures heat up due to stronger surface absorption of direct sunlight, while at night the surface cools more efficiently by emitting long-wave radiation. Slight differences in circulation may play a minor role, but those differences are likely also related to moisture advection. As the heat wave circulation develops, the existence of a moisture source to the south and/or east of southern California appears to make the difference between a primarily day or nighttime event. The intensity of the southwest monsoon, for example, can play an important role in this regard. As will be shown, there is also evidence for a warm sea surface temperature-associated moisture source directly to the south of the region. The atmospheric moisture content and its role in regulating the surface energy balance is the main reason why all large Californian heat waves can be classified into *primarily* daytime and nighttime events.

6.5.2 July 1972

The 1972 heat wave was the largest purely daytime event, but it differed considerably in its circulation from the other great heat waves. The associated spatial pattern of intense heat can be seen on Figure 6.4.3e and f. The 1972 event featured a surface High over British Columbia with a southeastern branch extending into the Great Basin. Together with a pronounced Low over the central California coast, creating a state-wide version of a Santa Ana condition, for example strong northeasterly flow from the high deserts down into the low valleys of interior and coastal California. This produced subsidence, drying and adiabatic heating. The upper-level anticyclonic circulation was displaced southwestward of its canonical location and moisture levels were below normal over California. For brevity, these results are not shown, but because

this event was, in terms of synoptic circulation, so different from the rest, researchers exclude it from daytime event composites.

6.5.3 July 2006

Figure 6.5.2: July 23 2006 Anomalies of MSLP and Wind at 995 Sigma Level (a), 500m Geopotential Height (b), and Precipitable Water (c)

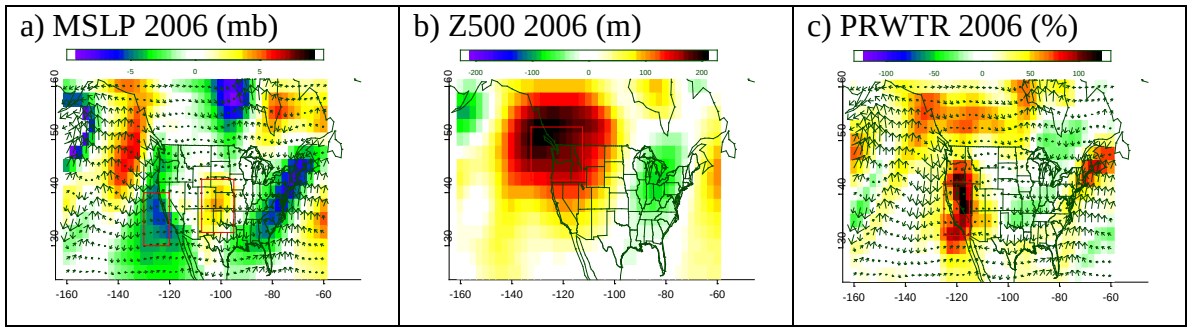

Units are the same as in Figure 6.5.1.

The peak of the 2006 event was characterized by surface circulation rather similar to other great heat waves, especially those of the daytime variety. In this case, the anomalous high over the central and southern Great Plains was somewhat weaker and the surface Low off the California coast was unusually strongly developed. Strong teleconnections were present upstream and downstream of these regional MSLP anomalies. At the 500mb level, the geopotential height over Washington State was impressive with a positive anomaly of 206 meters. There was enhanced moisture over the region, with a positive anomaly over Nevada reaching 121 percent of normal summertime moisture content there[8]. On July 23 2006, moisture over most of California reached levels that were comparable with other great nocturnal heat waves. While these values are impressive, they are only one component explaining why the July 2006 heat wave was so exceptional in its magnitude. To better understand its enormity requires a view of its time evolution rather than just a static snapshot of the peak date.

6.5.4 Synoptic Evolution of Great Heat Waves

Figure 6.5.3 more precisely compares the evolution of the 2006 event regional magnitude to the canonical day and nighttime event. Apparently, the moderate nighttime event peaks tend to precede large daytime event peaks. 2006 trumped all other nighttime events, it was more durable than most other intense heat waves, day or night, and it was also noteworthy in the fact that it was preceded by a sizeable day and nighttime warming occurring over several days and 3-5 days before the onset of the main event that peaked on July 23.

8 The main thrust of the event, however, was over California, especially intense over the central part of the state at night (Figure 5.10a and b).

Figure 6.5.3: Evolution July 2006

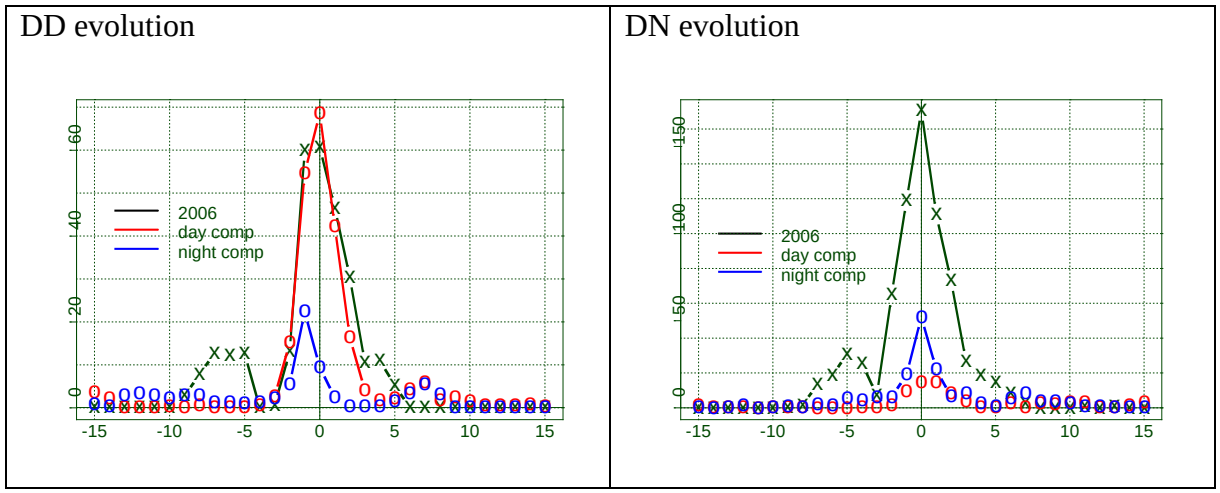

Regional DD_{99} (a) and DN_{99} (b) magnitude compared to composite evolution of 6 other major day and 5 nighttime events from 15 days before to 15 days after the peak magnitude of events. Degree Day (a) and Degree Night (b) evolution.

Figure 6.5.4,addresses the evolution of circulation and moisture anomalies in July 2006 compared to the canonical daytime and nighttime events. Results show the temporal evolution of key circulation and moisture indices of day and nighttime heat wave activity, for example, surface pressure gradient expressed as difference of MSLP anomalies over the central/southern Great Plains and coastal California waters, circulation aloft (Z500 over Washington, and precipitable water averaged over California and Nevada. Simultaneous examination of Figures 6.5.3 and 6.5.4 shows how typical intense events develop and how the 2006 event developed differently from most intense heat waves on record.

Figure 6.5.4: Evolution of Circulation Anomalies

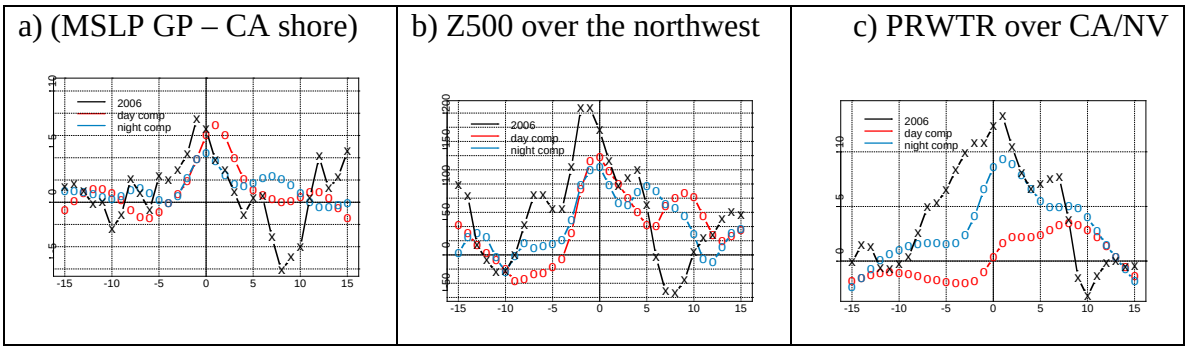

Evolution July 2006 compared to composite evolution of 5 other major day and 5 nighttime events from 15 days before to 15 days after the peak magnitude of events. All indices were averaged over rectangles outlined in red over relevant plates on Figures 6.5.2 and 6.5.3 and anomalies computed relative to JJA climatology. MSLP gradient (Great Plains box – California Shore box: a), Z500 averaged over the Washington box (b), and PRWTR anomaly averaged over the California/Nevada box (125 –115W, 42.5 – 32.5N, c). Thick red and blue lines with O's are canonical average daytime and nighttime event evolutions. Thick black and yellow lines punctuated with X's represent evolutions of the 2006 event.

Once the circulation associated with the typical day or nighttime event ramps up, Tmax heats up fast, and if the moisture source is available, moisture is advected over the region very quickly, which intensifies the nighttime magnitude while putting a cap on daytime warming. Daytime events apparently tend to be preceded by a low pressure aloft over the northwest and a quick build-up of the High. The circulation build-up to the nighttime events is more variable over this region and depends much more on moisture availability and a surface circulation conducive to advecting it over the region sometimes ahead of the developing heat wave. The 2006 event is an example of this early moisture advection coupled with an early development of the surface pressure gradient and the high pressure aloft. The circulation associated with the 2006 event set in very early and strong, especially aloft, where the timing was the earliest and the magnitude of the Z500 anomaly was also the largest of any other event on record. In 2006, moisture was available early and kept accumulating over the region throughout the event and also apparently to unprecedented levels compared to other events on record. This anomalous moisture was consistently pumped into the region from a Pacific source to the south of southern California (animation result cannot be shown). The early development of the heat wave circulation and the tremendous and early availability of moisture apparently gave rise to the hot and moist "prelude" that, after a short lull in the circulation, intensified into the heat wave of July 2006. The unprecedented moisture available so early coupled with a primer of hot temperatures and a suddenly intensifying circulation gave rise to a nighttime heat wave of enormous magnitude. Daytime temperatures were able to rise to remarkable levels and over an impressive space-time scale, much more so than during any other large nighttime event, largely because early mornings were so hot already before the solar heating set in. Tmin and Tmax interacted constructively and persistently to sear California over the last two weeks of July 2006.

6.6 Trends

From the above account, it is clear that the causes of heat waves over California and Nevada are complex and that numerous conditions coincided to create the unprecedented heat of July 2006. One of these conditions, touched on in the beginning of this article, is the trend especially in nighttime temperatures which intensified greatly since 2000 and must be related to the increased probability of larger nighttime heat waves. As the 2006 and 2003 events suggest, such events can spill over into, or prime the environment for, greater daytime heat associated with primarily nighttime events. This may account for part of the trend observed in daytime heat wave activity as well. In any case, the strongest trend and the best possibility for its physical explanation are shrouded in the hot and humid darkness of the night. In this last part of this article, researchers will try to shed some light on this matter by focusing on long-term changes in heat wave activity over this region.

The yet incomplete final decade on our record (1998 – 2006) has already produced much stronger heat wave activity than any of the previous five decades, during both day and night. For nocturnal heat waves especially, the trend towards greater heat wave activity is apparent as an orderly progression from one decade to the next (result not shown). The increasing relative magnitude of nighttime versus daytime heat waves is also apparent. This raises the obvious question: Is humidity increasing over the region? Our results, based on the available Reanalysis and sparse *in situ* dew point and radiosonde records, are inconclusive on this point[9]. There is a possibility that the relevant regional humidity changes are episodic, such as triggered by the synoptic nature of the heat wave circulations and therefore not clearly manifested except during heat waves. But what mechanism could possibly account for such a trend?

Let us now consider the connections between regional summer climate and large-scale Pacific sea surface temperature (PSST) patterns. Summertime Tmax and Tmin (Figure 6.2.1 c and d, respectively) should be differently related to PSST. Summertime Tmin and its predictability over the western and central U.S. are mainly related to Pacific SST, while Tmax is more strongly related to local soil moisture (Alfaro et al. 2006). At first glance it is not surprising then, that JJA average Tmin over California and Nevada is more strongly related to PSST than is Tmax (Figure 5.15a and b).

9 Warm humid nights are becoming more frequent, but apparently not more humid, while warm dry days are becoming a little more humid since the 1970s – although the overall trend is not significant due to an apparent moist bias in the reanalysis in the very early part of the record. Average seasonal and July PRWTR amounts are also on the rise since the 1970s but not significantly so, again because of the moist early 1950s in the Reanalysis. The in situ data do not support this moist anomaly in the 1950s, but these very sparse data they do not show clear and consistent trends either.

Figure 6.6.1: Correlations with Sea Surface Temperature

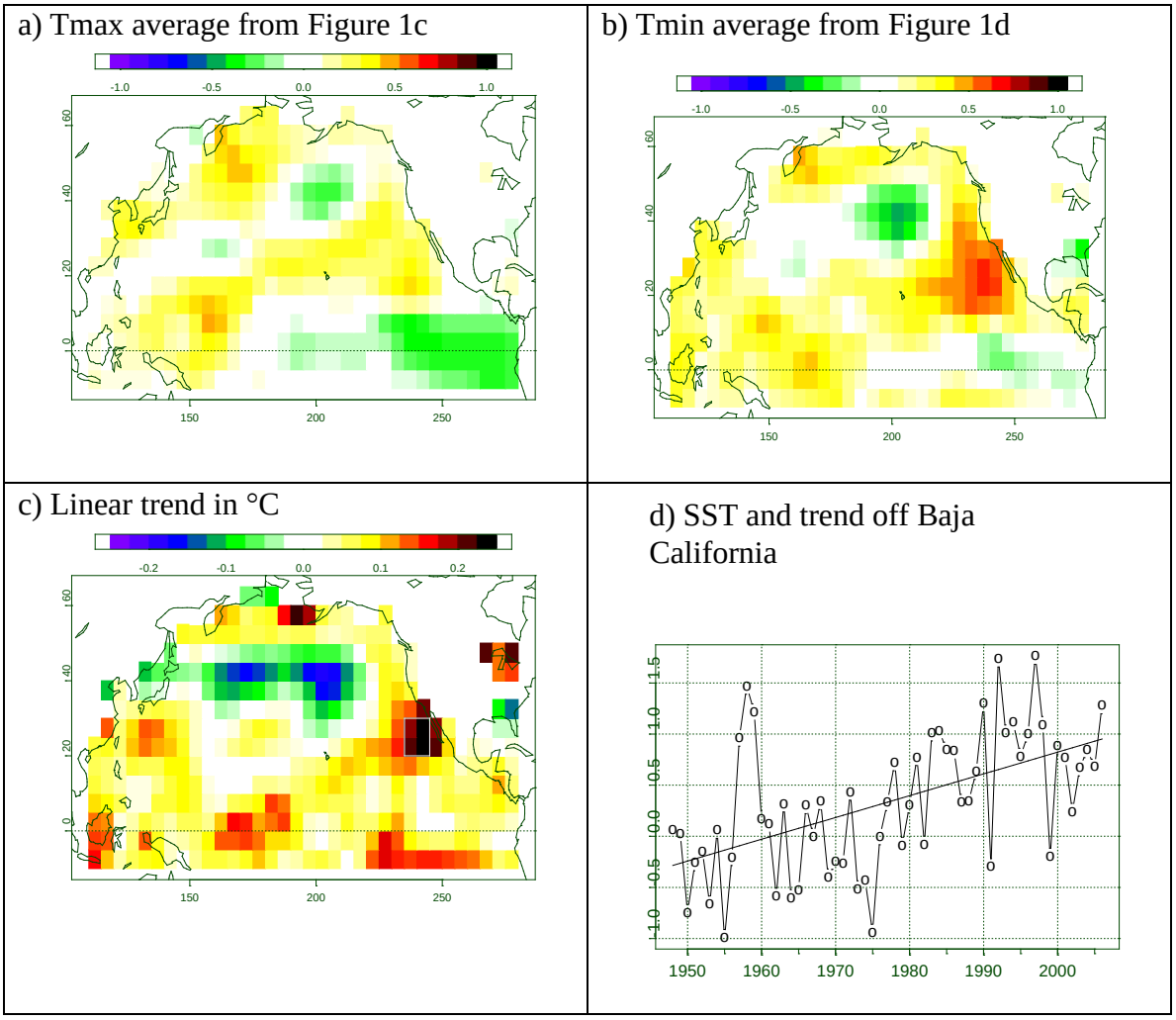

Figure 6.6.1 shows correlation coefficient between June-August averaged SST[10] and contemporaneous region-averaged Tmax (a) and Tmin (b) as shown in Figure 6.2.1c and d. Linear trends (c) in SST are predominantly positive. The time series of SST averaged in the white box off of Baja California (BSST) is shown with linear trend (d). The linear trend accounts for 33 percent of BSST variance. The correlation coefficient between BSST and average Tmin (Tmax) is 0.63 (0.32). Much of this correlation is due to the similar trend in the regional Tmin time series. Interannual correlations (with trends removed) are lower, but also significant at 0.44 (0.29).

10 Monthly SST anomalies from KAPLAN EXTENDED v2: Statistically homogenous concatenation of Kaplan et al. (1998) OS SST, Reynolds and Smith (1994), Smith and Reynolds (2004) NCEP OI analyses.

http://ingrid.ldeo.columbia.edu/SOURCES/.KAPLAN/.EXTENDED/.v2/.ssta

As noted by Alfaro et al. (2004), California summer temperature is clearly related to the North Pacific decadal Oscillation (NPO). It is curious, however, that the strongest correlations between regional average Tmin and Pacific SST are found not off the California State coast, but rather directly to the south, just east of Baja California, Mexico. This is a region where a strong positive trend in SST is observed (Figure 6.6.1c and d). Others have detected this regional trend as well, and it appears to be a prominent part of the global ocean warming observed in conjunction with anthropogenic climate change (Pierce et al. 2006, their Figure 6.7.4). Can the intriguing connection between SST off Baja California and the observed trend in average summertime Tmin arise in part from the influence of this regional SST trend on California nighttime heat wave activity? As seen, heat wave circulations advect air from this region off Baja California. Is the moisture content of this air affected by the underlying SST trend?

The spatial pattern of the trend in precipitable water is presented in Figure 5.16. Although researchers cannot see a moistening over California[11] and Nevada, Figure 5.16 (a and b) clearly shows a moistening over the region of warming SST east of Baja California (BSST, Figure 5.15c) where a strong correlation between SST and average Tmin was observed (Figure 6.6.2b). This trend makes anomalous moisture more readily available for California heat wave circulations to advect and more frequently and preferentially intensify the nocturnal expression of California heat waves. Great nocturnal heat waves are characterized by enhanced moisture availability east of Baja California for about 10 days before and after the peak of the event (Figure 6.6.2c). Heat wave circulations advect air northward from this region to California (Figure 6.6.2d). This is exactly what happened in 2006, but that time, the anomalous moisture was available earlier and advection occurred days before the onset of the main event (Figures 6.6.2c and d, 6.5.3c), preconditioning this great heat wave to be expressed most strongly at night.

11 There is a curious localized drying trend over southern California/Northern Baja and this is probably related to the wet (bias?) period in the late 1940s – early 1950s over the region in Reanalysis data (Figure 6.6.2). The point (localized) nature of that trend suggests that it may in fact be an artifact of an assimilated data point around the Salton Sea area. Is it due to the drying of the Salton Sea? This issue is interesting, but only tangential to the current focus.

Figure 6.6.2: (a) Linear Trend Computed at Each Pixel of the PRWTR Averaged for July. (b) July PRWTR in A Box 130-117.5W, 25-27.5N and Linear Trend, c) Daily PRWTR anomaly in the same box for 15 days around the peak of great daytime and nighttime heat waves as well as the 2006 event (as in Figure 6.5.4). (d) Same for the v-component of the surface-level wind in a box 125-117.5W, 32.5-25N, representing the northward advection from the region east of Baja to California.

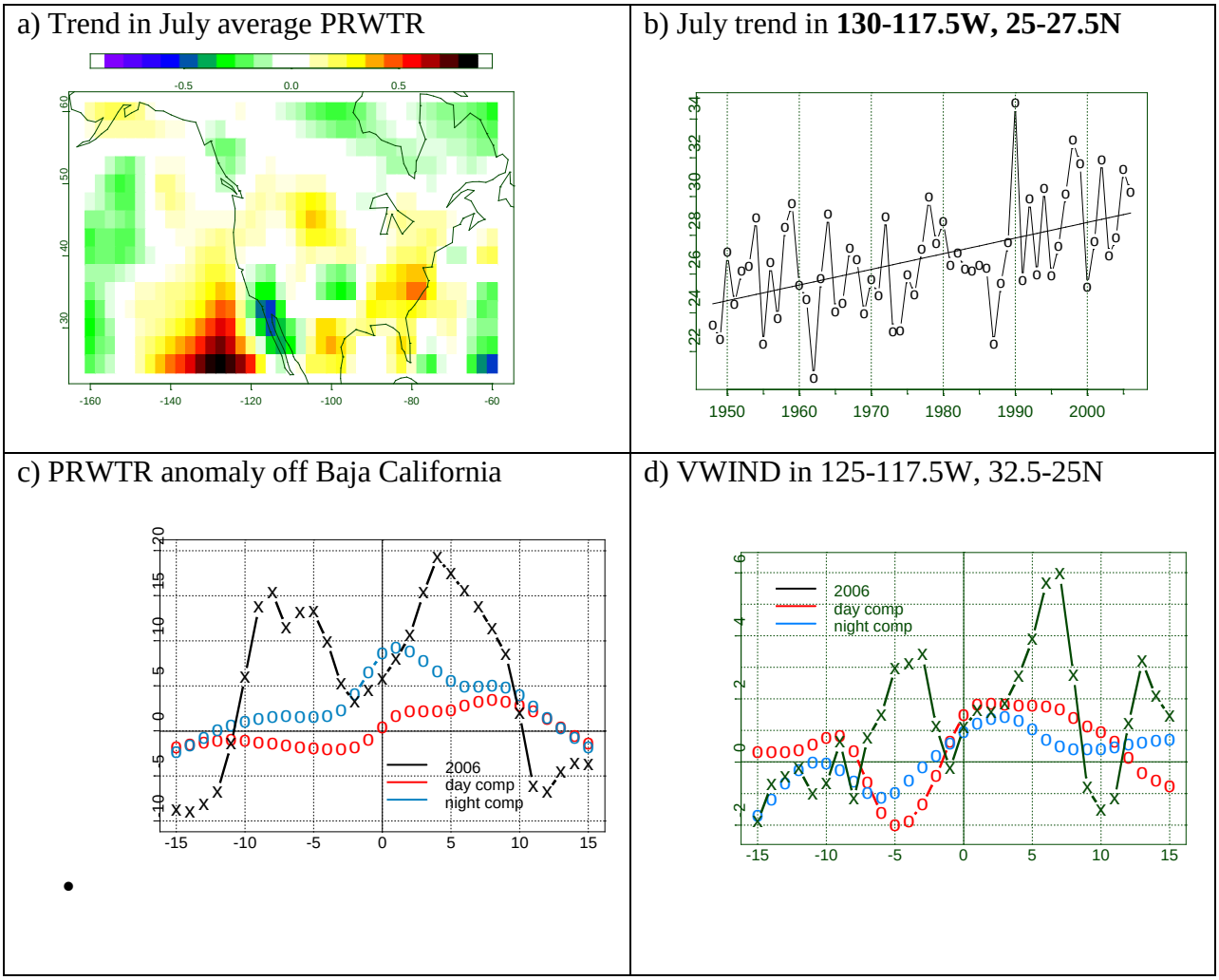

The trend explains 24% of the time series and is correlated at ρ=0.4 with regional average Tmin (Figure 6.2.1d), ρ= 0.15 without the trends.

The strong and trendy relationship between regional average summertime Tmin and BSST (Figure 6.6.1b) can therefore at least partially be explained by the effect of BSST via atmospheric moisture, advected via heat wave circulations, on Tmin extremes. This moistening does not occur frequently enough to make for clearly detectable summertime moisture trends over California and Nevada, but its episodic effect on Tmin extremes is apparently strong enough to be partially reflected in average summertime Tmin over the region. This at least partially explains the relationship between average Tmin and BSST (Figure 6.6.1b) as well as the observed trend in summertime average Tmin via nocturnal heat wave activity. This is an

inherently regional explanation[12]. Examination of mechanisms driving the BSST trend is beyond the scope of this study. The trend may be part of the NPO evolution, but does not display the NPO's shifty behavior. This trend has been observed as part of the general warming of the world's oceans (Pierce et al. 2006) and certainly merits closer investigation as it provides an important link between global climate change and regional weather extremes over the California region.

6.7 California Heat Waves, Predictability and Future Evolution

Our observational work on heat wave activity in the California region shows that heat waves are becoming more humid and expressed more strongly in nighttime temperatures. These changes are undoubtedly having significant impacts on public health and energy demand, both its magnitude and timing, as cooling is required more often at night and also more intensely and at lower temperature thresholds during the day because people have less tolerance for (and, especially in California, acclimatization to) humid heat than dry heat. Both the interannual and long-term variability in California heat wave activity has been shown to be related to sea surface temperature in the North Pacific and, especially, off the coast of Baja California (BCSST, Figure 6.6.1c and d). Can skillful seasonal forecasts of heat wave activity in California be made based on Pacific SST patterns? Can the observed trends in California heat wave activity be expected to continue? The main key to answering both questions appears to be in the interannual and long-term behavior of BCSST. Let us examine this behavior and its relevance for summertime temperature predictability in California.

12 Another part of the explanation for seasonal average Tmin warming may be similar to that which explains Tmin trends observed over most other regions around the globe (Easterling et al. 2000), but a clear mechanism that works for all regions has not yet been proposed. Regional mechanisms are being clarified for selected regions and they typically point to enhanced greenhouse gases including water vapor (Philipona et al. 2005).

Figure 6.7.1: Total Linear Trend in BCSST (1948 – 2006) by Month

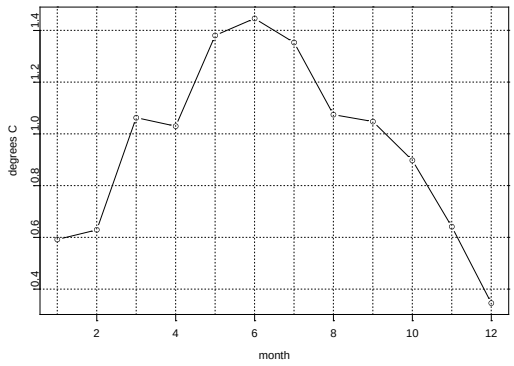

The trend in BCSST has a distinct seasonal cycle with maximum trend (1.4°C over the 59 years of record) observed in the May, June and July, more than twice that observed in winter and mostly associated with the 1970s shift in the Pacific Decadal Oscillation (PDO).

We know that California summertime temperatures are correlated with the spring PDO accounting for useful predictability (Alfaro et al. 2004). Some of this predictability may be related to BCSST. Computing the correlations between monthly BCSST and California nighttime summer temperature (Figure 6.2.1d) gives us maximum contemporaneous correlations (~0.65) with August BCSST and useful antecedent correlations (~0.45) with May and April BCSST. However, when the linear trend is removed from both series, the antecedent correlations fall below useful significance (see blue curve on Figure 6.7.2). Researchers conclude that, although BCSST explains a significant part of contemporaneous summer-to-summer minimum (and to a much lesser extent, maximum, figure not shown) temperatures in California, useful predictability is mostly associated with the long-term increasing trend in both series.

Figure 6.7.2: Correlation Between California Monthly BCSST and JJA Average Nighttime Temperature (Figure 6.2.1d)

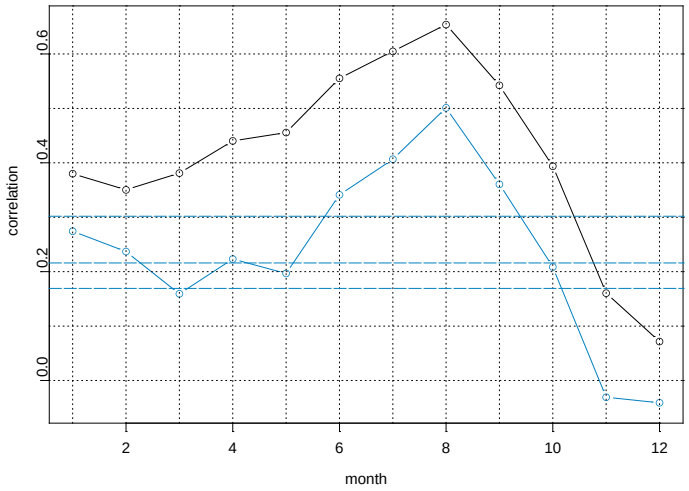

Black line – raw data, blue line – detrended series. Dashed blue lines represent 90, 95 and 99% significance levels for correlations coefficients of the detrended series.

Some of this potential predictability power of BCSST is related to BCSST's partial dependence on the PDO, the large scale structure of the North Pacific SST field (Alfaro et al. 2004). But BCSST is not entirely PDO-related. The PDO has very different seasonal structure of trends (Figure 6.7.3), peaking in February and March and mostly due to the mid-seventies PDO shift.

Figure 6.7.3: PDO Trend by Month Computed from De-Trended SST Using the Monthly Index of N. Mantua

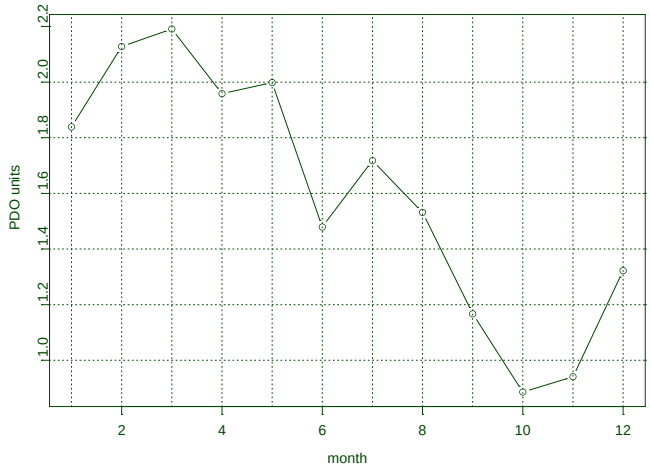

Source: http://jisao.washington.edu/pdo/PDO.latest

Noting that the summertime BCSST (JJA BCSST, as in Figure 6.6.1d) is best related to the antecedent May PDO index (Figure 6.7.3, but even the previous summer PDO can potentially provide a useful BCSST prediction at one year lead), researchers regress the May PDO, for example the large scale variability, out of the summertime BCSST to obtain the residuals, the regional part of the BCSST variability (Figure 6.7.5). We note that the regional BCSST index exhibits a significant trend.

Figure 6.7.4: Correlation Between JJA BCSST and Monthly PDO. Red Segment Shows the Months (JJA) Over Which the BCSST Index was Computed

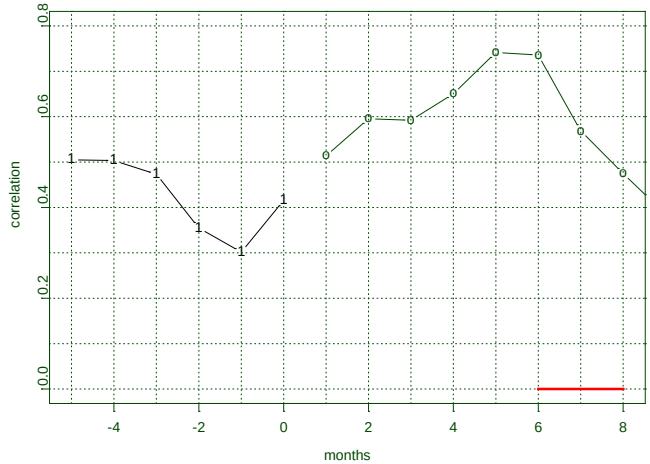

Figure 6.7.5: Residuals from the May PDO – JJA BCSST Regression and Trend. the Trend is Significant (P = 0.0327)

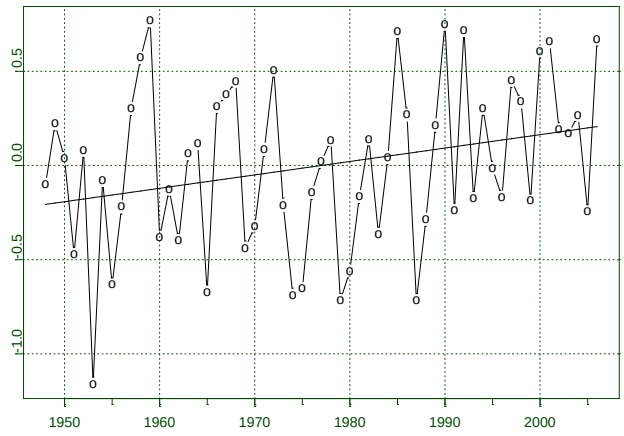

The regional BCSST index is composed both of interannual variability and a long-term trend. Researchers examined the relationship of this regional index with large-scale antecedent and contemporaneous Pacific sea surface temperature patterns and, interestingly, in spite of dynamical reasons to expect it, did not find any relationship between El Niño/Southern Oscillation (ENSO) and BCSST (Figure 6.7.6).

Figure 6.7.6: Correlations Between Monthly Pacific SST and JJA BCSST Residuals(Figure 6.7.5)

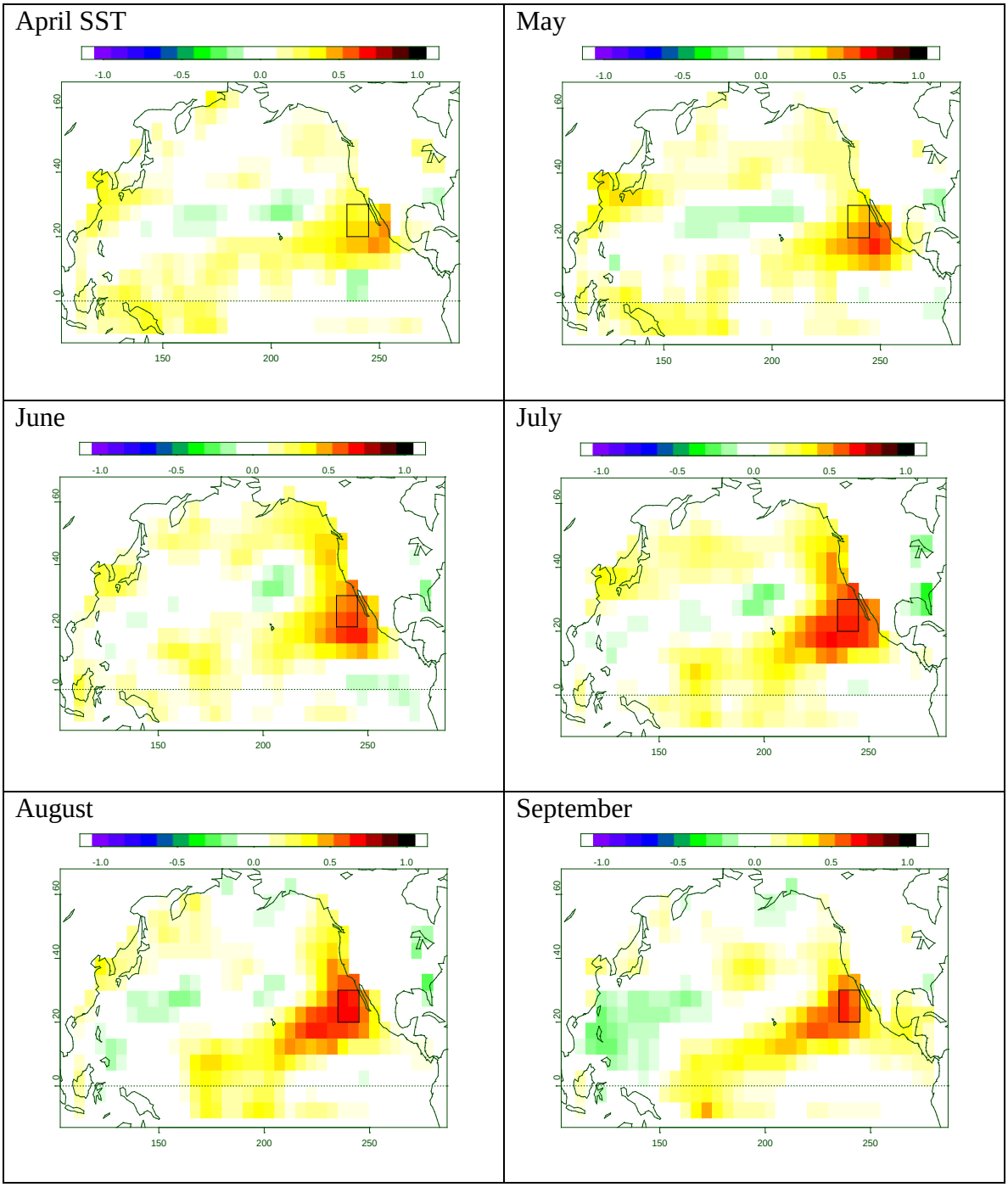

In an effort to find dynamical causes for the regional summertime BCSST variability, researchers have also examined relationships with atmospheric circulation (sea level pressure, surface wind, 500mb height) as well as with surface latent heat flux and evaporation and cloudiness. These results are not shown. They all point to the fact that this regional BCSST variability must be related to internal ocean dynamics and is itself the likely cause of contemporaneous atmospheric variability including the enhanced regional atmospheric moisture content that researchers have shown to be responsible for the observed variability and long-term changes in California heat wave activity. Although observed California heat wave evolution is consistent with observed climatic changes over many parts of the world, it does have a strong regional oceanographic origin and researchers cannot yet speak with certainty about the specific dependence of these regional changes on global climate processes of anthropogenic character.

We also note that examination of regional projections of summertime temperature and heat wave activity over California and Nevada by three global dynamical models (GCMs), although strongly trending upwards, do not, with one notable exception, capture the observed differences in trends between daytime and nighttime temperatures and heat wave expressions.

The one exceptional model, the CNRMcm3 fully coupled atmosphere-land-ocean model of the National Center for Meteorological Research of the French Meteorological Service (Météo-France), shows clear tendencies in California heat wave activity that are remarkably close to those observed (Figure 6.7.7).

Figure 6.7.7: Average (Top Panels) and Extreme (Bottom Panels) Maximum and Minimum Temperature Indices Over California and Nevada

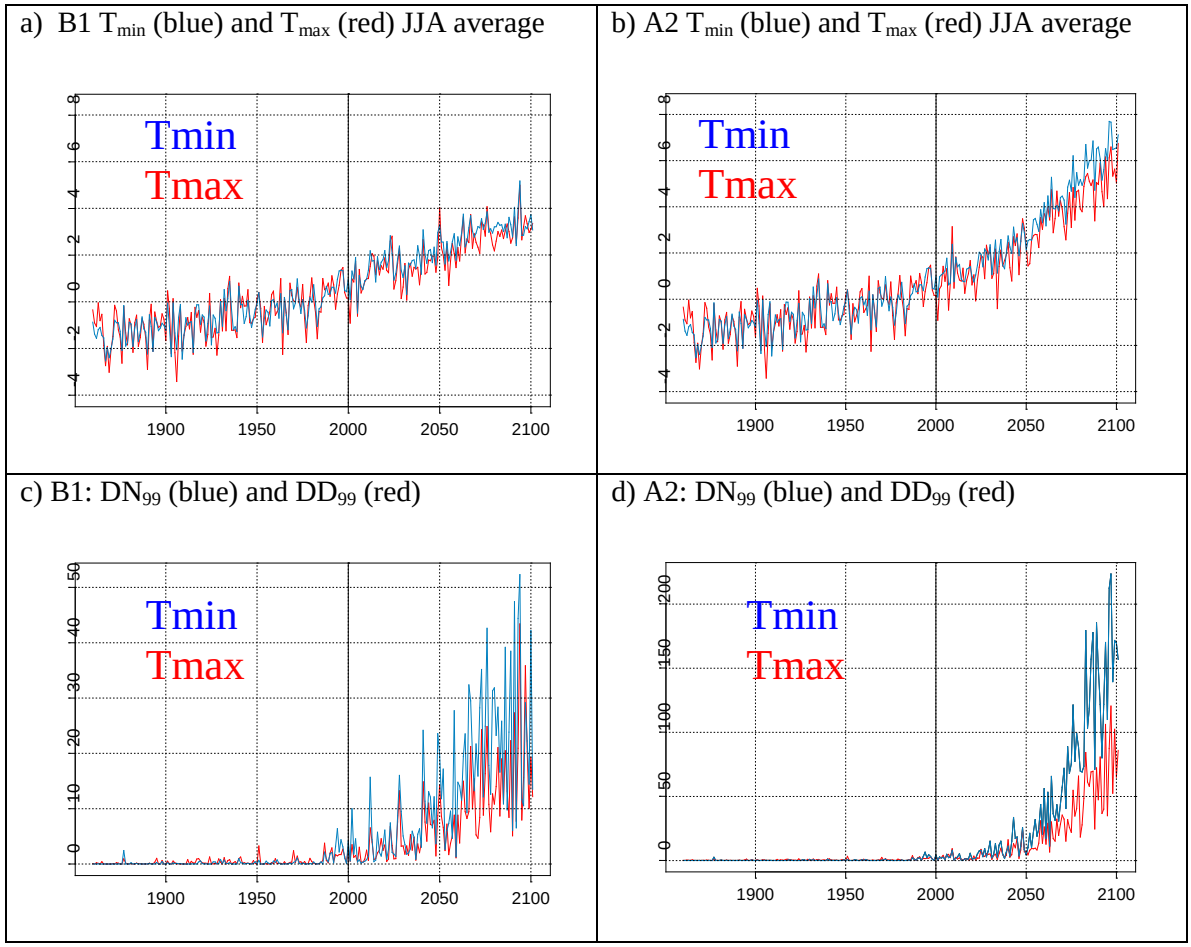

Integrated over the historical and future climates using the CNRM-cm3 global dynamical model.

The future climates follow the B1 (left panels) and A2 (right panels) global emissions scenarios. Scenario B1 assumes enlightened action on the part of governments to control emissions and population, while A2 represents the business-as-usual scenario. Panels a and b present model information complementing and extending the observations presented in the bottom panels of Figure 6.2.1. Bottom figures present model indices identical to the observations presented in Figure 6.2.3, top panels.

The CNRM model is able to capture the observed behavior of heat wave activity over the California region surprisingly well. Although negligible differences between the Tmin and Tmax average summertime trends are modeled during the historical period, heat wave events begin to show a preference for nighttime extreme temperature outbreaks at the very end of the 20th century. This preference turns into a clear trend during the 21st century. Moreover, under the business-as-usual (A2) scenario, the future trend towards enhanced nighttime heat wave

activity relative to the increasing daytime heat waves is much larger than that under the milder B1 scenario. This difference in A2 versus B1 heat wave activity is clearly seen on Figure 6.7.8.

Figure 6.7.8: Daytime – Nighttime Regional Heat Wave Indices ($DD_{99} - DN_{99}$)

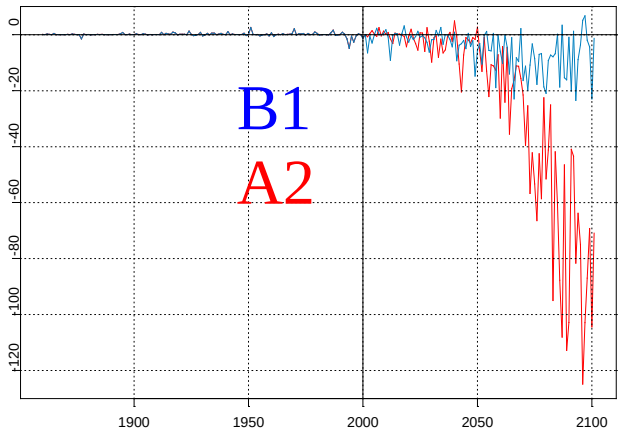

Negative values represent stronger nighttime relative to daytime heat waves over California and Nevada. Modeled by the CNRM-cm3 model.

The CNRM-cm3 model is able to capture the observed changing character of regional heat waves over California and Nevada. In this model, observed changes can be attributed to the regional effects of global anthropogenic climate change. Moreover, the enlightened governance (B1) scenario shows the nighttime preference of heat wave activity stabilizing after initial growth towards the last third of the 21st century, while the business-as-usual (A2) scenario continues to severely accelerate this tendency throughout the century. This acceleration is strong enough to be reflected clearly in average summertime maximum and minimum temperatures towards the end of the century (Figure 6.7.7b).

Another model, however, the GFDL-cm21, shows the opposite differential trends in California heat wave activity: stronger tendency for hot daytime temperatures relative to hot nighttime temperatures (Figure 6.7.9), while another model, the NCAR PCM1 does not show coherent differences.

Figure 6.7.9: Daytime – Nighttime Regional Heat Wave Indices (DD_{99} – DN_{99})

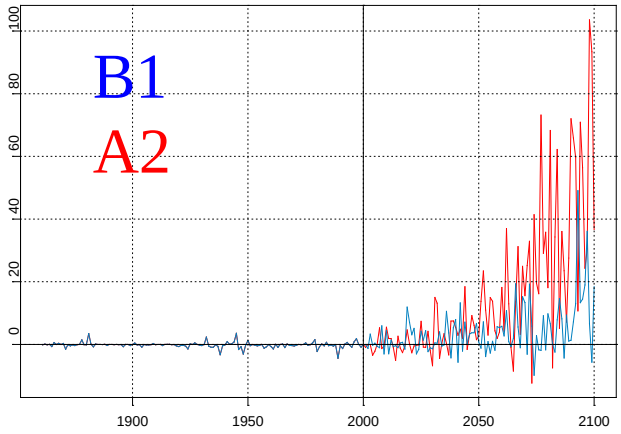

Positive values represent stronger daytime relative to nighttime heat waves over California and Nevada. Modeled by the GFDL-cm21 model.

In future work, these differences between models need to be scrutinized starting with validation of heat wave activity, such as making sure that heat waves in models occur for the right dynamical reasons and that the differences in nighttime vs. daytime trends are in fact due in large part to changes in atmospheric moisture content. Salient models could then be identified (CNRM is a good candidate at this point) and recommendations on how to improve the unsuccessful models could be made. The salient models could be used to project future risk of dangerous heat waves in response to anthropogenic climate change under various socio-economic development scenarios. This future modeling work will, of course, help clarify the ultimate causes of observed changes in heat wave activity.

Detailed examination of global climate models' data and regional ocean dynamics are beyond the scope of the present study. However, both these directions are key to understanding and forecasting future heat wave activity in California and will be pursued in future work. This work will eventually lead towards skillful seasonal prediction as well as long-range projection of California heat wave activity required for assessing short- and long-term future energy needs.

6.8 Summary, Discussion and Conclusions

We have quantified heat waves over California and Nevada in terms of their overall regional seasonal magnitude (relative to local climatology) as well as their components; intensity, spatial extent and duration; down to local and daily scales. Great Californian heat waves can be classified into primarily dry daytime and humid nighttime events, those with the greatest regional magnitudes expressed in Tmax or Tmin, respectively. Daytime (nighttime) events typically have significant but far smaller expressions in Tmin (Tmax). Heat waves can occur anytime in summer, but show a preference for late July, near the climatological peak in the

seasonal cycle of regional temperature. Nighttime heat wave magnitude and all its components display a clear and increasing regional trend. Daytime heat wave activity is more variable and sporadic. It is also increasing, but a large part of this daytime increase has occurred as a shift in the 1970s. Interestingly, interior highlands have tended to experience progressively stronger daytime heat waves relative to the lowland valleys throughout the 59-year record. Extreme heat waves typically last about a week where temperatures exceed the threshold (the hottest one percent of climatological Tmax or Tmin) over a large part of the region and, during their peak date, these events can affect vast parts of the region. The most recent great heat waves on our record, namely 2003 and 2006, were primarily nighttime events, they lasted over two weeks each, far exceeded previously set nighttime magnitude records, and have had overall daytime expressions to match or exceed, in the case of 2006, the greatest observed daytime events on record.

With one notable exception (1972), the atmospheric circulation anomalies responsible for great day and nighttime California heat waves are remarkably similar consisting mainly of a strong surface pressure gradient across the region set up between a high pressure anomaly over the Great Plains and a Low off the California coast. The circulation anomaly aloft consists of a great anticyclone above Washington State. The circulation associated with these features results in low-level convergence into California, especially from the south and east. The main difference between day and nighttime heat waves is the presence of a moisture source that may sometimes be associated with an active southwest monsoon, but more typically is a moist marine air mass to the south. If available, this moisture source is advected northward over the region by the heat wave circulation. The anomalous moisture thus advected over California and Nevada typically reaches twice the normal levels for this arid region and promotes the greatest relative warming at night mainly via the elevated greenhouse effect of a moist atmosphere. When the moisture source is unavailable, nighttime surface temperatures cool off efficiently by radiation as is normal for this arid region. A moisture source to the south of California, east of Baja California has been growing in association with a warming SST trend in this region. This regional SST trend explains the bulk of the increasing trend in nighttime heat wave activity over California and Nevada and is apparently related to the warming of the world's oceans.

The frequency and magnitude of nighttime heat waves has clearly and steadily been on the rise and the trend appears to be accelerating. Out of the largest 6 nighttime (daytime) events occurring over almost six decades between 1948 and 2006, 3 (1) have occurred in the last six years[13]. The heat wave that spanned the second half of July 2006 reached a nighttime spatial extent of almost ¾ of the area, at its peak on July 23 (for example, local Tmin anomalies were in the hottest one percent of the summertime climatological Tmin distributions, as measured at 74 percent of stations, roughly uniformly distributed across California and thinning into Nevada). Its overall nighttime magnitude was roughly twice that of the next largest recorded nighttime

13 However, the daytime expression of these most recent nighttime heat waves has been on par with the greatest daytime events on record. This observation is alarming. Health impacts of daytime temperature expressions of humid nighttime events are expected to be larger since humidity can exacerbate heat stress, for example humid heat feels worse than dry heat as reflected in apparent temperature.

event (July 2003[14]) and its overall daytime magnitude was also unprecedented, due particularly to the unusual combination of its duration and intensity.

What made the 2006 event so special? Circulation and humidity anomalies were remarkably strong and early without precedent. Humidity in excess of previous events was advected from the south and was already present in the area during the prelude (July 15-20)[15] to the onset of the most intense and extensive temperature anomalies. During this prelude, a local surface low developed just off the California coast advecting moisture from the south (Figures 6.5.4 and 6.6.2, and animation, not shown), collecting more than twice the normal summer atmospheric precipitable water over California and Nevada and setting the stage for the greatest night (and daytime) heat wave on record. When the broad surface High spilled into the Great Plains (July 20– 22), the coastal Low persisted, it intensified as the High came down the Great Plains and dissipated, while the anomalous coastal Low kept pumping moisture and heat from the south into California keeping temperatures high, especially at night[16]. The persistent coastal Low and moisture availability upstream, for example south of the Low, led to a moisture build-up that nocturnalized and "super-sized" what would have otherwise been merely another great daytime event. As it happened, its overall daytime expression surpassed all *daytime* heat waves on record. Intense and extensive nighttime heat without observed precedent, helped to intensify daytime warming and make the heat wave more intense and durable via the positive feedback between Tmax and Tmin.

While coincident and persistent key circulation anomalies of late July 2006 and the availability of a great moisture source played their pivotal roles in making the greatest heat wave on record, the strong and accelerating trend in regional nocturnal heat wave activity suggests that the probabilities are mounting for synoptic conditions to combine more often in ways conducive to the occurrence of nighttime heat waves. The summertime average Tmax and Tmin trends (Figure 6.2.1) go hand-in-hand with heat wave occurrences expressed in day and nighttime temperature extremes, which these average trends partially reflect and partially determine via association to large-scale teleconnections. As pointed out previously, the main factor that determines whether a heat wave will be primarily expressed in day or nighttime temperatures is the availability of an anomalous moisture source upwind of the synoptic circulation that converges hot surface air into the region. A warming SST trend east of Baja California appears to have been instrumental in making this moisture source more readily available. This SST trend is part of the global ocean surface and subsurface warming known to be due to anthropogenic climate change (Barnett et al., 2001, 2005, Pierce et al. 2006). Important questions to be addressed by future studies emerge. How much of the trend in BSST is caused by global

14 July10 – August 2, 2003, was the most intense and extensive nighttime event to date, 3X greater in overall magnitude than the previous record (2001). It had a strong daytime expression as well, placing it third on the list of *daytime* events.

15 July 19th, 2006, saw the 7th greatest one-night spatial extent of extreme heat on the 59-summer record.

16 The extremely strong and persistent upper-level circulation with the blocking high over the Northwest, must have encouraged the persistence of the low-level circulation.

warming? How strongly can it be expected to continue? How much of the climb in nocturnal heat wave activity that is now being witnessed over California and Nevada partly a regional expression of a global process? Answering these questions unequivocally is beyond the scope of this study and requires an augmented set of tools including dynamical modeling. We intend to address these questions in future studies. For now researchers simply note that the results presented here are fully consistent with global warming and they do intuit a plausible scenario for future summertime heat wave activity in California: more, hotter, more extensive and durable humid nighttime heat waves with a slowly growing daytime signature.

Assuming a global – regional climate change connection physically exists in this case, an interesting question, of the chicken-and-egg variety, is whether this type of regional development should be regarded as a regional effect of global warming or a regional expression of one of the main internal sources of global warming, one of the specific ways that the water vapor feedback acts regionally to accelerate global warming due to anthropogenic forcing? Such questions border on philosophy and are useful to improve the understanding and awareness of global climate change. More readily answerable climatological questions can also be asked. We do not know, for instance, how global climate change may be expressed in the regional synoptic circulation that brews up heat waves in the western U.S.. For example, it is not known if the frequency of summertime blocking over the Northwest and/or the behavior of surface anticyclones dropping down into the Great Plains should be expected to change in the future. To understand the physical causes of possible future changes and to physically validate dynamical models, these are the types of questions important to address in historical model integrations and long-term projections. Regional results based on global model projections (Hayhoe et al. 2004) can and should be verified with respect to their regional realism relevant for a specific extreme, for example regional circulation and moisture anomalies associated with large heat wave events.

Although most severely impacting California, the July 2006 heat wave extended across the conterminous United States as well as into adjacent parts of Canada and Mexico. A contemporaneous heat wave, although not as severe as the 2003 event, also affected most of Europe. The event can, therefore, be viewed in a much larger geo-spatial context. In a similar way, the heat wave activity of summer 2003 was unprecedented over Western Europe and over California/Nevada. We do not know to what extent such extreme events are coincidental. We plan to adopt a broader and longer viewpoint in a follow-up article. Global climate warming is becoming and is expected to increasingly become more apparent in the mounting spatial scale of regional summertime heat (Gershunov and Douville 2007). Together with our more focused regional results, this further suggests a direct and increasing link between regional heat waves and global climate change. It shows in more detail that a smooth global warming trend consists to some extent of regional extremes. California is likely not unique in terms of its rising nighttime heat wave activity, although it may very well be unique in its specific regional causes and detail. Fortunately, the likely antropogenic forcing behind the observed trend, if verified, will provide an excellent basis for longer-term regional projection. Towards this goal, regional coupling mechanisms (such as between day and nighttime temperatures under various humidity conditions) should be explored in detail and especially in models which can then be

used to explore causal mechanisms for the observed trends in regional heat wave activity. Regional climate change, especially as manifested in extreme events, must be better understood via examination of synoptic dynamics (and hydro-dynamics) typical for the region. Climate change models should be scrutinized for their ability to simulate the salient dynamical features for the region of interest and then used selectively to project these features into the future. Then three will be the ability to dynamically validate regional manifestations of global climate change and project them in their extreme detail.

More intense, spatially extensive, durable and frequent nighttime heat, especially coupled with high humidity, increases the detrimental effects of individual heat waves on the well-being of individuals and society. Improved understanding of the anatomy of heat waves should lead to better outlooks on seasonal, interannual and multi-decadal time scales. This is needed for intelligent allocation of resources required to mitigate the risks associated with extreme weather and climate events.

CHAPTER 7:
Modeling Stream Flow and Hydropower Across Three Basins

Hydropower is an important energy resource in the western U.S., providing a relatively inexpensive and renewable alternative to fossil fuel-based technologies such as natural gas turbines. Hydropower resources in the western U.S. are strongly coupled to cool season precipitation variability, which explains approximately 85 percent of the variance in annual stream flow in the Columbia River basin (PNW), 90 percent of the variance in the Sacramento San Joaquin (SSJ) basins, and 55 percent of the variance in the Colorado River basin (CRB). Persistent changes in cool season precipitation variability have been observed since the mid-1970s, and include increased variance, coefficient of variation, lag1 autocorrelation, and inter-regional covariation. Changes in warm season precipitation, by comparison, are most evident in increased lag1 autocorrelation since the mid-1970s.

Using long term temperature and precipitation data sets from 1916-2003 to drive the Variable Infiltration Capacity hydrologic simulation model, researchers simulate monthly stream flows from 1916-2003 at a number of river locations which in turn are used to drive three reservoir simulation models for the PNW, SSJ, and CRB. Despite differences in climate and water resources infrastructure and management in the three regions examined, changes in stream flow and hydropower variability since the 1970s have largely mirrored changes in cool season precipitation variability. These changes have increased vulnerability to energy shortages in the western U.S. because droughts since the mid-1970s have tended to be longer and more intense, and more coincident from region to region. Similar changes are apparent for high flow conditions, when abundant hydropower resources have been available west-wide.

Paleoclimatic records from 1858-1977 suggests that the observed pattern of variability from 1977-2003 is unusual in the context of natural variability over the past 150 years or so. Longer paleoclimatic records for the SSJ and CRB alone show that similar episodes have occurred at most three times in the last 500 years, at roughly 200 year intervals. The changes in cool season precipitation variability, stream flow and hydropower resources coincide with strong anthropogenically forced warming at the global scale, however it remains to be seen if these changes are systematic and physically related to global warming in some way, or if they are simply a temporary feature of natural variations in precipitation that have been unusual in the earlier parts of the 20th century record. If these changes are in fact systematic in nature, ongoing changes in energy and water management to cope with the altered variability may be needed.

7.1 Introduction

Regional hydropower resources are related to global incoming solar energy resources redistributed via the global water cycle and atmospheric circulation patterns associated with the earth's climate system. Typically, hydropower resources are analyzed as a function of observed

stream flow in rivers and water management policies that determine the operation of dams. Here a more fundamental approach is taken by examining the effect of observed cool season (October-March) climate variations on annual stream flow and hydropower resources in three large river basins in the western U.S.

Hydropower plays an important role in the mix of energy sources in the western U.S. because it is usually the lowest cost energy source, and is relatively abundant in comparison with other regions of the U.S. This is particularly true in the Pacific Northwest (PNW), where, on average, local hydropower resources supply about 65-70 percent of the total electrical energy demand in the region (BPA 1991). Because hydropower resources displace more expensive fuel-based energy systems, availability of hydropower resources is also an important factor in determining variations in fossil fuel consumption and markets from year to year (Voisin et al. 2005). Natural gas market analysts, for example, frequently cite hydropower production in the PNW Columbia River basin as an important factor controlling natural gas prices in the U.S., second only to variations in U.S. winter heating degree days, and of greater importance than hurricane damage to gas supply infrastructure in the Gulf of Mexico.

Variations in hydropower production are a complex function of water availability (climate variability affecting precipitation and river flow), demand for water and energy, and water resources infrastructure and management policies that determine the operation of dams. Because all of these factors can change markedly through time, models (which impose self-consistent infrastructure, demands, and operating policies through time), are an essential component of any analysis of the effects of climate variations on hydropower production over long periods of time. In the PNW, for example, the Columbia River's active storage capacity was almost doubled in the late 1960s and early 1970s due to the Columbia River Treaty (ratified by Canada in 1964) and other agreements (BPA, 1991). Thus, any evaluation of climatic effects on current energy production capability prior to the mid 1970s cannot be based on observed energy production data.

In this study researchers will examine the changing nature of cool season precipitation variability and variations in annual hydropower production in three large hydropower producing water resources systems in different parts of the western U.S.: the Columbia River basin in the PNW, the Sacramento/San Joaquin (SSJ) system in California (CA), and the Colorado River basin (CRB) in the southwest U.S.. This work follows previous investigation of variations in seasonal hydropower production in the PNW and CA related to the El Niño Southern Oscillation and Pacific Decadal Oscillation (Voisin et al. 2005).

A number of previous studies have identified changes in late 20th century climate variability and stream flows in the western U.S. Studies by Cayan et al. (2003), Jain et al. (2005) and Pagano and Garen (2005), for example, showed that the variability and/or synchronicity of river flow has increased in the late 20th century in the western U.S. Hamlet and Lettenmaier (2007) further demonstrated that these changes in hydrologic variability are consistent with observed changes in cool season precipitation variability since about 1973 which have (in modeling studies) increased natural flood risks over most of the western U.S. Our objectives in this study are to more fully quantify the observed changes in precipitation variability observed in the 20th

century, and relate them to changes in annual flow and hydropower production in the PNW, SSJ, and CRB.

At the time of this writing the root causes of the observed changes in cool season precipitation variability since the mid-1970s are largely unknown, however two main hypotheses present themselves: 1) systematic large-scale changes in the global climate system (such as related to global warming) are responsible and 2) the observed changes in variability in the late 20th century are a normal part of the climate system which has simply been rare in the relatively short 20th century record. The first hypothesis is supported by the fact that the observed changes seem to be affecting the entire western U.S. (suggesting a large-scale change in the climate system). The timing of the change has also been coincident with the period most clearly associated with greenhouse forced warming at the global level (IPCC 2001), which at face value would seem to support hypothesis 1). Such an argument is weakened by the fact that large scale changes in the Pacific Ocean and cool season climate in the western U.S. associated with the Pacific Decadal Oscillation and other factors (Gershunov and Barnett 1998; Mantua et al. 1997; Zhang et al. 1997) have occurred over essentially the same time frame, suggesting that natural variability alone could explain the observed behavior.

Paleoloclimatic stream flow reconstructions based on tree-ring records have shown that multi-decadal synchronicity between reconstructed stream flows in the SSJ and the CRB has been relatively rare, but has occurred in the past (Meko and Woodhouse 2005). Similar studies in the PNW (Gedalov et al. 2005), however, are not able to resolve the annual variations in stream flow, which makes direct comparisons with the CRB and SSJ time series reconstructions problematic. To avoid these problems researchers instead take the approach of comparing reconstructed natural flows in the Columbia River from 1858 to 1977 with long-term stream flow reconstructions for the SSJ and CRB to establish a longer record of variability (see following section for more detail).

7.2 Methods

In order to construct a self-consistent time series of annual hydropower production in the three hydropower systems discussed above, researchers use stream flow simulations from the Variable Infiltration Capacity (VIC) hydrologic model (Liang et al. 1994), implemented at 1/8th degree over the western U.S. (see Hamlet et al. 2005 for more details). The hydrologic model is driven by a long-term daily-time-step gridded temperature and precipitation data set from 1916-2003 (Hamlet and Lettenmaier 2005). The naturalized stream flows produced by the hydrologic model are bias corrected using quantile mapping techniques (Smith 1992; Snover et al. 2003; Voisin et al. 2005), and are then used as driving data for three reservoir simulation models: ColSim (Hamlet and Lettenmaier 1999b) which simulates the operation of the Columbia River Hydro system in the PNW, CVMod (Van Rheenen et al. 2004) which simulates the operation of the SSJ water resources system in CA, and CRSim (Christensen et al. 2004) which simulates the operation of the Colorado River water resources system in the southwest. Together these linked models simulate the physical relationships between climate (temperature and precipitation), stream flow, and hydropower production in the three regions for a

consistent set of water resources infrastructure, reservoir operating policies, and water demands.

We establish the relationship between basin runoff and cool season precipitation using a regression model for observed naturalized flows based on spatially averaged warm or cool season precipitation from the VIC driving data (see above) used as a single explanatory variable. Naturalized flows are from the Columbia River at The Dalles, OR (USGS gage 14105700), the Colorado River below Hoover Dam (USGS gage 09421500), and the Sacramento River near Shasta Dam (USGS gage 11377200) in the SSJ.

In examining the changing statistics of cool season precipitation and hydropower production researchers use the apparent break points (1947 and 1977) in the historic time series of the Pacific Decadal Oscillation index (Mantua et al. 1997) to define specific periods for analysis. These break points have previously been associated with changing precipitation and stream flow regimes in the western U.S. (see Cayan et al. 1998; Gershunov and Barnett 1998; Hamlet and Lettenmaier 1999a; Hidalgo et al. 2004; Mote et al. 2003; Voisin et al. 2005).

Statistical significance at 95 percent confidence of mean, standard deviation, and lag1 autocorrelation is tested using an assumption of normally distributed variables (probably not strictly true in the case of CA and the CRB). Statistical significance of the coefficient of variation is tested using the methods described by Verrill and Johnson (2007). The significance of the sample correlation coefficient is tested using a Fisher r-to-z transformation scheme (see Devore 1991). Sample sizes are not identical in the three time periods, but in identifying a statistically significant change researchers require that the statistics derived from 1977-2003 (n=27) be statistically significant in comparison with both 1916-1946 (n=31) and 1947-1976 (n=30) which provides a more robust test.

To help put observed changes in precipitation variability in the late 20th century into a longer context, researchers use long-term reconstructions of natural stream flow for large basins in each region. In the PNW researchers use reconstructed natural flow in the Columbia River at The Dalles, OR based on observed peak stage records (available from 1858-1877), naturalized gage records from 1878-1928 (Naik et al. 2005), and naturalized gage records from 1929-1989 (derived by the authors from modified flows and estimates of net diversions prepared for the Bonneville Power Administration by A.G. Crook (1993)). Annual flows from 1858-1877 are estimated from peak daily discharge records, which explain about 75 percent of the variance in annual flow using linear regression. These observed records are compared to tree-ring-based composite stream flow reconstructions in the SSJ (Meko 2001) and in the CRB at Lees Ferry, AZ (Woodhouse et al. 2006) for the overlapping period 1858-1977 (120 water years). For the SSJ and CRB only, much longer paleological reconstructions are available. For these two regions alone the overlapping period 1500-1977 was analyzed.

To analyze these long records researchers employ metrics which sum a 21-year running coefficient of variation (CV), lag 1 autocorrelation, and regional covariation over the three watersheds (for stream flow) or regions (for precipitation). These metrics allow us to identify periods in which each of these statistics is high or low in all three regions at the same time.

7.3 Results and Discussion

We begin by exploring the relationships between cool and warm season climate and stream flow variability for the three basins examined in detail in this study (see Hamlet et al. 2007 for a more general discussion of the hydrologic response of these basins in response to seasonal climate). In the PNW and the SSJ (Figure 7.8.1), cool season precipitation explains about 83 and 91 percent of the variance in annual flow respectively. Effects of warm season precipitation (not shown) are small in the PNW and SSJ, explaining less than four percent of the variance in the case of the PNW and less in the SSJ. In the CRB (Figure 7.8.2), the relationship between cool season climate and annual runoff is weaker than in the PNW and SSJ, with cool season precipitation anomalies explaining only 56 percent of the variance in annual flow. This is expected since the PNW and CA have strongly Mediterranean climates (wet winters, dry summers), whereas the CRB receives a significant portion of the annual precipitation in the warm season monsoon (explaining about 18 percent of the variance in annual flow,Figure 7.8.2).

7.4 Observed Changes in Precipitation Variability

Comparing spatially averaged cool season precipitation and statistics for three periods in the 20th century record associated with predominantly warm and cool PDO conditions, observed changes in cool season precipitation from 1977 forwards in comparison with earlier periods include increased variance, coefficient of variation (CV), and lag 1 autocorrelation (Table 7.8.1). The changes in variance are statistically significant in all four regions (For completeness the Great Basin (GB) is also analyzed, although researchers will not examine stream flow records in that region) at the 95 percent confidence limit. In the PNW, the increase in the CV and lag1 autocorrelation are also significant. With the exception of the mean precipitation in the CRB, none of the other statistics calculated for 1977-2003 are significant at the 95 percent confidence level in comparison with both earlier periods.

The inter-regional correlation (for example the correlation between the cool season precipitation time series in two regions) also increases in all but one case (CRB-GB correlation is the same in 1916-1924 as in 1977-2003) (Table 7.8.1b). Changes in interregional correlation coefficient, however, are only statistically significant in the case of the PNW-GB and CA-GB correlations.

In summary, cool season precipitation has become significantly more variable at the end of the 20th century, and wet and dry periods are more persistent, particularly in the PNW. The data also show changes in mean precipitation that are consistent with many previous studies describing decadal variability in the 20th century discussed in the introduction. In particular the PNW is dryer in 1977-2003 than in 1947-1976, and the CRB is wetter in 1977-2003 than in 1947-2003. All three regions were relatively dry from 1916-1946 due to widespread drought in the 1930s and 40s. With the possible exception of the CRB, the changes in mean precipitation from 1977-2003 are not statistically significant, however.

By comparison, the statistics of warm season precipitation have been much more stationary (Figure 7.8.4, Table 7.8.3, 7.8.4). The PNW and SSJ have been somewhat wetter in warm season

from 1977-2003, and the lag 1 autocorrelation from 1977-2003 is higher in all regions in comparison with the two earlier periods. The variance and coefficient of variation for warm season precipitation, however, do not show any meaningful changes. Long-term increasing trends in warm season precipitation the PNW have been apparent from about 1928-1995 (4.6 percent per decade), but since the mid 1990s there have been dramatic downward trends in warm season precipitation in the PNW (-8 percent per decade) from 1977-2003.

7.5 Observed Changes in Regional Synchronicity of Precipitation

To further examine the changes in regional synchronicity, researchers use a running 21-year correlation analysis. Figure 7.8.4 shows the correlation between cool and warm season precipitation in different regions, and Figure 7.8.5 shows the correlation between warm season precipitation in the CRB and cool season precipitation in the PNW and SSJ. Although synchronous behavior was apparent in most of the western U.S. early in the 20th century in cool season (Figure 7.8.5 upper panel), relatively asynchronous behavior became common around 1940, and precipitation has become increasingly synchronous between regions since that time. Warm season precipitation shows a similar overall pattern for the PNW-CRB and SSJ-CRB pairs, but the PNW and SSJ have been synchronous and asynchronous at different times in the record with no clear trends in this relationship (Figure 7.8.5 lower panel).

Correlations between cool season precipitation in the PNW and SSJ and warm season precipitation in the CRB are potentially important in terms of correlation in annual flows because warm season precipitation in the CRB accounts for a substantial portion of the variance in annual flow in the CRB. Cool season precipitation in the PNW and warm season precipitation in the CRB has become much more synchronous in the 20th century, whereas correlation between cool season precipitation in the SSJ and warm season precipitation in the CRB has varied and shows no clear trends (Figure 7.8.6).

7.6 Simulated Changes in Annual Hydropower Production

The time series response of hydropower production from a reservoir system integrates cool-season precipitation anomalies in space and time in a complex manner. This is particularly true in snowmelt dominant basins (like the ones examined in this paper), which store much of the cool season precipitation at higher elevations as snow and then release this storage over a relatively short period of time in the spring and summer (Hamlet et al. 2007).

Although at monthly time scales different reservoir systems can display very different time series behavior, at annual time scales the storage in a reservoir system primarily acts as a low frequency filter for the annual inflows to the system. Hydropower production, which is a function of both head (reservoir surface elevation) and inflow, thus tends to be more strongly auto correlated than the inflow time series that drives it. These fundamental characteristics of hydropower systems can effectively amplify changes in the lag1 autocorrelation and/or inter-regional correlation of the inflow time series to produce more pronounced changes in the resultant hydropower time series.

Figure 7.8.7 shows the simulated time series of annual hydropower production from the three river basins from 1916-2003. Although considerably less noisy (smaller CV) and more auto correlated (larger lag 1 correlation), the changes in statistics for hydropower production broadly mirror those for cool season precipitation (Table 7.853). The post 1977 period is characterized by increased variance, increased coefficient of variation, increased autocorrelation, and increased regional covariance. Note especially the strongly amplified increase in inter-regional correlation post 1977.

As noted above, some of the observed covariance between the PNW and the CRB hydropower may also be related to strongly increased covariance between cool season precipitation in the PNW (which explains most of the variance in annual flow in the PNW) and warm season precipitation in the CRB (which explains about 18 percent of the variance in annual flow in the CRB) from 1977-2003.

7.7 Evidence from Long-Term Stream Flow Records in the PNW and Paleoclimatic Reconstructions in the SSJ and CRB

As discussed in the introduction, the changes in variability, persistence, and inter-regional coherence observed in the late 20th century raise some important questions about how often patterns of variability such as these have occurred in the past due to natural variations in climate. In this section researchers compare stream flow reconstructions in the CRB, SSJ, and PNW (see methods section) to quantify these relationships, comparing them to a similar analysis of cool season precipitation for the shorter record from 1916-2003. Figure 7.8.8a shows a 21-year running coefficient of variation summed over the three time series (SumCV), a 21-year running lag1 autocorrelation summed over the three time series (SumL1A), and 21-year running inter-regional correlation summed over the three time series (SumIRC) for the reconstructed stream flow time series. Figure 7.8.8b shows the same metrics for the cool season precipitation time series in each region.

Taking into account the apparent bias between the SumCV for the stream flow reconstructions and cool season precipitation records, it is apparent that the CV over the western U.S. has been unusually high towards the end of the record. Furthermore, periods of simultaneously high SumL1A and SumIRC have not occurred from 1858-1977. Instead the normal pattern of variability prior to 1977 is for weak negative correlation (R = -0.12) between SumL1A and SumIRC. That is, when lag-1 autocorrelation is strong in all three regions, interregional correlation is relatively weak, and vice versa. Post 1977, SumL1A and SumIRC climb simultaneously to high values.

Longer paleological records for the SSJ and CRB alone from 1500-1977 show that periods of high SumCV, SumL1A and SumIRC (for these two regions alone) have occurred in the past (Figure 7.8.9). Two periods in particular, centered around 1580 and 1780 respectively, stand out as analogues of the 1977-2003 period. Although probably a coincidence, these periods of high variance, strong year-to-year persistence, and strong inter-regional correlation are fairly uniformly spaced about 200 years apart for the SSJ and CRB. Note also that the weak anti-

correlation of SumL1A and SumIRC discussed above seems only to have emerged after about 1800 in the longer record.

Although the root causes of the changes in precipitation variability from 1977-2003 are not currently known, this analysis demonstrates that these changes have been unusual in the context of normal patterns of variability in the last 200 years or so, but similar events over the southern half of the western U.S. may have occurred several times in the last 500 years (based on stream flow reconstructions for the SSJ and CRB alone).

7.8 Conclusions

20th century records from 1916-2003 show substantial and persistent changes in the statistics of cool season precipitation variability from 1977-2003 in comparison with earlier parts of the 20th century. Statistical changes include increased variance, coefficient of variation, and lag-1 autocorrelation, and increased inter-regional covariation. Positive and negative anomalies have become larger, more persistent, and more regionally synchronous. In the CRB, warm season precipitation also plays a significant role in stream flow generation and hydropower production. The autocorrelation of warm season precipitation in the CRB and the inter-regional correlation between warm season precipitation in the CRB and PNW cool season precipitation has also increased in late 20th century records, although the coefficient of variation of warm season precipitation has remained relatively stationary. These changes in variability, although they may not be permanent, are clearly long-lived, having persisted for more than 30 years so far.

Because cool season precipitation plays such a strong role in determining annual stream flows (particularly in the PNW and SSJ) changes in the statistics of simulated annual hydropower production broadly mimic the changes cool season precipitation.

Although direct comparison between paleo stream flow reconstructions and observed cool season precipitation records are somewhat problematic, the paleologic record suggests that periods in which the CV, lag 1 auto-correlation, and inter-regional correlation are simultaneously high in the CRB, SSJ, and PNW have never occurred from 1858-1977. For the longer paleological record from 1500-1977 for the SSJ and CRB alone, however, two broadly similar periods centered around 1580 and 1780 are apparent, suggesting that similar episodes affecting all three regions may have occurred in the past (roughly once every 200 years).

The west-wide nature of the observed effects since 1977 supports the hypothesis that these changes are related to persistent, large-scale changes in cool season circulation. Whether these changes can be directly related to systematic changes in the global climate system (such as related to changes in greenhouse forcing) is unclear. From a statistical standpoint the likelihood of successfully attributing these relatively small changes to an anthropogenic forcing seems unlikely. Improving the paleoclimatic reconstructions of stream flow in the PNW would perhaps be helpful in this regard, because it would be possible then to compare much longer periods for all three regions.

Regardless of the cause, the changes in cool season precipitation variability observed over the past 30 years or so have important implications for energy planning. In particular, the observed changes in variability, persistence, and inter-regional covariation in hydropower resources increase the risks of west-wide hydropower shortfalls during droughts. Because conventional fuel-based energy resources must ultimately be used to mitigate these shortfalls when they occur, there are important implications associated with energy infrastructure (both supply and transmission) needed to supply reserve capacity, natural gas supplies (storage and transmission capacity), and the analysis of fuel markets, particularly in CA, which is affected by hydropower resources in all three regions. Equally important in the context of natural gas markets are the periods of relative abundance in hydropower production, which are also enhanced post 1977. The time series behavior of simulated hydropower resources suggests, for example, that "boom and bust" cycles associated with natural gas markets are now more likely to occur in response to the changing time series behavior of hydropower resources. Similar issues related to conjunctive use of water (for example, use of abundant water resources in one area to offset losses in another) in the SSJ and CRB are also implied by these findings.

Table 7.8.1: Statistics for Regionally Averaged Cool Season (Oct-Mar) Precipitation for Three Time Periods

		PNW	SSJ	CRB	GB
1916-1946	mean (mm)	574.7	443.9	174.7	172.2
	Std deviation	88.8	100.1	30.6	23.6
	CV	0.15	0.23	0.17	0.14
	lag 1auto corr	-0.15	0.06	0.11	0.60
	trend (% per decade)	-1.1	6.9	-3.5	3.7
1947-1976	mean (mm)	640.3	477.1	168.6	180.7
	Std deviation	84.4	99.3	34.0	23.9
	CV	0.13	0.21	0.20	0.13
	lag 1auto corr	-0.42	0.12	-0.29	0.15
	trend (% per decade)	1.5	2.8	3.8	-0.1
1977-2003	mean (mm)	594.3	488.1	**190.8**	185.3
	Std deviation	**126.2**	**141.9**	**50.8**	**41.4**
	CV	**0.21**	0.29	0.27	**0.22**
	lag 1auto corr	**0.22**	0.12	0.15	0.46
	trend (% per decade)	4.2	2.4	-9.7	-5.1

Bold entries for 1977-2003 are statistically significant in comparison with both previous periods.

Table 7.8.2: Inter-Regional Correlation Coefficients for Regionally Averaged Cool-Season (Oct-Mar) Precipitation

	PNW-CA	PNW-CRB	PNW-GB	CA-CRB	CA-GB	CRB-GB
1916-1946	0.51	-0.17	0.17	0.37	0.75	0.63
1947-1976	0.29	-0.46	0.14	0.30	0.72	0.54
1977-2003	0.65	-0.06	**0.52**	0.50	**0.87**	0.63

Bold entries for 1977-2003 are statistically significant in comparison with both previous periods.

Table 7.8.3: Statistics for Regionally Averaged Warm Season (Apr-Sept) Precipitation for Three Time Periods

		PNW	SSJ	CRB	GB
1916-1946	mean (mm)	250.5	98.5	178.9	121.2
	Std deviation	47.0	24.1	27.8	28.2
	CV	0.19	0.24	0.16	0.23
	lag 1auto corr	0.12	-0.19	-0.29	-0.33
	trend (% per decade)	4.1	2.0	-3.8	2.2
1947-1976	mean (mm)	275.7	99.3	167.7	130.3
	Std deviation	41.8	29.7	25.6	24.4
	CV	0.15	0.30	0.15	0.19
	lag 1auto corr	0.15	-0.36	-0.06	-0.12
	trend (% per decade)	0.3	-3.9	2.1	4.3
1977-2003	mean (mm)	**303.3**	107.9	179.0	**142.2**
	Std deviation	53.0	31.3	33.1	34.1
	CV	0.17	0.29	0.18	0.24
	lag 1auto corr	0.21	-0.04	0.15	**0.36**
	trend (% per decade)	-8.1	-1.2	-2.4	-7.4

Bold entries for 1977-2003 are statistically significant in comparison with both previous periods.

Table 7.8.4: Inter-Regional Correlation Coefficients for Regionally Averaged Warm-Season (Apr-Sept) Precipitation

	PNW-CA	PNW-CRB	PNW-GB	CA-CRB	CA-GB	CRB-GB
1916-1946	0.51	0.30	0.48	0.42	0.59	0.51
1947-1976	0.45	0.04	0.28	0.23	0.41	0.78
1977-2003	0.42	0.30	0.54	0.15	0.59	0.61

Bold entries for 1977-2003 are statistically significant in comparison with both previous periods.

Table 7.8.5: Statistics for Simulated Total Annual Hydropower Production for Three Time Periods

		PNW (ColSim)	SSJ (CVMod)	CRB (CRSim)
1916-1946	mean (GW-hr)	104.58	8.07	20.21
	variance	15.41	2.36	4.42
	CV	0.15	0.29	0.22
	lag 1auto corr	0.00	0.21	0.72
	trend (% per decade)	-0.6	11.4	-11.3
1947-1976	mean (GW-hr)	126.90	9.82	19.29
	variance	13.28	2.44	2.51
	CV	0.10	0.25	0.13
	lag 1auto corr	-0.53	0.19	0.14
	trend (% per decade)	1.6	5.7	-1.5
1977-2003	mean (GW-hr)	123.59	9.77	22.56
	variance	21.07	3.52	5.80
	CV	0.17	0.36	0.26
	lag 1auto corr	0.53	0.44	0.62
	trend (% per decade)	-3.8	5.6	-5.0

Figure 7.8.1: Comparison of Observed Annual Naturalized Stream Flow and Regressed Value

A)

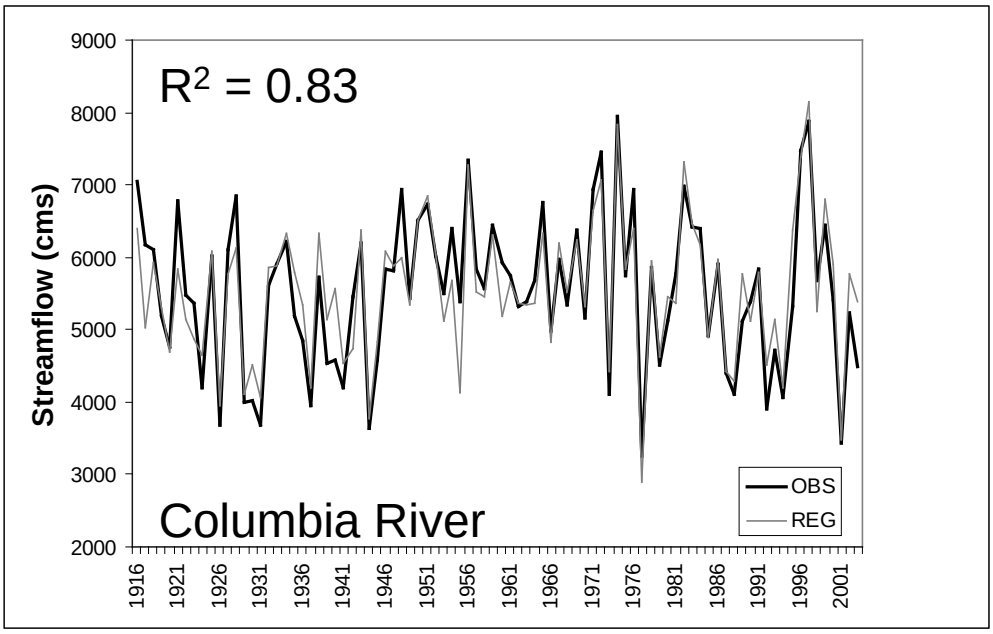

B)

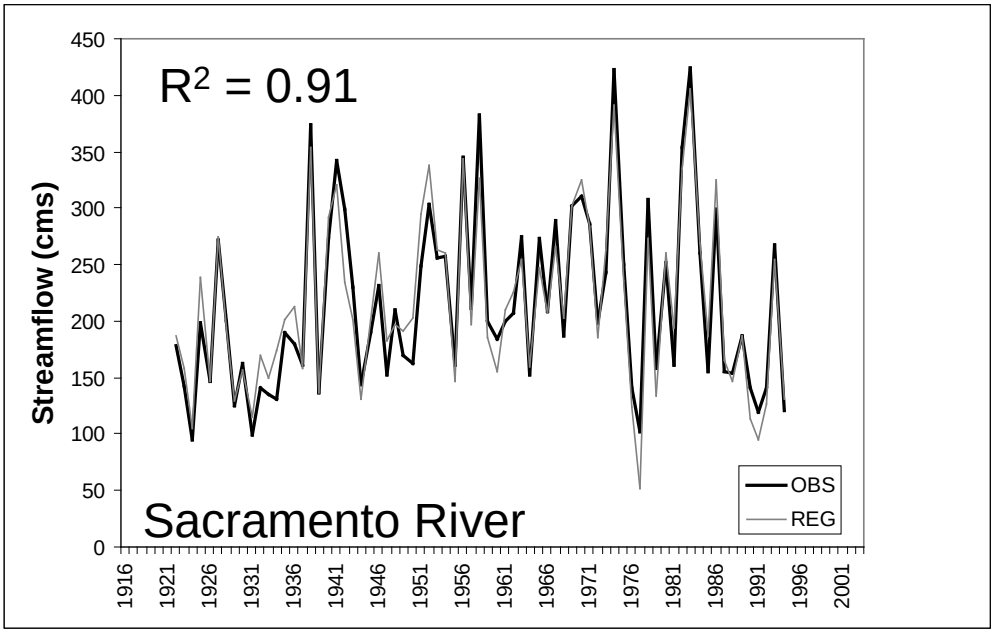

Based on estimated basin-average cool season (Oct-Mar) precipitation from the VIC driving data: A) Columbia River at The Dalles, OR (basin area = 614,000 km2), B) Sacramento River at Shasta Dam (basin area 16,800 km2)

Figure 7.8.2: Comparison of Observed Annual Naturalized Stream Flow in the Colorado River at Hoover Dam (Basin Area 388,000 Km2) and Regressed Value

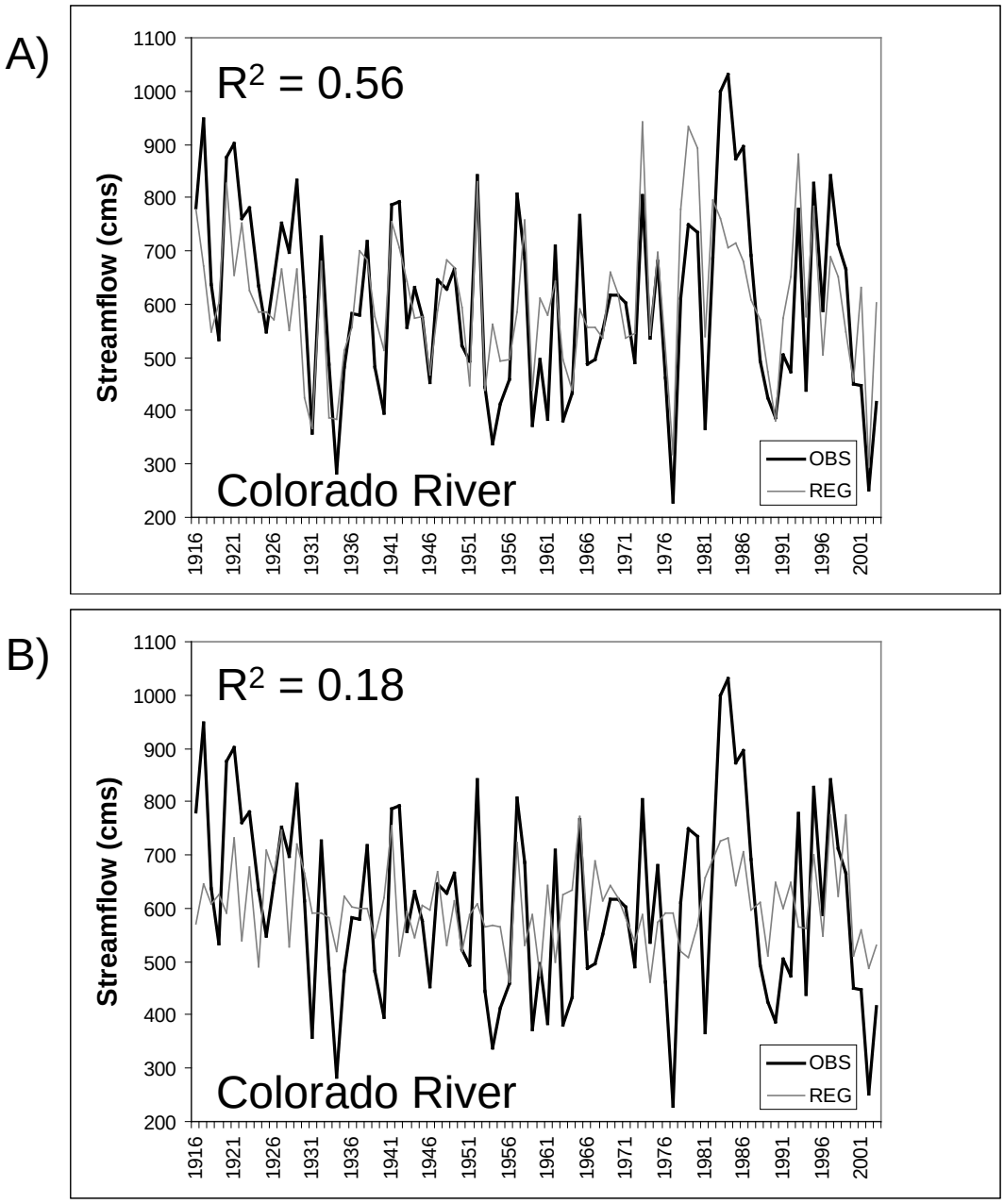

Based on A) estimated basin-average cool season (Oct-Mar) precipitation from the VIC driving data, and B) estimated basin average warm season (Apr-Sept) precipitation from the VIC driving data.

Figure 7.8.3: Time Series of Standardized Anomalies (Relative to 1961-1990) of Regionally Averaged Cool Season (Oct-Mar) Precipitation from Water Year 1916-2003

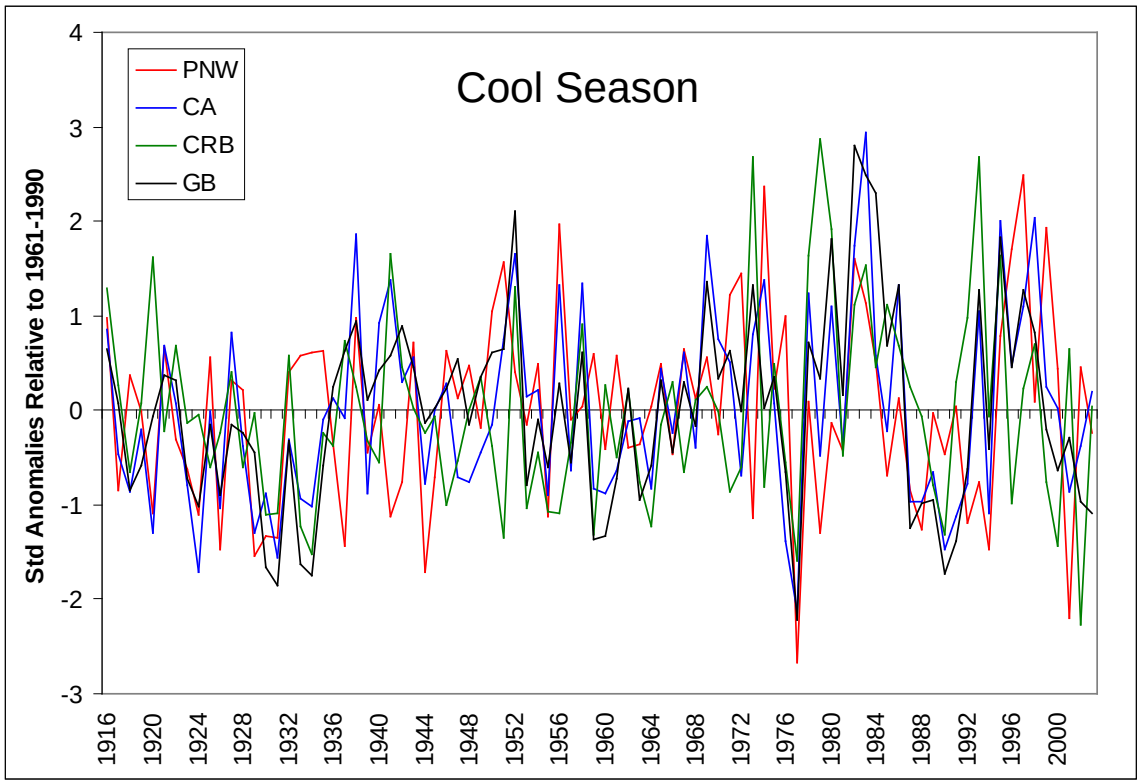

Figure 7.8.4: Time Series of Standardized Anomalies (Relative to 1961-1990) of Regionally Averaged Warm Season (Apr-Sept) Precipitation from Water Year 1916-2003

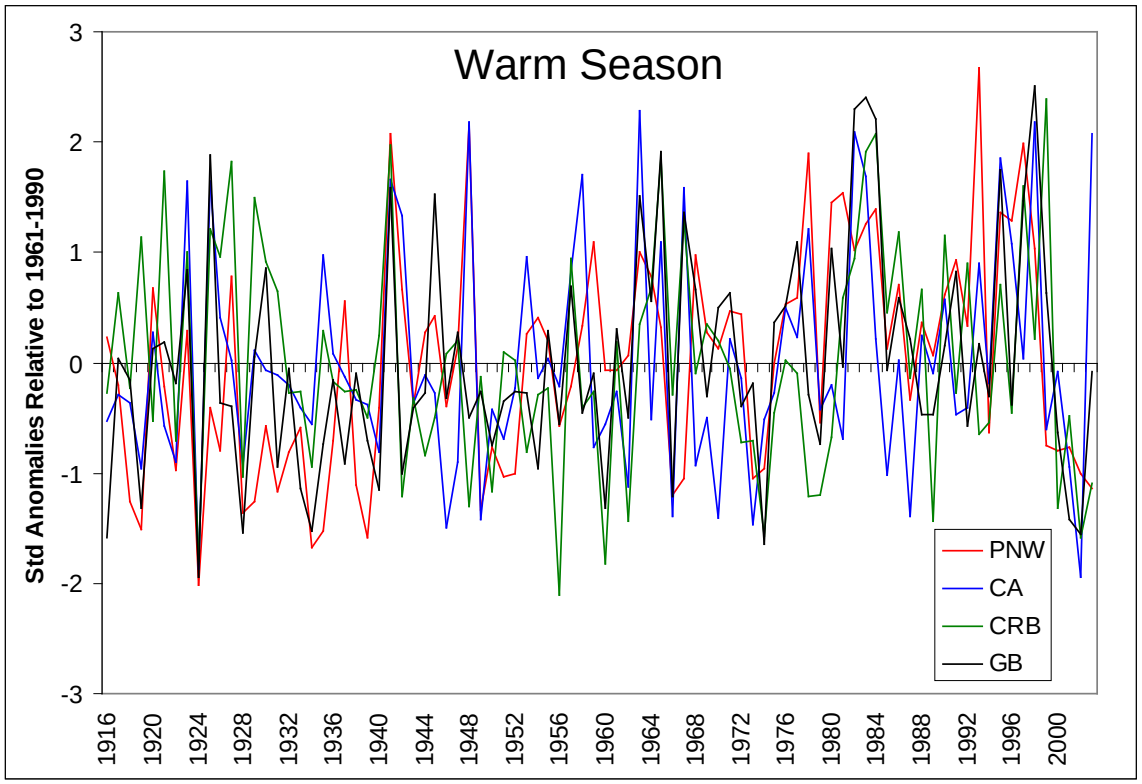

Figure 7.8.5: 21-Year Running Correlation Analysis of Regionally Averaged Precipitation

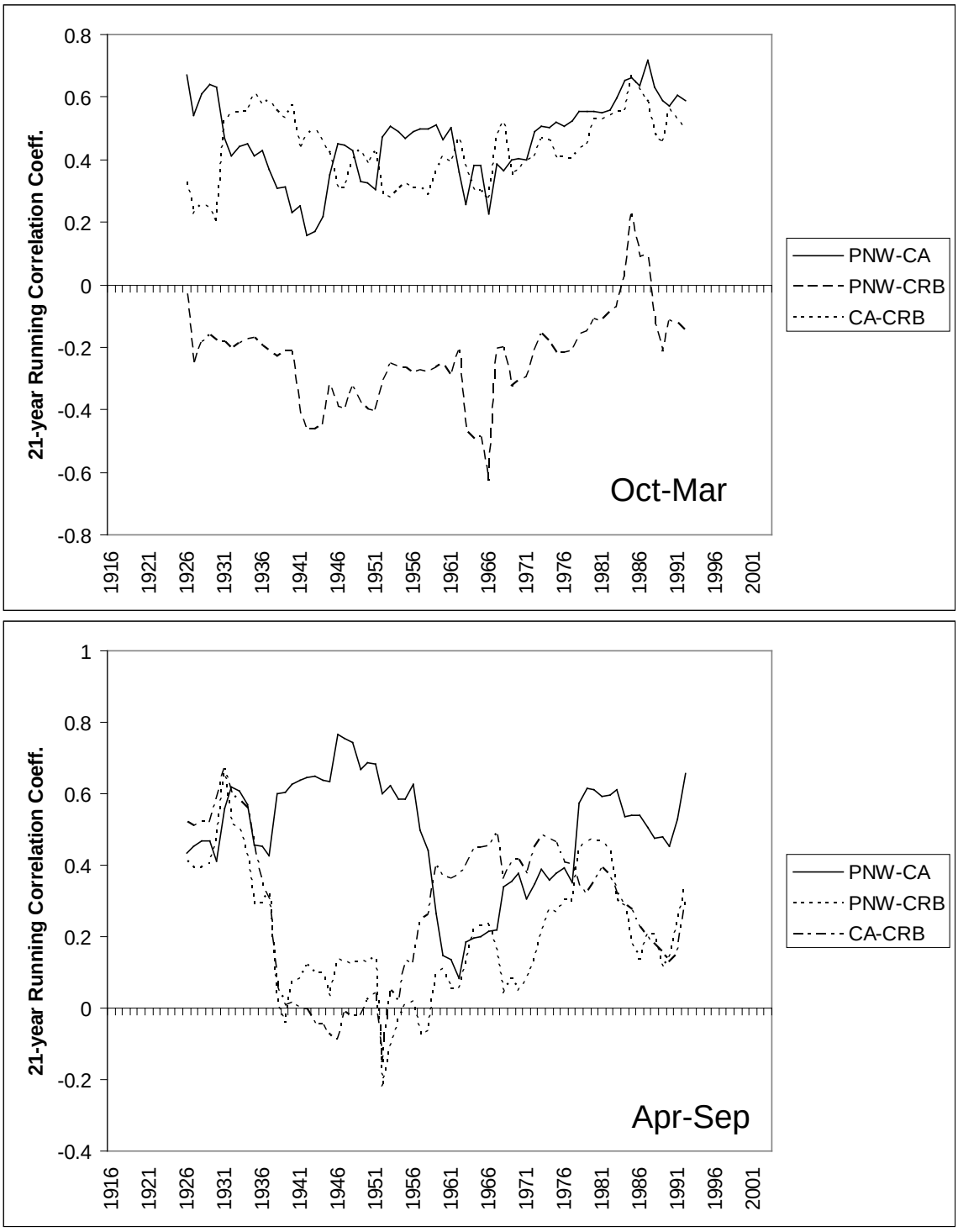

Upper panel shows correlation between cool season precipitation in each region (shown in Fig 6.3). Lower panel shows correlation between warm season precipitation in each region (shown in Fig 6.4).

Figure 7.8.6: 21-Year Running Correlation Analysis of Regionally Averaged Precipitation for Cool Season Precipitation in the PNW and CA(shown in Fig 6.3) and warm season precipitation in the CRB (shown in Fig 6.4).

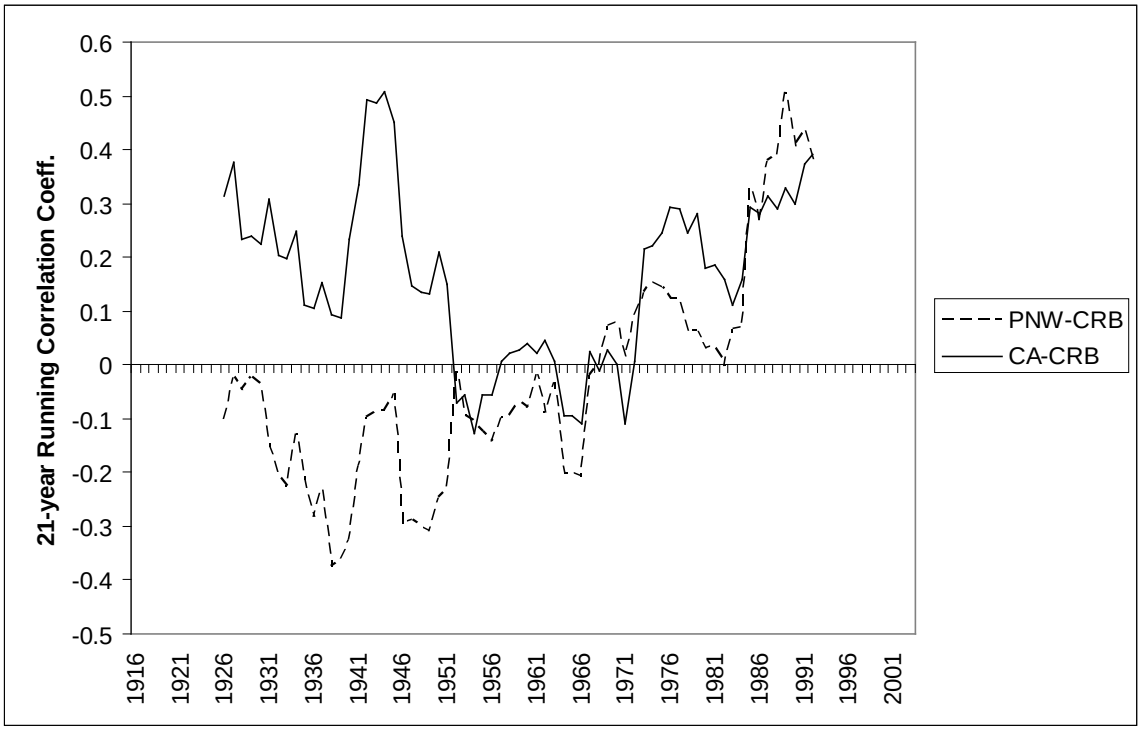

Figure 7.8.7: Time Series of Simulated Annual Hydropower Production

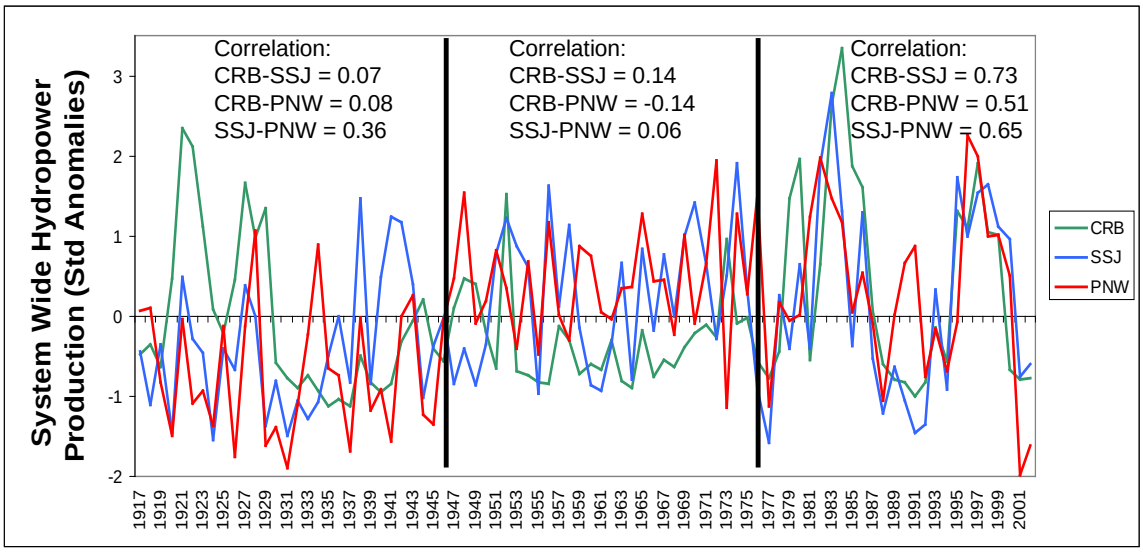

From the ColSim (PNW) CVMod (SSJ), and CRSim (CRB) reservoir simulation models from 1916-2003 with inter-regional correlation statistics for 1916-1946, 1947-1976, 1977-2003 (inset tables).

Figure 7.8.8: Sum of 21-Year Running Lag-1 Autocorrelation, Inter-Regional Correlation, and CV for the PNW, SSJ, and CRB

A)

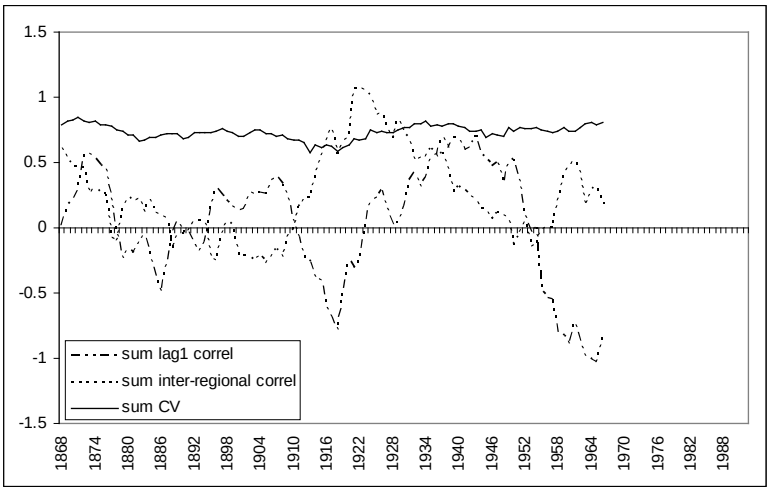

B)

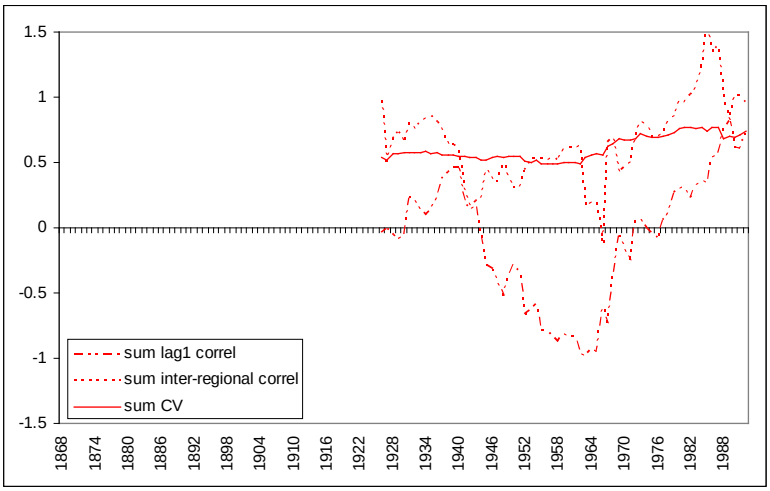

C)

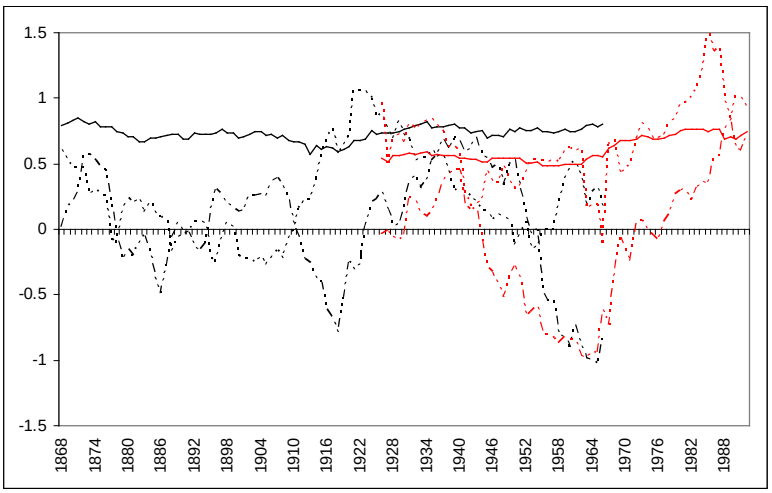

Based upon: A) Stream flow reconstructions (1858-1977) , B) Regionally averaged cool Season precipitation (1916-2003), C) superposition of results from A) and B).

Figure 7.8.9: Sum of 21-Year Running Lag-1 Autocorrelation, Inter-Regional Correlation, and CV for the SSJ and CRB Only

A)

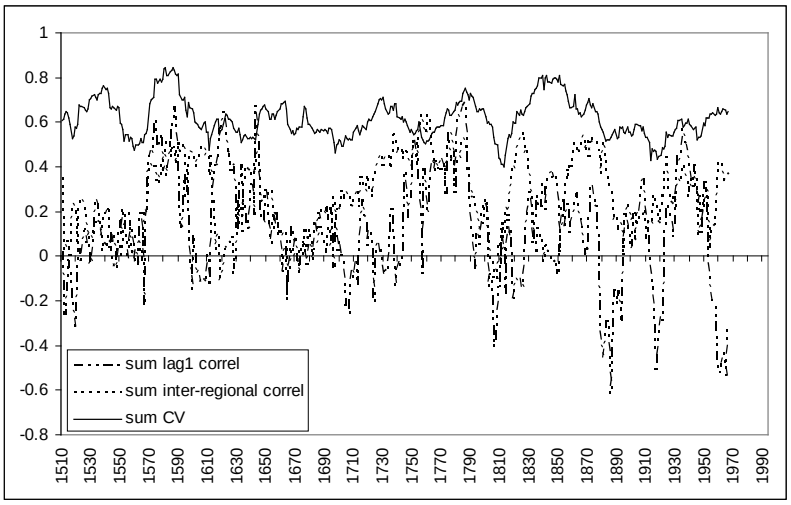

B)

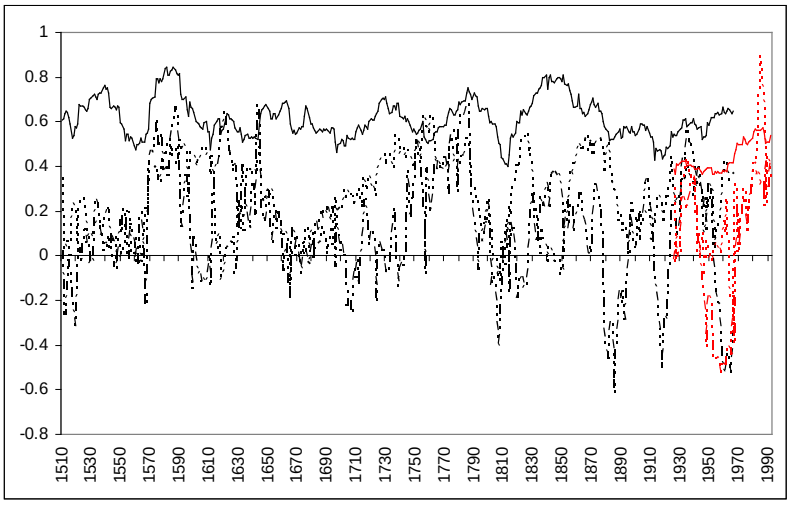

Based upon stream flow reconstructions (1500-1977), and regionally averaged cool-season precipitation (1916-2003). A) shows analysis of reconstructions only, B) shows superimposed analysis of reconstructions and cool-season precipitation.

CHAPTER 8:
Stakeholder Partnership: California Department of Water Resources

8.1 Research Objectives and Approach

Water managers in the western United States have long faced the challenge of meeting a variety of demands with limited and uncertain supplies. Seasonal climate outlooks offer the potential to improve decision-making by extending the planning horizon for resource managers, yet the value of these forecasts is largely untapped. Among the most cited barriers to their use are low forecast skill, difficulties with interpretation, and lack of demonstrated application. This research is aimed at improving the use and usability of NOAA seasonal forecast information through a case study involving California's Department of Water Resources (DWR), managers of water for the most populous state, largest irrigated agricultural industry, and arguably, most publicized conflicts over water allocation in the country.

This project addressed the following science and applications questions:

- How can NOAA climate forecast products be effectively translated and integrated into decision-making to reduce the vulnerability and impacts of drought? How can seasonal climate forecasts result in improved seasonal stream flow forecasts and in turn more efficient water management?
- How can a process of working with stakeholders be developed that will help to promote the integration of forecast information into decision-making? How can researchers more effectively bridge the gap between forecasts and their potential beneficial uses, through a process of understanding socio-organizational factors, opportunities and barriers?

Building upon previous and ongoing research funded by NOAA, this project focused on the transition of these products to operations, and the evaluation of their potential benefits in decision-making, rather than solely the development of new technologies.

8.2 Research Accomplishments

Our research produced results in two main categories. First, researchers conducted a comprehensive statistical analysis of climate forecast skill and correlation with water year classification systems. Second, researchers established collaborative relationships with DWR, and identified the types of decisions and decision-makers that could potentially benefit from these forecasts. These accomplishments are described in more detail in the paragraphs below.

8.2.1 Statistical Analysis

Our analysis of forecast skill focused on the source of water for the state's two largest water projects – the State Water Project, operated by DWR, and the Central Valley Project, operated by the Bureau of Reclamation. Broadly covered by Climate Prediction Center (CPC) forecast divisions 88 and 91, the region encompasses the watersheds of the Sacramento and San Joaquin Rivers, also the state's largest (see Figure 8.2.1).

Figure 8.2.1: The Forecast Divisions Under Study and Their Location with Respect to the Major Rivers of Northern California

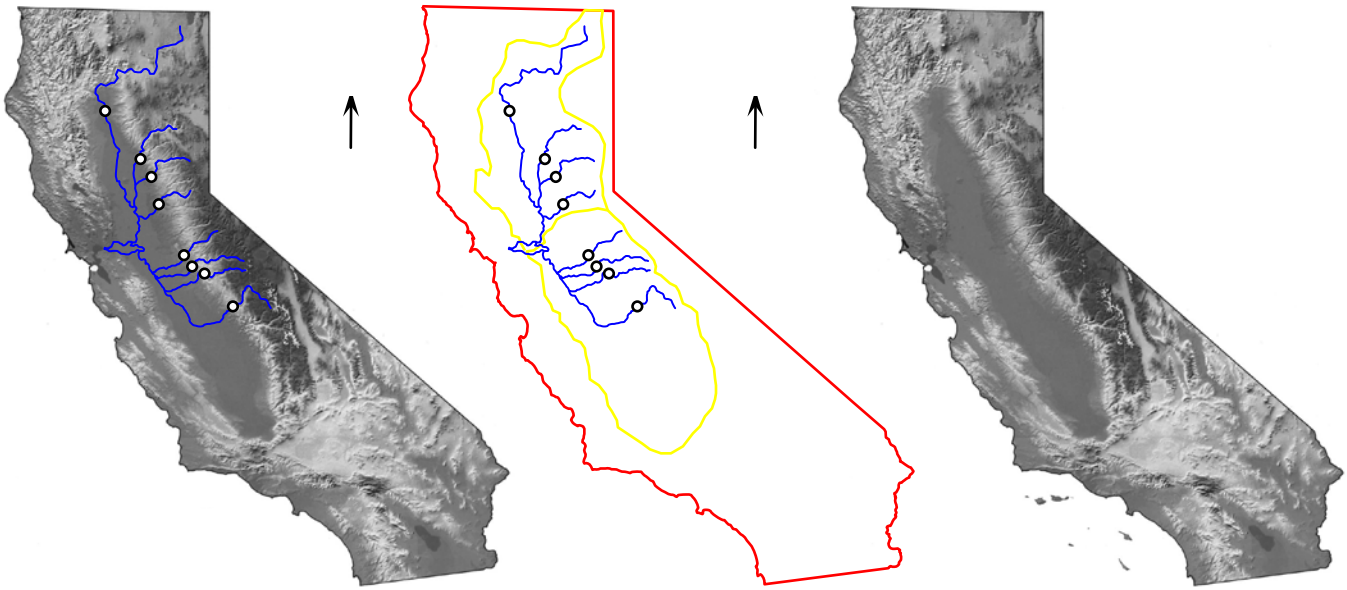

Yellow lines outline (from north to south) forecast divisions 88 and 91. Blue lines represent (from north to south) the Sacramento, Feather, Yuba, American, Stanislaus, Tuolumne, Merced, and San Joaquin Rivers, converging at the Sacramento-San Joaquin Delta just east of San Francisco Bay. Circles are forecast locations for unimpaired flow that are used to calculate Water Supply Indices critical for Delta operations.

As inputs for the analysis, researchers employed seasonal precipitation and temperature outlooks archived in two sources–the official dataset of CPC forecasts, which have been generated by a continually changing set of algorithms since their earliest public release in December 1994, and an objective dataset of forecasts, retrospectively generated by the latest methods to January 1982, and provided by David Unger of CPC.

Results from this analysis include the following:

- Seasonal forecast skill scores are generally highest during the summer and winter months. Interestingly, for the key target seasons of DJF, JFM, and FMA, when precipitation makes up the bulk of the runoff for the peak demand months of April to July, the objective forecasts showed higher skill than the official forecasts for precipitation, but lower skill than the official forecasts for temperature (see Tables 8.4.1 and 8.4.2).
- ENSO and PDO analyses revealed slightly higher skill scores during the warm phases for both cycles. Lead time was found to have a much smaller influence on skill than target season.
- "False alarms," defined as those "misses" in which the precipitation forecast was below-normal and the observation was above-normal, were found to be much more likely than "false assurances," defined as those misses in which the precipitation forecast was above-normal and the observation was below-normal. Water managers are typically less concerned with the former than the later, with respect to drought situations. When averaged over all 12 target seasons, the ratio of false alarms to false assurances was 0.27:0.08 for FD 88 and 0.34:0.06 for FD 91 (see Table 8.4.3).
- About 65 percent of temperature observations were warmer than climatology over the period of record, although precipitation tended to be lower than climatology on average. Interestingly, precipitation forecasts tended to be conservative, with roughly 80-85 percent being for below normal conditions.
- In both Sacramento and San Joaquin River basins, October to March runoff is most highly correlated with precipitation falling during NDJ, while April to July runoff is most highly correlated with precipitation falling during JFM (see Tables 8.4.4 and 8.4.5). These runoff quantities make up two out of the three components in the Sacramento Valley 40-30-30 and the San Joaquin Valley 60-20-20 Water Year Indices, employed by DWR as indicators of expected water availability for allocation purposes. Both systems define one "wet" classification, two "normal" classifications (above and below normal), and two "dry" classifications (dry and critical), for a total of five water year types.
- Contingency tables that plotted seasonal precipitation forecasts vs. observed Water Supply Indices (WSIs) were unable to provide statistical confirmation that forecasts could be used as predictor variables (see Tables 8.4.6 and 8.4.7). Tables plotting seasonal precipitation forecasts vs. April to July runoff terciles offered little improvement (see Tables 8.4.8 and 8.4.9). Fisher tests revealed p-values too large to conclude any significant association.
- Efforts at breaking tabulations down by forecast lead time were met with minimal correlation. Attempts to correlate runoff with aggregate forecasts for successive seasons were also inconclusive, most likely because forecasts for one season tend to be the same as the forecasts for the next. Efforts at separating out those forecasts with lower degrees of confidence (for example, lower probability anomalies) were unsuccessful as well. Research in this area is ongoing.

8.2.2 Applications and Value for Water Resource Management

Through consultations with DWR personnel, researchers identified potential applications of seasonal climate forecasts in water resources decision-making. Working directly and continuously with potential users of forecast information has enabled us to focus our research on products that would be most valuable to decision-making. Research in this area is ongoing under funding from NASA.

- WSIs were developed as a tool for establishing annual flow requirements in the Bay-Delta Estuary, where the Sacramento and San Joaquin Rivers converge to flow westward through San Francisco Bay. While the Delta serves as a transfer point for both the State Water Project (SWP) and the Central Valley Project (CVP), it is also an important migration corridor for fish and wildlife, and home to a diverse recreational and agricultural economy.

Figure 8.2.2: Chronological Summary of Delta Flow Conditions Required by State Water Resources Control Board Decision 1641

[4] Minimum monthly average Delta outflow (cfs). If monthly standard ≤ 5,000 cfs, then the 7-day average must be within 1,000 cfs of standard; if monthly standard > 5,000 cfs, then the 7-day average must be ≥ 80% of standard.

Year Type	All	W	AN	BN	D	C
Jan	4,500					
Jul		8,000	8,000	6,500	5,000	4,000
Aug		4,000	4,000	4,000	3,500	3,000
Sep	3,000					
Oct		4,000	4,000	4,000	4,000	3,000
Nov-Dec		4,500	4,500	4,500	4,500	3,500

Flow objectives are functions of Sacramento Valley 40-30-30 Water Year Type, as shown in the example at right. (from Http://Wwwoco.Water.Ca.Gov/)

- WSIs offer a means of satisfying these competing interests by providing for an equitable allocation of Delta inflows. Figure 8.2.2 presents some of the flow objectives required by DWR to maintain adequate levels of salinity and dissolved oxygen, ensure sufficient water depths for navigation, and limit the entrainment of migratory fish in export pumps.
- DWR relies on snow surveys to forecast stream flows for its peak demand season of April to July. As such, the earliest estimates of WSIs are available each January when the first snow surveys are conducted. Between the beginning of the water year in October and that point, DWR bases its Delta operations on historical climatology. By providing an advanced indication of projected water supplies, seasonal climate forecasts offer the potential for more efficient water management, particularly in years of dryer conditions.
- Another strategy for ensuring sufficient environmental flows involves the use of water markets. In California, the mechanism for these transactions is the Environmental Water Account (EWA), operated by various state and federal agencies on behalf of endangered fish populations. Through a combination of long-term, spot market, and option purchases, the EWA obtains water on the statewide market to reimburse both the SWP and the CVP for reduced exports from the Delta. The single best predictors of EWA costs are the WSIs, as they affect the market price of water, availability of operational assets and cross-Delta transfer capacity, and quantity of export cuts. As earlier indicators of WSIs, seasonal climate forecasts offer opportunities to reduce these costs, particularly with respect to spot market transfers, which vary substantially in response to hydrology and tend to increase as the water year progresses.
- In addition to their possible value to Delta operations, NOAA products offer opportunities to improve water management in general. Like all reservoir operators, DWR faces the challenge of maintaining high enough water levels to meet demands while providing enough open volume to store floodwaters. Such decisions, which are typically made on a seasonal basis, could potentially be aided by climate forecasts. Quantification of benefits would require simulation of complex reservoir models such as CALSIM. Furthermore, full management benefits could only be realized by the incorporation of adaptive decision rules into existing operating policies.
- NOAA seasonal forecasts also hold the potential to improve DWR's credibility with its long-term contractors. Inaccurate hydrologic forecasts may not be costly to DWR financially, but could be very costly to the agency in terms of public relations. NOAA products could thus be highly beneficial in years that start off wet but become dry, or vice-versa. Interestingly, Climate Prediction Center (CPC) outlooks are already vaguely referenced in WSI forecasts that are released to some of the larger water supply contractors, although officially, they are not factored in to calculations.
- Although efforts thus far have focused on potential benefits to DWR, it is entirely possible that seasonal climate forecasts could offer greater advantages to water supply agencies under contract with DWR, which are shown in Figure 8.2.3. In dry years, after

all, it is the contractors who must explore alternative water sources like water bank purchases, groundwater pumping, and even reclamation or reuse, and earlier indications of anticipated water deliveries could result in significant cost savings. Discussions with some of the larger contractors, like the Metropolitan Water District of Southern California, are needed to explore this potential.

- Finally, a potential application exists within the hydropower division of DWR. Other studies have shown that the nominal skill of climate forecasts is perhaps better suited to the energy sector, due to the greater number of opportunities for their application. Potential benefits exist not only on the supply side of the sector, but also the demand side, as temperature forecasts could be used to better project electrical loads. Research in this area is ongoing.

Figure 8.2.3: Locations of Water Supply Agencies Under Long-Term Contracts with DWR

8.3 Conference Presentations

Rosenberg, E. and Steinemann, A.C. (2008). "Utility of seasonal climate outlooks for water supply forecasts in northern California." *The Water Center's 18th Annual Review of Research,* February 14, Seattle, WA.

Rosenberg, E., Wood, A., Tang, Q., Steinemann, A., Imam, B., Sorooshian, S., and Lettenmaier, D. (2007). "Improving water resources management in the western United States through use of remote sensing data and seasonal climate forecasts," *5th Annual Climate Prediction Applications Science Workshop,* March 20-23, Seattle, WA.

8.4 Communications, Outreach, User Interactions

This project involved extensive interactions with personnel from DWR's Division of Flood Management, Division of Operations and Maintenance, the California Energy Resources Scheduling Division, and the CPC. The following individuals were involved in this study:

Aaron Miller	Department of Water Resources	Senior Engineer
Andy Chu	Department of Water Resources	Chief of Export Management
Art Hinojosa	Department of Water Resources	Chief of Hydrology Branch
Boone Lek	Department of Water Resources	Senior Engineer
David Rizzardo	Department of Water Resources	Chief of Forecasting Section
David Unger	NOAA Climate Prediction Center	Meteorologist
John King	Department of Water Resources	Senior Engineer
Steve Nemeth	Department of Water Resources	Senior Engineer
Tuan Bui	Department of Water Resources	Supervising Engineer

Table 8.4.1: Results of the Skill Analysis for the Study Regions, Precipitation

	Precipitation											
	Forecast Division 88						Forecast Division 91					
	Official (SS = 429)			Objective (SS = 1565)			Official (SS = 361)			Objective (SS = 1574)		
	HR	S_{MAE}	S_{RMSE}	HR	S_{MAE}	S_{RMSE}	HR	S_{MAE}	S_{RMSE}	HR	S_{MAE}	S_{RMSE}
SON	0.80	0.23	0.20	0.77	0.15	0.17	0.75	0.12	0.11	0.72	0.05	0.10
OND	0.33	-0.27	-0.21	0.39	-0.05	-0.10	0.29	-0.01	0.00	0.44	-0.02	-0.05
NDJ	0.10	-0.04	-0.03	0.35	-0.08	-0.07	0.57	0.00	-0.01	0.36	-0.07	-0.05
DJF	*0.50*	*0.00*	*0.02*	*0.58*	*0.00*	*0.00*	*0.45*	*-0.01*	*0.05*	*0.52*	*-0.01*	*0.00*
JFM	*0.62*	*0.05*	*0.08*	*0.76*	*0.09*	*0.08*	*0.47*	*0.03*	*0.06*	*0.64*	*0.05*	*0.07*
FMA	*0.65*	*0.07*	*0.09*	*0.76*	*0.07*	*0.03*	*0.61*	*0.06*	*0.08*	*0.54*	*0.02*	*0.00*
MAM	0.42	0.07	0.07	0.49	0.00	-0.01	0.52	0.04	0.04	0.57	0.02	-0.01
AMJ	0.20	-0.07	-0.03	0.44	-0.03	-0.01	0.56	-0.01	0.00	0.40	-0.05	-0.05
MJJ	0.48	-0.02	0.00	0.72	0.06	0.04	0.51	0.00	0.00	0.58	0.00	0.04
JJA	0.44	0.01	-0.01	0.72	0.10	0.06	0.50	0.00	0.03	0.57	0.08	0.06
JAS	0.97	0.21	0.15	0.92	0.32	0.33	0.96	0.24	0.20	0.91	0.44	0.46
ASO	0.82	-0.01	0.02	0.85	0.20	0.16	0.82	0.02	0.01	0.75	0.20	0.06
All	*0.63*	*0.03*	*0.03*	*0.65*	*0.02*	*-0.01*	*0.65*	*0.03*	*0.04*	*0.59*	*0.02*	*0.00*

Table 8.4.2: Results of the Skill Analysis for the Study Regions, Temperature

	Temperature											
	Forecast Division 88						Forecast Division 91					
	Official (SS = 1398)			Objective (SS = 1842)			Official (SS = 1414)			Objective (SS = 1876)		
	HR	S_{MAE}	S_{RMSE}	HR	S_{MAE}	S_{RMSE}	HR	S_{MAE}	S_{RMSE}	HR	S_{MAE}	S_{RMSE}
SON	0.44	-0.04	0.04	0.57	-0.07	-0.03	0.49	0.01	0.02	0.46	-0.05	-0.01
OND	0.60	0.00	0.01	0.57	-0.02	-0.02	0.67	0.03	0.03	0.62	-0.01	-0.01
NDJ	0.52	0.00	0.03	0.43	-0.01	-0.01	0.43	-0.01	0.03	0.48	-0.02	0.01
DJF	*0.56*	*0.02*	*0.05*	*0.50*	*-0.01*	*-0.01*	*0.75*	*0.02*	*0.02*	*0.66*	*-0.04*	*0.03*
JFM	*0.66*	*0.04*	*0.06*	*0.60*	*0.01*	*0.01*	*0.77*	*0.08*	*0.07*	*0.71*	*0.03*	*0.04*
FMA	*0.59*	*0.01*	*0.01*	*0.59*	*0.02*	*-0.01*	*0.58*	*-0.03*	*0.01*	*0.57*	*-0.06*	*-0.06*
MAM	0.59	-0.02	0.01	0.57	-0.01	0.01	0.47	-0.04	0.02	0.52	-0.03	0.00
AMJ	0.64	0.03	0.01	0.56	0.02	0.01	0.63	0.02	0.00	0.63	0.01	-0.01
MJJ	0.80	0.04	0.02	0.43	-0.01	-0.01	0.80	0.05	0.03	0.56	0.01	0.00
JJA	0.74	0.06	0.07	0.51	0.01	0.01	0.74	0.06	0.07	0.64	0.00	0.01
JAS	0.75	0.11	0.11	0.68	0.14	0.14	0.85	0.11	0.11	0.78	0.25	0.22
ASO	0.51	-0.06	0.02	0.53	-0.10	-0.01	0.52	0.03	0.06	0.51	-0.07	0.05
All	*0.63*	*0.02*	*0.03*	*0.55*	*0.00*	*0.00*	*0.65*	*0.03*	*0.03*	*0.60*	*0.00*	*0.01*

SS = sample size; HR = directional hit rate, defined as the percentage of forecasts predicted in the correct direction with respect to the climatological mean; SMAE = mean absolute error skill score, defined as 1 – (MAE/MAEclim); SRMSE = root mean squared error skill score, defined as 1 – (RMSE/RMSEclim). Values for directional hit rates can range from 0 to 1, with 0.50 indicating the skill of climatology, and values for MAE and RMSE skill scores can range from -∞ to 1, with positive scores indicating forecasts better than climatology. Target seasons are shown at left and ordered by water year, which begins October 1. Shown highlighted are the key target seasons of DJF, JFM, and FMA; precipitation falling during this period makes up the bulk of the runoff during the peak demand months of April to July. So that skill scores were not unduly "penalized" for forecasts of climatology (equal chances), which essentially indicate that the probability of the most likely category cannot be predicted, these outlooks were removed from the datasets.

Table 8.4.3: Extended Directional Hit Rate Analysis for DJF, JFM, FMA, and All 12 Target Seasons. See Key Below for Explanation. BN = Below Normal; AN = Above Normal

	Precipitation (objective)						Temperature (objective)					
	FD 88			FD 91			FD 88			FD 91		
DJF	0.25	0.35	0.61	0.29	0.37	0.65	0.10	0.19	0.29	0.00	0.10	0.10
	0.07	0.33	0.39	0.12	0.23	0.35	0.31	0.41	0.71	0.24	0.66	0.90
	0.32	0.68	0.58	0.40	0.60	0.52	0.40	0.60	0.50	0.24	0.76	0.66
JFM	0.41	0.09	0.50	0.37	0.23	0.59	0.06	0.13	0.20	0.02	0.06	0.08
	0.15	0.35	0.50	0.13	0.28	0.41	0.27	0.54	0.80	0.22	0.69	0.92
	0.55	0.45	0.76	0.50	0.50	0.64	0.33	0.67	0.60	0.24	0.76	0.71
FMA	0.36	0.08	0.44	0.40	0.35	0.75	0.06	0.07	0.13	0.04	0.06	0.09
	0.16	0.40	0.56	0.11	0.14	0.25	0.34	0.52	0.87	0.37	0.53	0.91
	0.53	0.48	0.76	0.51	0.49	0.54	0.41	0.59	0.59	0.41	0.59	0.57
All	0.52	0.27	0.79	0.51	0.34	0.85	0.08	0.17	0.25	0.03	0.09	0.12
	0.08	0.13	0.21	0.06	0.07	0.13	0.29	0.47	0.75	0.32	0.57	0.88
	0.60	0.40	0.65	0.57	0.42	0.59	0.36	0.64	0.55	0.34	0.66	0.60

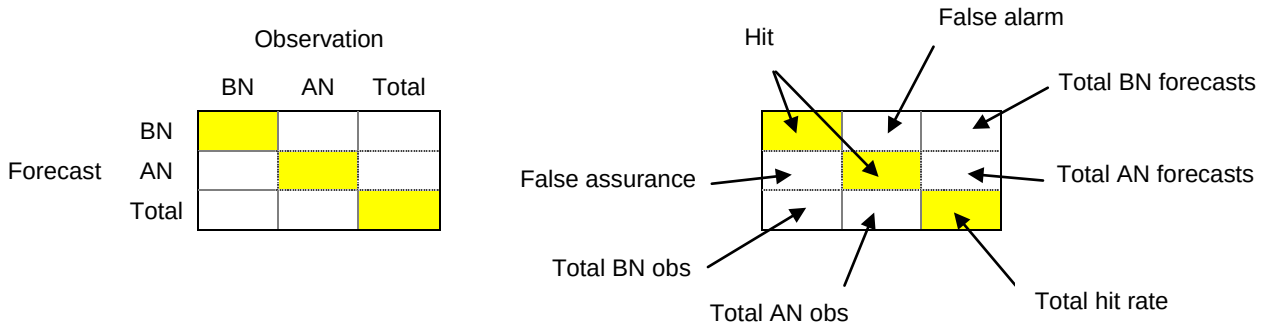

Table 8.4.4 and Table 8.4.5: Results of the Correlation Analysis for Precipitation and Stream flow

	Oct – Mar runoff	
	FD 88	**FD 91**
OND	0.4052	0.3628
NDJ	0.5675	0.5660
DJF	0.5412	0.4805
JFM	0.3763	0.3378
NDJF	0.6673	0.6182
NDJFM	0.7305	0.6400
ONDJFM	0.7603	0.6743

	Apr – Jul runoff	
	FD 88	**FD 91**
NDJ	0.3764	0.4436
DJF	0.4031	0.5638
JFM	0.4584	0.6145
FMA	0.4219	0.5011
DJFM	0.5852	0.7637
DJFMA	0.6740	0.8384
NDJFMA	0.6966	0.8557

Numbers represent R^2 values for the sum of observed precipitation during the specified months and the indicated runoff. Analysis included data from 1906 to the present.

Table 8.4.6 and Table 8.4.7: Tabulation of Seasonal Precipitation Forecasts and Water Year Types Over the Length of the Objective Dataset (1982 To Present)

FD 88 Precipitation Forecast			Sacramento Valley 40-30-30 Water Year Type				
			C	D	BN	AN	W
JFM		B	20	13	3	9	18
		N	3	6	0	7	8
		A	10	19	3	11	28
FMA		B	11	13	2	4	11
		N	7	4	0	5	9
		A	15	22	3	17	40

FD 91 Precipitation Forecast			San Joaquin Valley 60-20-20 Water Year Type				
			C	D	BN	AN	W
JFM		B	31	18	3	15	38
		N	11	11	2	3	15
		A	22	6	3	7	23
FMA		B	18	7	1	13	23
		N	15	14	4	5	16
		A	33	15	4	8	40

Results are shown for target seasons JFM and FMA, since these periods exhibited not only the highest skill out of the winter months with respect to precipitation forecasts, but also the highest degrees of correlation with April to July runoff. B below normal; N = near normal; A = above normal; C = critical; D = dry; BN = below normal; AN = above normal; W = wet.

Table 8.4.8 and Table 8.4.9: Tabulation of Seasonal Precipitation Forecasts and April to July Runoff Terciles Over the Length of the Objective Dataset (1982 To Present)

			Sacramento Valley April to July Runoff		
			B	N	A
FD 88 Precipitation Forecast	JFM	B	32	15	16
		N	9	9	6
		A	35	18	18
	FMA	B	24	12	5
		N	9	7	9
		A	43	22	32

			San Joaquin Valley April to July Runoff		
			B	N	A
FD 91 Precipitation Forecast	JFM	B	49	28	28
		N	22	8	12
		A	28	15	18
	FMA	B	25	16	21
		N	29	14	11
		A	48	23	29

Runoff terciles were determined from historic record of WSIs provided by DWR. B = below normal; N = near normal; A = above normal.

GLOSSARY

BSST/BCSST	Baja California Sea Surface Temperature
CCA	Canonical Correlation Analysis
CPC	Climate Prediction Center
CRB	Colorado River Basin
CVP	Central Valley Project
CVP	Coefficient of Variation
DD	Degree Days
DFJ	December-January-February
DN	Degree Nights
DWR	Department of Water Resources
ENSO	El-Nino/Southern Oscillation
EWA	Environmental Water Account
FMA	February-March-April
GB	Great Basin
GCm	Global Dynamical Model
JJA	June-July-August
NCDC	National Climatic Data Center
NDJ	November-December-January
NOAA	National Oceanographic and Atmospheric Administration
NPO	North Pacific Decadal Oscillation
OLS	Ordinary Least Squares
PCA	Principle Components Analysis
PDF	Probability Distribution Function
PDO	Pacific Decadal Oscillation
PNW	Pacific Northwest (Columbia River Basin)

PSST	Pacific Sea Surface Temperature
SSJ	Sacramento San Joaquin Basin
SST	Sea Surface Temperature
SWP	State Water Project

REFERENCES

Alfaro, A., A. Gershunov, D. Cayan, A. Steinemann, D. Pierce and T. Barnett, 2004: A Method for Prediction of California Summer Air Surface Temperature. EOS, 85(51), 553, 557-558.

Alfaro, E.J., A. Gershunov and D. Cayan, 2006: Prediction of summer maximum and minimum temperature over the central and western United States: The role of soil moisture and sea surface temperature. J. Climate, 19(8), 1407-1421, doi: 10.1175/JCLI3665.1.

Azzalini, A. and Capitanio, A. (2003). Distributions generated by perturbation of symmetry with emphasis on a multivariate skew *t* distribution. The full version of the paper published in abridged form in *J.Roy. Statist. Soc. B* 65, 367–389, is available at http://azzalini.stat.unipd.it/SN/se-ext.ps.

Dettinger,M.D.,D.R.Cayan,H.F.Diaz, and D.M.Meko, North-south precipitation patterns in western North America on interannual-to-decadal time scales,J.Clim.,11,3095,1998.

Gershunov, A., T.P. Barnett and D.R. Cayan, 1999: North Pacific inter-decadal oscillation seen as factor in ENSO-related North American climate anomalies. EOS, 80 (3), 1, 25-30.

Bonneville Power Administration (BPA), U.S. Army Corps of Engineers (North Pacific District), Bureau of Reclamation (Pacific Northwest Region) (BPA et al.), 1991: The Columbia River System: The Inside Story. Report published for the Columbia River System Review by the U.S. Army Corps of Engineers and the Bureau of Reclamation #DOE/BP-1689.

Cayan, D. R., M. D. Dettinger, H. F. Diaz, and N. Graham, 1998: Decadal variability of precipitation over western North America. J. Climate, 11 (12): 3148–3166.

Cayan, D. R., M. D. Dettinger, R. T. Redmond, G. J. McCabe, N. Knowles, and D.H. Peterson, 2003: The transboundary setting of California's water and hydropower systems, linkages between the Sierra Nevada, Columbia, and Colorado hydroclimates. Climate and Water: Transboundary Challenges in the Americas, H. Diaz and B. Morehouse, Kluwer Press, Chapter 11.

Christensen, N.S., Wood, A.W., Voisin, N., Lettenmaier, D.P. and R.N. Palmer, 2004: Effects of Climate Change on the Hydrology and Water Resources of the Colorado River Basin, Climatic Change, 62 (1-3): 337-363.

Crook, A.G. 1993: 1990 Level Modification Streamflow 1928-1989, Report of A.G. Crook Company to Bonneville Power Administration, Contract #DE-AC79-92BP21985.

Devore, J.L., 1991: Probability and Statistics for Engineering and the Sciences, Brooks/Cole Publishing, CA, pp 492-494.

Gershunov, A., and T.P. Barnett, 1998: Interdecadal modulation of ENSO teleconnections, Bulletin of the American Meteorological Society, 79 (12): 2715-2725.

Hamlet, A. F. and D. P. Lettenmaier, 1999a: Columbia River streamflow forecasting based on ENSO and PDO climate signals, American Society of Civil Engineers Journal of Water Resources Planning and Management, 125 (6): 333-341.

Hamlet, A. F. and D. P. Lettenmaier, 1999b: Effects of climate change on hydrology and water resources in the Columbia River Basin, Journal of the American Water Resources Association, 35 (6): 1597-1623.

Hamlet A.F., and D.P. Lettenmaier, 2005: Production of temporally consistent gridded precipitation and temperature fields for the continental U.S., J. Hydrometeorology, 6 (3): 330-336.

Hamlet A.F., P.W. Mote, M.P. Clark, and D.P. Lettenmaier, 2005: Effects of temperature and precipitation variability on snowpack trends in the western U.S., J. Climate, 18 (21): 4545-4561.

Hamlet A.F., P.W. Mote, M.P. Clark, D.P. Lettenmaier, 2007: 20th Century Trends in Runoff, Evapotranspiration, and Soil Moisture in the Western U.S., J. Climate, 20 (8): 1468-1486

Hamlet, A.F., D.P. Lettenmaier, 2007: Effects of 20th Century Warming and Climate Variability on Flood Risk in the Western U.S., Water Resour. Res., 43, W06427, doi:10.1029/2006WR005099.

Hidalgo H.G., and J.A. Dracup, 2003: ENSO and PDO effects on hydroclimatic variations of the Upper Colorado River basin, J. Hydrometerology, 4 (1): 5-23.

IPCC, 2001: Climate Change 2001: The Scientific Basis. Contribution of Working Group I to the Third Asessment Report of the Intergovernmental Panel on Climate Change [Houghton, J.T., Y. Ding, D.J. Griggs, M. Noguer, P.J. Van der Linden, X. Dai, K. Maskell, and C.A. Johnson (eds.)], Cambridge University Press, Cambridge, UK and New York, NY, USA, 881pp.

Jain, S., M. Hoerling and J. Eischeid J., 2005: Decreasing reliability and increasing synchroneity of Western North American streamflow. J. Climate, 18 (5): 613-618

Liang X., D.P. Lettenmaier, E.F. Wood, and S.J. Burges, 1994: A Simple hydrologically based model of land surface water and energy fluxes for general circulation models, J. Geophys. Res., 99 (D7): 14,415-14,428.

Mantua, N., S. Hare, Y. Zhang, J. M. Wallace, and R. Francis, 1997: A Pacific interdecadal climate oscillation with impacts on salmon production, Bulletin of the American Meteorological Society, 78: 1069-1079.

Meko, D.M., 2001: Reconstructed Sacramento River System Runoff From Tree Rings, Report prepared for the California Department of Water Resources, July.

Meko, D.M. and C.A. Woodhouse, 2005: Tree-ring footprint of joint hydrologic drought in Sacramento and Upper Colorado river basins, western USA. Journal of Hydrology, 308 (2005): 196-213.

J. L. Monteith, "Evaporation and the Environment" Symp. Soc. Expl. Biol. 19 (1965).

Mote, P.W., E.A. Parson, A.F. Hamlet, K.G. Ideker, W.S. Keeton, D. P.,Lettenmaier, N.J. Mantua, E.L. Miles, D.W. Peterson, D.L. Peterson, R., Slaughter, and A.K. Snover, 2003: Preparing for climatic change: the water, salmon, and forests of the Pacific Northwest, Climatic Change, 61 (1-2): 45-88.

Naik, P.K., D.A. Jay, 2005: Estimation of Columbia River virgin flow: 1879 to 1928.

Hydrological Processes, 19 (9): 1807-1824.

Pagano T., and D. Garen, 2005: A recent increase in western U.S. streamflow variability and persistence, J. of Hydrometeorology, 6 (2): 173-179.

H. L. Penman, Proc. of the Royal Soc. of London, A193 (1948).

Smith, J.A., G.N.Day, M.D. Kane, 1992: Nonparametric Framework for Long-Range Streamflow Forecasting, ASCE J. of Water Res. Planning and Management, 118 (1): 82-92.

Snover, A.K., A.F. Hamlet, D.P. Lettenmaier, 2003: Climate-change scenarios for water planning studies, Bulletin of the American Meteorological Society, 84 (11): 1513-1518.

Woodhouse, C.A., S.T. Gray, and D.M. Meko, 2006: Updated Streamflow Reconstructions for the Upper Colorado River Basin,Water Resources Research, Vol. 42, W05415.

Van Rheenen, N.T., A.W. Wood, R.N. Palmer and D.P. Lettenmaier, 2004: Potential Implications of PCM Climate Change Scenarios for Sacramento - San Joaquin River Basin Hydrology and Water Resources, Climatic Change, 62 (1-3): 257-281.

Verrill, S.P., R.A. Johnson, 2007: Confidence bounds and hypothesis tests for normal distribution coefficients of variation, USDA Forest Service, Research Paper FPL-RP-638.

Voisin, N., A. F. Hamlet, L. P. Graham, D. W. Pierce, T. P. Barnett, and D. P. Lettenmaier, 2006: The role of climate forecasts in western U.S. power planning, Journal of Applied Meteorology, 45(5): 653-673.

Zhang Y., Wallace, J.M., Battisti, D.S., 1997: ENSO-like interdecadal variability: 1900-93, J. of Climate, 10 (5): 1004-1020

Alfaro, E., A. Gershunov, D.R. Cayan, A. Steinemann, D.W. Pierce and T.P. Barnett, 2004: A method for prediction of California summer air surface temperature. Eos. 85. 553, 557-558.

Alfaro, E., A. Gershunov and D.R. Cayan, 2006: Prediction of summer maximum and minimum temperature over the Central and Western United States: The role of soil moisture and sea surface temperature. Journal of Climate. 19, 1407-1421.

Barnett, T.P., D.W. Pierce and R. Schnur, 2001: Detection of anthropogenic climate change in the world's oceans. Science, 292, 270-274.

Barnett, T.P., D.W. Pierce, K.M. AchtaRao, P.J. Gleckler, B.D. Santer, J.M. Gregory and W.M. Washington, 2005: Penetration of human-induced warming into the world's oceans. Science, 309, 284-287.

Beniston, M., 2004: The 2003 heat wave in Europe: A shape of things to come? An analysis based on Swiss climatological data and model simulations. Geophys. Res. Lett., 31, L02202, doi:10.1029/2003GL018857.

Beniston, M. and H.F. Diaz, 2004: The 2003 heat wave as an example of summers in a greenhouse climate? Observations and climate model simulations for Basel, Switzerland. Global and Planetary Change, 44, 73-81.

Bonfils, C. and D. Lobell, 2007: Empirical evidence for a recent slowdown in irrigation-induced cooling. Proc. Natl. Acad. Sci., doi:10.1073/pnas.0700144104.

Bonfils, C., P. Duffy, D. Lobell, 2007: Comments on "Methodology and results of calculating central California surface temperature trends: Evidence of human-induced climate change?" by J.R. Christy et al., J. Clim., 20, 4486-4489.

Cayan D.R., S.A. Kammerdiener, M.D. Dettinger, J.M. Caprio, D.H. Peterson, 2001: Changes in the onset of spring in the western United States. Bull. Amer. Meteor. Soc. 82, 399-415.

Davis, A., 2006: Heat claims as many as 38 people, tests state energy supply. Associated Press, appearing in San Jose Mercury News, July 25.

Duffy, P.B., C. Bonfils and D. Lobell, 2007: Interpreting recent temperature trends in California. Eos, 88, 409-410.

Easterling, D. R., and Coauthors, 1997: Maximum and minimum temperature trends for the globe. Science, 277, 364–367.

Easterling, D.R., G.A. Meehl, C. Parmesan, S.A. Changnon, T.R. Karl and L.O.Mearns, 2000a: Climate extremes: Observations, modeling, and impacts. Science, 289, 2068-2074.

Easterling, D.R., J.L. Evans, P.Ya. Groisman, T.R. Karl, K.E. Kunkel and P. Ambenje, 2000b: Observed variability and trends in extreme climate events: A brief review. Bull. Am. Meteorol. Soc., 81, 417-425.

Fischer, P., B. Brunekreef and E. Lebret, 2004: Air pollution related deaths during the 2003 heat wave in the Netherlands. Atmospheric Environment. 38, 1083-1085.

Gershunov A. and H. Douville, 2007: Extensive summer hot and cold extremes under current and possible future climatic conditions: Europe and North America. In: H. Diaz and R. Murnane (Eds.), Climate Extremes and Society. Cambridge University Press, in press.

Grize, L., A. Huss, O. Thommen, C. Schindler and C. Braun-Fahrländer, 2005: Heat wave 2003 and mortality in Switzerland. Swiss Med Wkly, 135, 200-205.

Hansen, J.E., R. Ruedy, Mki. Sato, M. Imhoff, W. Lawrence, D. Easterling, T. Peterson, and T. Karl, 2001: A closer look at United States and global surface temperature change. J. Geophys. Res., 106, 23947-23963, doi:10.1029/2001JD000354.

Hayhoe, K., and coauthors, 2004: Emissions pathways, climate change, and impacts on California. PNAS, 101, 12422-12427.

Hemon, D. and E. Jougla, 2003: Estimation de la surmortalité et principales caracteristiques epidemiologiques. Paris: ISERM 25 septembre 2003.

Kaplan, A., M. Cane, Y. Kushnir, A. Clement, M. Blumenthal and B. Rajagopalan, 1998: Analyses of global sea surface temperature 1856-1991, Journal of Geophysical Research, 103, 18,567-18,589.

Kistler, R., E. Kalnay, W. Collins, et al., 2001: The NCEP-NCAR 50-year reanalysis: Monthly means CD-ROM and documentation. Bull. Amer. Meteor. Soc., 82 (2), 247-267.

Knowles, N., M.D. Dettinger and D.R. Cayan, 2006: Trends in snowfall versus rainfall in the Western United States. J. Clim., 19, 4545-4559.

Lobell, D. and C. Bonfils, 2007: The effect of irrigation on regional temperatures: An analysis of spatial and temporal trends in California, 1934-2002. J. Clim., in press.

Lobell, D., G. Bala and P.B. Duffy, 2006: Potential bias of model projected greenhouse warming in irrigated regions. Geophys. Res. Lett., 33, L13709, doi:10.1029/2006GL026770.

Los Angeles Times, 2006: High nighttime temperatures set records too. July 25.

Meehl, G.A. and C. Tebaldi, 2004: More intense, more frequent, and longer lasting heat waves in the 21st century. Science, 305, 994-997.

Mote, P., A.F. Hamlet, M.P. Clark and D.P. Lettenmaier, 2005: Declining mountain snowpack in western North America. Bull. Am. Meteorol. Soc., 86, 39-49.

Munoz, O., 2006: 139 deaths later, heat wave appears over. Associated Press, appearing in Forbes, July 28.

NCDC, 2003: Data documentation for data set 3200 (DSI-3200): Surface land daily cooperative summary of the day. National Climatic Data Center, Asheville, NC, 36 pp. [Available online at http://www.ncdc.noaa.gov/pub/data/documentlibrary/tddoc/td3200.pdf].

Philipona, R., B. Dürr, A. Ohmura, and C. Ruckstuhl, 2005: Anthropogenic greenhouse forcing and strong water vapor feedback increase temperature in Europe, Geophys. Res. Lett., 32, L19809, doi:10.1029/2005GL023624.

Pierce, D.W., T.P. Barnett, K.M. AchtaRao, P.J. Gleckler, J.M. Gregory, W.M. Washington, 2006: Anthropogenic warming of the oceans: observations and model results. J.Clim. 19, 1873-1900.

Reynolds R. W. and T. M, 1994: Smith. Improved global sea surface temperature analyses. J. Clim., 7.

Smith T. M. and R. W. Reynolds, 2004: Improved extended reconstruction of SST (1654-1997). J. Clim., 17, 2466-2477.

Schar, C., P.L. Vidale , D. Luthi, C. Frei, C. Haberli, M.A. Liniger and C. Appenzeller, 2004: The role of increasing temperature variability in European summer heat waves. Nature, 427, 332-336.

Stedman, J., 2004: The predicted number of air pollution related deaths in the UK during the August 2003 heat wave. Atmospheric Environment, 38, 1087-1090.

Stewart, I.T., D.R. Cayan and M.D. Dettinger, 2005: Changes toward earlier streamflow timing across western North America. J. Clim., 18, 1136-1155.

Stott, P.A., D.A. Stone and M.R. Allen, 2004: Human contribution to the European heat wave of 2003. Nature, 432, 610-613.

Tebaldi, C., K. Hayhoe, J.M. Arblaster and G.A. Meehl, 2006: Going to the extremes: An intercomparison of model-simulated historical and future changes in extreme events. Clim. Change, 79, 185-211.

Trenberth, K. E. and C. J. Guillemot, 1998: Evaluation of the atmospheric moisture and hydrological cycle in the NCEP/NCAR reanalyses. Climate Dynamics, 14, 213-231.

USAgNet, 2006: California's cattle death toll surpasses 25,000. July 31.

Bonneville Power Administration (BPA), U.S. Army Corps of Engineers (North Pacific District), Bureau of Reclamation (Pacific Northwest Region) (BPA et al.), 1991: The Columbia River System: The Inside Story. Report published for the Columbia River System Review by the U.S. Army Corps of Engineers and the Bureau of Reclamation #DOE/BP-1689.

Cayan, D. R., M. D. Dettinger, H. F. Diaz, and N. Graham, 1998: Decadal variability of precipitation over western North America. J. Climate, 11 (12): 3148–3166.

Cayan, D. R., M. D. Dettinger, R. T. Redmond, G. J. McCabe, N. Knowles, and D.H. Peterson, 2003: The transboundary setting of California's water and hydropower systems, linkages between the Sierra Nevada, Columbia, and Colorado hydroclimates. Climate and Water: Transboundary Challenges in the Americas, H. Diaz and B. Morehouse, Kluwer Press, Chapter 11.

Christensen, N.S., Wood, A.W., Voisin, N., Lettenmaier, D.P. and R.N. Palmer, 2004: Effects of Climate Change on the Hydrology and Water Resources of the Colorado River Basin, Climatic Change, 62 (1-3): 337-363.

Crook, A.G. 1993: 1990 Level Modification Streamflow 1928-1989, Report of A.G. Crook Company to Bonneville Power Administration, Contract #DE-AC79-92BP21985.

Devore, J.L., 1991: Probability and Statistics for Engineering and the Sciences, Brooks/Cole Publishing, CA, pp 492-494.

Gershunov, A., and T.P. Barnett, 1998: Interdecadal modulation of ENSO teleconnections, Bulletin of the American Meteorological Society, 79 (12): 2715-2725.

Hamlet, A. F. and D. P. Lettenmaier, 1999a: Columbia River streamflow forecasting based on ENSO and PDO climate signals, American Society of Civil Engineers Journal of Water Resources Planning and Management, 125 (6): 333-341.

Hamlet, A. F. and D. P. Lettenmaier, 1999b: Effects of climate change on hydrology and water resources in the Columbia River Basin, Journal of the American Water Resources Association, 35 (6): 1597-1623.

Hamlet A.F., and D.P. Lettenmaier, 2005: Production of temporally consistent gridded precipitation and temperature fields for the continental U.S., J. Hydrometeorology, 6 (3): 330-336.

Hamlet A.F., P.W. Mote, M.P. Clark, and D.P. Lettenmaier, 2005: Effects of temperature and precipitation variability on snowpack trends in the western U.S., J. Climate, 18 (21): 4545-4561.

Hamlet A.F., P.W. Mote, M.P. Clark, D.P. Lettenmaier, 2007: 20th Century Trends in Runoff, Evapotranspiration, and Soil Moisture in the Western U.S., J. Climate, 20 (8): 1468-1486.

Hamlet, A.F., D.P. Lettenmaier, 2007: Effects of 20th Century Warming and Climate Variability on Flood Risk in the Western U.S., Water Resour. Res., 43, W06427, doi:10.1029/2006WR005099.

Hidalgo H.G., and J.A. Dracup, 2003: ENSO and PDO effects on hydroclimatic variations of the Upper Colorado River basin, J. Hydrometerology, 4 (1): 5-23.

IPCC, 2001: Climate Change 2001: The Scientific Basis. Contribution of Working Group I to the Third Asessment Report of the Intergovernmental Panel on Climate Change [Houghton, J.T., Y. Ding, D.J. Griggs, M. Noguer, P.J. Van der Linden, X. Dai, K. Maskell, and C.A. Johnson (eds.)], Cambridge University Press, Cambridge, UK and New York, NY, USA, 881pp.

Jain, S., M. Hoerling and J. Eischeid J., 2005: Decreasing reliability and increasing synchroneity of Western North American streamflow. J. Climate, 18 (5): 613-618.

Liang X., D.P. Lettenmaier, E.F. Wood, and S.J. Burges, 1994: A Simple hydrologically based model of land surface water and energy fluxes for general circulation models, J. Geophys. Res., 99 (D7): 14,415-14,428.

Mantua, N., S. Hare, Y. Zhang, J. M. Wallace, and R. Francis, 1997: A Pacific interdecadal climate oscillation with impacts on salmon production, Bulletin of the American Meteorological Society, 78: 1069-1079.

Meko, D.M., 2001: Reconstructed Sacramento River System Runoff From Tree Rings, Report prepared for the California Department of Water Resources, July.

Meko, D.M. and C.A. Woodhouse, 2005: Tree-ring footprint of joint hydrologic drought in Sacramento and Upper Colorado river basins, western USA. Journal of Hydrology, 308 (2005): 196-213.

Mote, P.W., E.A. Parson, A.F. Hamlet, K.G. Ideker, W.S. Keeton, D. P.,Lettenmaier, N.J. Mantua, E.L. Miles, D.W. Peterson, D.L. Peterson, R., Slaughter, and A.K. Snover, 2003: Preparing for climatic change: the water, salmon, and forests of the Pacific Northwest, Climatic Change, 61 (1-2): 45-88.

Naik, P.K., D.A. Jay, 2005: Estimation of Columbia River virgin flow: 1879 to 1928.

Hydrological Processes, 19 (9): 1807-1824.

Pagano T., and D. Garen, 2005: A recent increase in western US streamflow variability and persistence, J. of Hydrometeorology, 6 (2): 173-179.

Smith, J.A., G.N.Day, M.D. Kane, 1992: Nonparametric Framework for Long-Range Streamflow Forecasting, ASCE J. of Water Res. Planning and Management, 118 (1): 82-92

Snover, A.K., A.F. Hamlet, D.P. Lettenmaier, 2003: Climate-change scenarios for water planning studies, Bulletin of the American Meteorological Society, 84 (11): 1513-1518.

Woodhouse, C.A., S.T. Gray, and D.M. Meko, 2006: Updated Streamflow Reconstructions for the Upper Colorado River Basin,Water Resources Research, Vol. 42, W05415.

Van Rheenen, N.T., A.W. Wood, R.N. Palmer and D.P. Lettenmaier, 2004: Potential Implications of PCM Climate Change Scenarios for Sacramento - San Joaquin River Basin Hydrology and Water Resources, Climatic Change, 62 (1-3): 257-281.

Verrill, S.P., R.A. Johnson, 2007: Confidence bounds and hypothesis tests for normal distribution coefficients of variation, USDA Forest Service, Research Paper FPL-RP-638

Voisin, N., A. F. Hamlet, L. P. Graham, D. W. Pierce, T. P. Barnett, and D. P. Lettenmaier, 2006: The role of climate forecasts in western U.S. power planning, Journal of Applied Meteorology, 45(5): 653-673.

Zhang Y., Wallace, J.M., Battisti, D.S., 1997: ENSO-like interdecadal variability: 1900-93, J. of Climate, 10 (5): 1004-1020.